DRAPER LABORATORY

EXTRACTION OF ANTIPARTICLES CONCENTRATED IN PLANETARY MAGNETIC FIELDS

JAMES BICKFORD
PRINCIPAL INVESTIGATOR
jbickford@draper.com

NIAC PHASE I
FINAL REPORT

APRIL 2006

555 TECHNOLOGY SQUARE
CAMBRIDGE, MA 02139

TABLE OF CONTENTS

ACKNOWLEDGEMENTS

Jim Bickford would like to acknowledge the numerous contributions from the people and organizations that enabled or directly contributed to the success of the phase I program. Funding was provided by the NASA Institute for Advanced Concepts (NIAC) under a contract administered by the Universities Space Research Association (USRA). The team members are William Schmitt (radiation transport analysis), and Joseph Kochocki (cosmic ray physics) from Draper, Walther Spjeldvik (radiation belt modeling) from the Weber State University Department of Physics and Nordmann Research and Development, Oleg Batishchev (plasma physics) from the MIT Space Propulsion Lab, and Harlan Spence (space physics) from the BU Center for Space Physics.

Galina Pugacheva and Anatoly Gusev, who are both now at the Space Research Institute in Moscow, along with Walther and other colleagues, completed much of the work that laid the foundation for the phase I antiparticle radiation belt analysis. Richard Selesnick from The Aerospace Corporation provided helpful pointers during modeling of the CRAND effect, John West from Draper Laboratory was the program manager, and Joe Donis, Don Fyler, Pete Maragilia, Rick Metzinger, Darryl Sargent, and Marc Weinberg from Draper provided technical assistance in a variety of topic areas. Finally, I would like to thank Shari Bickford for patiently listening to all of my stories and providing valuable feedback.

CHAPTER 1 - EXECUTIVE SUMMARY

BACKGROUND AND OVERVIEW

Small quantities of antimatter have enormous potential in a variety of space, medical, and sensing applications. In particular, it has been suggested that tens of nanograms to micrograms of antiprotons can be used to catalyze nuclear reactions and propel spacecraft to velocities up to 100 km/sec. This is well beyond the capability of traditional chemical propellants and opens up new exciting options for space exploration. Larger supplies of antiprotons would eventually enable spacecraft capable of relativistic velocities. The revolutionary potential of this technology is due to the fact that antiparticles release an enormous amount of energy when they come into contact with regular matter. The energy density is two to three orders of magnitude higher than nuclear reactions and nearly ten orders of magnitude greater than the best chemical propellants used in spacecraft such as the space shuttle.

However, the intrinsic advantages of antimatter have not yet been realized due to the inherent limitations associated with the production and storage of antiprotons. Currently, high energy particle accelerators used for physics research provide the only controllable supply of antiprotons. The generation and trapping of the antiparticles is an extremely inefficient process with limited throughput since it relies on extracting the particles from sub atomic collision debris. The generated particles must be stored in a high vacuum environment and levitated in magnetic and/or electric fields to avoid having them contact standard matter. The worldwide output is currently in the low nanogram per year range at an estimated cost of up to $160 trillion per gram with additional overhead for infrastructure and personnel.

In comparison, high energy galactic cosmic rays (GCR) bombard the upper atmosphere of planets and material in the interstellar medium to naturally generate antiparticles through pair production. The antimatter is created by converting the kinetic energy of the incident GCR particle into mass during a high energy collision with another particle. Orbital and high altitude balloon measurements have confirmed the fractional existence of antiprotons in the normal background of ionizing radiation. (Figure 1) The GCR background represents a nearly infinite source of antiprotons though the natural flux is extremely low, making it difficult to collect a large number of particles with conventional systems. However, the properties of the natural environment surrounding planets with magnetic fields can generate much larger fluxes as the particles interact with the magnetic field and atmosphere.

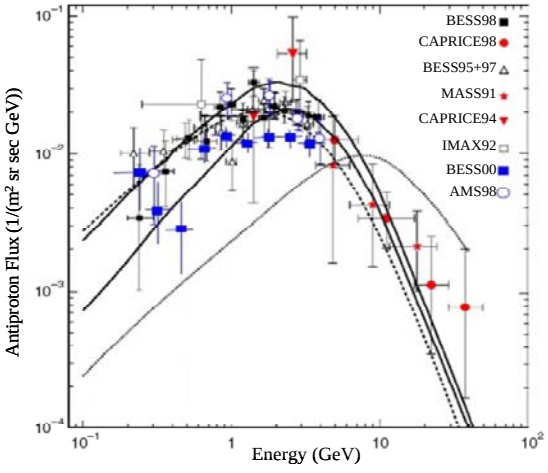

Figure 1 – Measured GCR antiproton spectrum. (Picozza and Morselli, 2003)

There are four fundamental processes that can cause antiprotons to be concentrated in or around planetary magnetic fields. They are:

- Cosmic Ray Albedo Antineutron Decay (CRANbarD)
- Direct pair production and trapping of antiprotons in the exosphere
- Transient GCR focusing
- Artificial augmentation

During this phase I study, the efficiencies of each of these processes were evaluated to determine the overall effectiveness of generating high fluxes of antiprotons near planets. A subset of these processes can also occur at other locations in the solar system (e.g. comet tails) to locally increase the antiproton flux well beyond the natural GCR background. The potential natural supply of positrons was also evaluated. Ultimately, these natural fluxes can be concentrated and the antiparticles trapped for use in space propulsion and/or other innovative applications.

The proposed collection system employs electric current flowing through one or more rings made from high temperature superconductors. The current loop induces a magnetic dipole moment which can influence the trajectory of a charged particle over a very large spatial extent. This is the basic premise of the Bussard magnetic scoop first proposed for interstellar travel. However, our concept is to use the system on a spacecraft in an equatorial orbit to direct and then trap antiparticles trapped in the radiation belts as they bounce between their mirror points in the Northern and Southern hemispheres. The magnetic field induced by the concept shown in Figure 2 can be used to first concentrate the antiparticles and then to store them within the mini-magnetosphere formed around the spacecraft. The same field can also assist in directing ejecta products from the propulsion system and to partially shield equipment or astronauts within the vehicle from external radiation sources.

Figure 2 – Artist's concept of the proposed collection system formed of superconducting rings.

IN SITU PRODUCTION AND TRANSPORT

A natural antiproton radiation belt can be generated in a manner analogous to the traditional Van Allen radiation belts which surround the Earth. The high energy portion (E>30 MeV) of the proton belt is primarily formed by the decay of neutrons in the Earth's magnetosphere. The GCR flux interacts with the planet's upper atmosphere to release free neutrons with a half life of just over 10 minutes. A fraction of these neutrons travel back into space (albedo) and decay into a proton, electron, and an anti-neutrino while still within the influence of the magnetosphere.

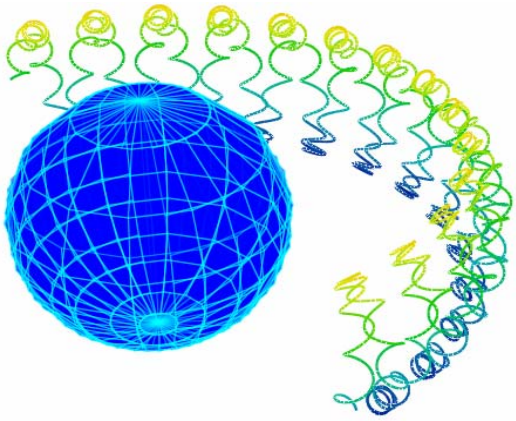

Figure 3 – Motion of a charged particle trapped in a planet's magnetosphere.

The magnetic field of the planet forms a bottle to stably hold the protons and electrons from the decay process. If the trajectory of the ejected proton from the decay process is outside of the planet's loss cone for magnetic confinement, the proton will be trapped on the magnetic field line (L-shell) on which it was formed. The periodic motion (Figure 3) is explained by the Lorentz force which causes the particles to spiral along the magnetic field lines and mirror between the North and South magnetic poles. In addition, the particles have a slow drift motion around the planet. As particles are lost through diffusion and loss processes, new ones are generated to maintain a quasi-static supply trapped in the near dipole field of the Earth.

The interaction of cosmic radiation with the upper atmosphere also produces antiparticles from pair production. Figure 4 shows computer simulations of the nuclear transport phenomena that generates antineutrons from the incident particle flux. The produced antineutrons follow a trajectory primarily along the path of the original cosmic ray, but can be backscattered after interacting with the atmosphere. These albedo antineutrons decay in a manner similar to the regular neutrons. However, the antineutron will decay into a positron, antiproton, and neutrino and therefore acts as a supply for the antiparticle radiation belts surrounding the Earth. The physics that govern the trapping and motion are identical between the particle and its antiparticle counterpart with the exception that the antiparticle with the opposite charge will spiral and drift in the opposite direction.

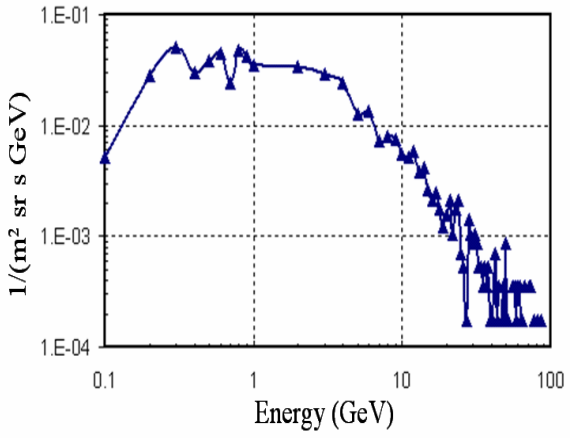

Figure 4 – Production spectrum for antineutrons generated in the Earth's atmosphere.

The residual atmosphere of Earth extends thousands of kilometers from the planet. The trapped antiprotons can annihilate with these atmospheric constituents, especially at low altitudes where this becomes the primary loss mechanism. Figure 5 shows the estimated loss rates for particles at several energies as a function of its altitude. At radiation belt altitudes, this loss rate is extremely slow enabling a large supply of generated antiprotons to be built up relative to the source flux.

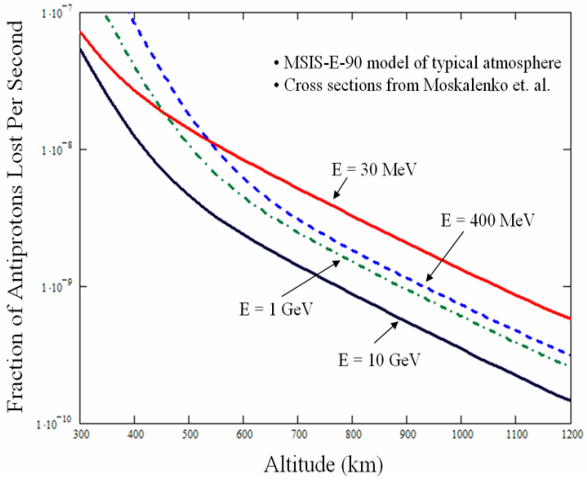

Figure 5 – Fraction of antiprotons lost per second due to annihilation with the atmosphere. (Earth)

Figure 6 shows the estimated flux of antiprotons trapped in the Earth's magnetosphere due to the CRANbarD source. The values were determined by combining empirical models of the proton belt and normalizing it by the estimated antiproton to proton ratio for the source function. Computer modeling of the production of albedo antineutrons relative to albedo neutrons yielded an energy dependent ratio of 1 antineutron for every 10^5 to 10^9 neutrons. Based on this and the subtraction of the solar proton contribution, the antiproton content of the Earth's magnetosphere from this effect is estimated to be between 0.15 and 15 nanograms. This is replenished every few years.

Antiprotons can also be directly trapped after pair production in the exosphere. However, there is a fine balance between the generation and loss processes. Unlike the neutral antineutrons which can travel unimpeded through the magnetosphere to decay somewhere deep in the radiation belts, antiprotons are immediately trapped along the L-shell where the pair production took place. Therefore, most of the antiprotons will be produced deep in the atmosphere where loss rates are high thereby yielding a negligible trapped flux. Loss rates are lower at higher altitudes but there is

less source material (atmosphere) which results in a low interaction cross section for pair production. The peak production and trapping occurs at an altitude of approximately 1200 km (L=1.2).

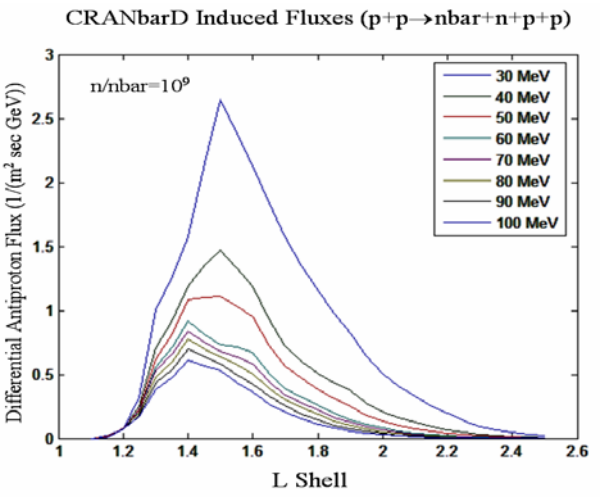

Figure 6 – Estimated antiproton flux around Earth.

The total antiproton content of the magnetosphere is relatively low due to the inefficiency of the antineutron backscatter process as derived by a slab model of the nuclear transport phenomena. The predicted flux is very sensitive to the input parameters which may have resulted in an estimate that is too conservative. The influence of incident GCR protons which strike the atmosphere at a grazing angle (and are therefore not modeled) will be more efficient at generating viable antineutrons since they do not have to go through the full backscatter process to travel through and decay in the magnetosphere. A full source, loss, and transport analysis for antiprotons should be completed in the future.

The strong magnetic fields and large size of the Jovian planets in the outer solar system make these bodies far more efficient at generating and trapping antiprotons. A series of basic extrapolations of the source functions were used to estimate the relative antiproton content of the outer planets. The antiproton source is stronger relative to Earth since the loss cone is reduced allowing a larger fraction of the decay products to be trapped; the much larger magnetosphere increases the time of flight through the trapping region, allowing far more of the antineutrons to decay within the magnetosphere; and the larger surface area and other production targets (rings, etc…) can produce a greater number of pair produced antiparticles.

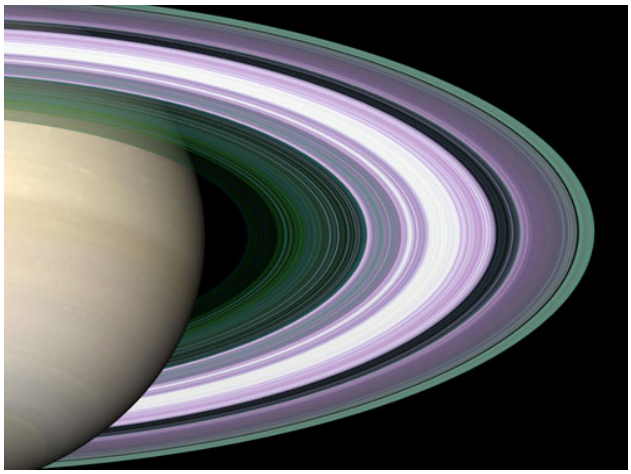

Figure 7 – The largest antiproton source in the solar system. (Cassini radio occultation experiment)

Surprisingly, Jupiter was not found to be the best source of antiprotons in the solar system. Even though it is the largest in terms of size and field strength, the magnitude of the magnetic field shields much of the atmosphere from the GCR production spectrum which reduces the overall effectiveness of the process. In comparison, a larger portion of the flux reaches the atmosphere of Saturn. In addition, antineutrons are copiously produced in the rings of the planet which do not need to be backscattered to yield stable trapping. Therefore, Saturn likely has a stable antiproton population of hundreds of micrograms based on extrapolations from the conservative Earth estimate. A full radiation belt model of Saturn system with antiproton generation and loss sources needs to be completed to more precisely determine the fluxes.

The background GCR flux can also be concentrated by a planetary magnetic field. On a yearly basis, approximately 4 grams of antiprotons will impinge on the magnetosphere of the Earth and nearly 10 kg will pass through the magnetosphere of Jupiter. Simulations of the motion of these particles (Figure 8) were completed to determine how effectively the planet could help concentrate the particles and improve the efficiency of collection. It was found that static magnetic fields provide a one half to one and a half order of magnitude increase in flux relative to the background near the magnetic poles of the planet. This is valuable though placing a spacecraft in an orbit optimized for such collection may not be practical since it will spend much of its orbit passing through equatorial regions where the flux is lower. A spacecraft optimized for collecting trapped fluxes in equatorial regions is likely to be more practical though the total supply is limited by the source function. Of more interest is the hint that quasi-stable trapping of incident GCR antiprotons may be possible due to minor energy degradation in the magnetosphere. This could potentially happen naturally (unlikely) or be induced artificially by degrading the incident particle's energy with RF or electric fields.

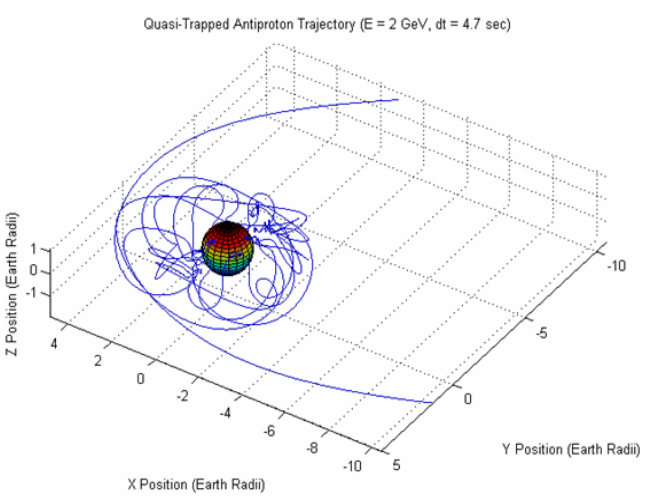

Figure 8 – Example GCR antiproton trajectory through the Earth's magnetosphere.

The magnetosphere of the Earth, or a miniature version created via artificial means around a satellite in orbit, could efficiently hold antiprotons that are generated artificially by a particle accelerator placed in orbit. Production in the space environment offers an intrinsic advantage for space exploration since the particles are generated and stored in orbit, therefore mitigating the need to transport them from the ground in bulky and heavy traps. A generator system placed in orbit will be far more efficient at collecting the antiparticles since the natural radiation trap will capture a wide angular distribution and energy range with minimal complexity. In a departure from convention, the large storage volumes enable the generator to be placed within the trap. This is a very efficient way to trap nearly all of the generated antiprotons. A 100 kWe generator would produce approximately 10 micrograms per year. Scaling this to a 1 GWe power source would enable nearly 100 milligrams of antiprotons to be produced per year. This level of antiproton generation is sufficient to enable the first interstellar missions to nearby stars.

COLLECTION SYSTEM

In the phase I program we have evaluated the efficiency and collection rate of a magnetic scoop designed to extract large quantities of trapped antiparticles present in the natural space environment. The principles of a magnetic scoop, first proposed for relativistic propulsion, have been adapted for use on a satellite in a planetary orbit. Particles bouncing between mirror points near the planet's poles will pass through and be concentrated by the superimposed magnetic field. Near the throat of the collection device, the particle energy can be degraded or electric/RF fields can be used to transfer the incoming particle onto a closed field line of the device. The antiparticle can safely be stored in this artificial radiation belt which forms in the space surrounding the exterior to the vehicle. The radiation belts of planets successfully hold particles for periods of months to years and artificial systems are also capable of providing long term storage stability.

The magnetic dipole of the scoop is formed by generating high currents in superconducting loops around the spacecraft. Incident antiprotons will follow the magnetic field lines to the throat where they can be transferred to the closed external field lines where they are stored. Optionally, the particles can be trapped in a magnetic bottle formed by the field lines on the interior of a two coil configuration. The collection efficiency and rate are influenced by a number of internal and external factors including the magnitude of the induced dipole moment (total current, number of loops, loop radius), ambient field strength, incident energy spectrum, angle of incidence, and the trap location.

There are two fundamental processes that limit the ability of particles to enter the throat area of the scoop. First, depending upon the initial trajectory of the particle, the induced magnetic field may cause the particle to reflect away from the vehicle before it can be trapped. Second, depending upon the trajectory and particle energy, the spiral radius for the incoming particles may be larger than the entire collection system which ultimately eliminates the ability to influence the trajectory. Figure 9 shows the estimate collection rate based on these limiting factors as a function of the superconducting coil radius based on the worst case GCR background flux.

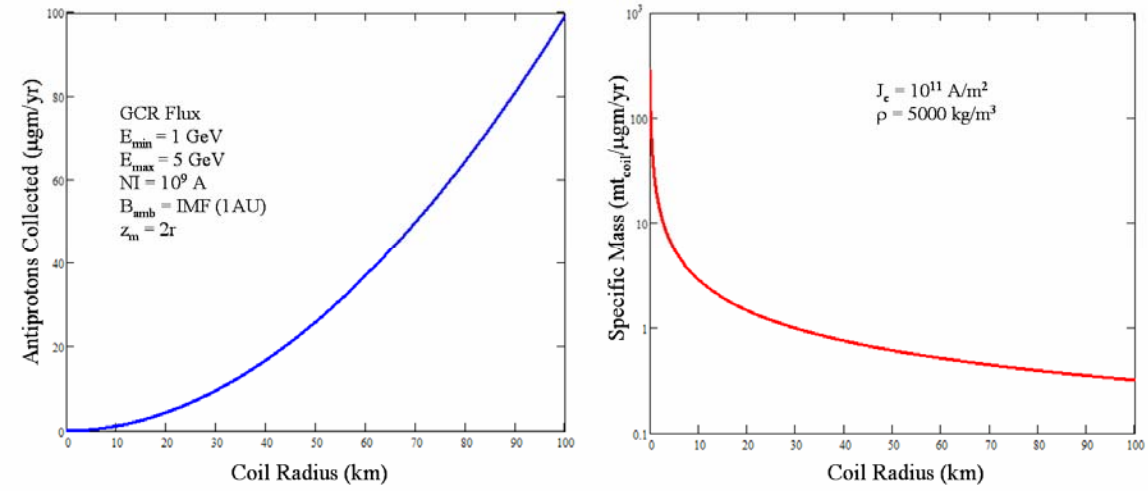

Figure 9 – Antiproton collection rate based on the background interstellar GCR flux.

The potential collection rate with the GCR antiproton flux can be tens of micrograms per year for some of the larger systems. Much smaller vehicles which are more practical from a total mass and logistics perspective will likely work in the microgram per year range at these flux levels. Operating the vehicle in regions with higher natural fluxes can significantly increase the overall collection rate. In addition, operating the vehicle in the radiation belts where the characteristic energy of the antiprotons tends to be lower will improve the collection efficiency. Ultimately, the total amount collected will be limited by the available source of antiprotons locally contained within the magnetosphere.

Several technology developments need to occur before the proposed collection system is feasible at a large scale. In particular, the performance of high temperature superconductors must improve substantially to reduce the coil mass to practical levels. The ability to produce long continuous sections of the wire must also be demonstrated for a robust space qualified system. Improvements in the ability to provide in orbit power are also essential, especially if artificially augmented systems are desired and developed. Finally, improvements in passive cooling systems and a reduction in the cost to orbit will help make the system more economically feasible.

CHAPTER 2 - BACKGROUND

UTILITY OF ANTIMATTER

The annihilation of antimatter with its normal matter counterpart liberates the total amount of energy predicted by Einstein's famous equation, $E=mc^2$. As shown in Table 1, on a mass basis this is about 10^{10} times more efficient than chemical reactions and 10^2 -10^3 times more efficient than nuclear reactions. To put this in perspective, the annihilation of 1 kg of antimatter releases the energy equivalent to 30 million barrels of oil. The total worldwide energy consumption per year corresponds to approximately 2200 kg of antimatter.

The extremely high energy content and other properties of antiparticles enable new applications in both space and on the Earth. In particular, the annihilation of antimatter with its regular matter counterpart enables extremely high performance space propulsion systems. As early as 1953, Eugene Sanger [1] suggested utilizing positrons for propulsive applications. Beamed core antiproton propulsion approaches the theoretical ISP limit of about 30 x 10^6 seconds. Compared to the best chemical propulsion (ISP ~400 seconds), antimatter rockets have extremely good mass fractions due to the ISP influence on the rocket equation. Schmidt et al. [2, 3] reviewed the performance of several antimatter propulsion methods in the context of aggressive interplanetary and interstellar precursor missions. Antimatter Catalyzed Microfission/Fusion (ACMF) requires only nanogram quantities of antiprotons to achieve spacecraft ΔVs in the range of 100 km/sec. Small scale thruster experiments with this technology are already underway in another NIAC funded program [4]. This, along with other antimatter based programs, would suddenly be enabled if antiparticles could successfully be created and safely stored for extended periods of time in the space environment.

Fuel	Energy Density (J/kg)	Notes
Battery	7.2 x 10^5	Lithium Ion
Chemical	1.4 x 10^7	LO_2/LH_2
Fission	8.2 x 10^{13}	U^{235}
Fusion	3.4 x 10^{14}	DT
Antimatter	9.0 x 10^{16}	$E=mc^2$

Table 1 – Relative energy density of various systems.

The high ΔV potential enables new classes of aggressive space exploration missions. Less than 10 micrograms of antiprotons are required to send a 100 metric ton payload on a one year round trip mission to Jupiter. Similar class missions include fast trips beyond the heliopause (100+ AU) and to the Sun's gravity focus point (550 AU) which effectively enables the Sun to be used as a giant telescope with unprecedented resolution. More traditional missions, such as those to Mars as envisioned in NASA's current vision for space exploration, are also improved substantially. For example, a traditional low energy Mars trajectory entails an average one way flight time of approximately 180 days while a 30 nanogram antiproton driven ACMF variant [5] would have a flight time of about 45 days and also reduce the overall mass needed to be launched into LEO for each mission.

New non-space applications are also enabled and have been proposed, provided antimatter can be produced and collected effectively. One of the most promising applications is to use antiprotons to image the interior of solids. Material properties and their distribution in the solid can be determined by examining the annihilation products [6]. This has profound implications in both medical diagnostics and homeland security. Also in the medical area, pictogram quantities of antiprotons can be used to locally treat inoperable tumors [7]. Finally, from a pure science perspective, improving the availability of antimatter will allow new experiments to be performed to confirm theoretical predictions in atomic and gravitational physics.

CURRENT PRODUCTION AND STORAGE CAPABILITIES

Currently, the primary source of controlled antiprotons is from high energy particle accelerators. Both CERN in Switzerland and the Fermi National Accelerator Laboratory (FNAL) produce antiprotons during the collision of high energy proton beams with a solid target. Resulting reactions produce copious numbers of various particles through pair production. A small percentage of the ejecta can be magnetically confined and focused to separate out the antiprotons which are then decelerated and placed in a confinement ring for use in subsequent experiments.

At FNAL, approximately 10^7 antiprotons per pulse can be 'stacked' in the accumulator ring. At present, 10^{11} antiprotons per hour can be produced for 4500 hours per year [3]. If the facility was used to exclusively create and accumulate antiprotons, a total of almost 1 nanogram would be produced over this period. A number of improvements have been discussed which could enhance this by a factor of 10 or more by increasing the efficiency of the collection process. It has been suggested that a dedicated facility could be built for $3-$10 billion (FY 1988) which could increase production still further [8].

Schmidt et al. [2] discusses some of the fundamental energy cost constraints of producing antiprotons in particle accelerators. Currently, only one in about 10^5 proton collisions produces an antiproton which can be collected. Due to the energy requirements for accelerating the proton beam, even with a wall plug efficiency of 50%, $0.10 per kilowatt-hour yields a net antiproton production cost of $62.5 trillion per gram collected due to electricity costs alone. In another analysis, LaPointe estimated the current electricity costs to be $160 trillion per gram. [9]

A number of alternative production capabilities have been proposed. Hora [10] and Crowe [11] have suggested using high intensity lasers to produce antimatter. However, efficiently generating laser pulses with sufficient energy remains an obstacle. Chapline [12] proposed using heavy ions instead of proton beams to increase accelerator production, though the antiprotons are generated isotropically making it difficult to collect the antiprotons from the ejecta debris. Cassenti [13] has suggested redirecting pions generated during collisions, though this approach also suffers from the difficulty of containing and redirecting the debris. These variations all have similar energy cost limitations. LaPointe proposed using the Casimir force to suppress local vacuum fields as a means to generate steep gradients required for antiproton production at a potential boundary [9]. However, like the other techniques, it has not been demonstrated in practice.

After production in Earth based facilities, antiprotons must be stored in a high vacuum environment and suspended in magnetic/electric fields to avoid losses due to annihilation with air nuclei and the container walls. The long term storage of the antiprotons is limited by the hardness of the vacuum since introduced particles will annihilate with antiprotons (or positrons) in the trap. Currently, the most advanced portable trap (HiPAT) can in principle store approximately 10^{12} (~1 picogram) of antiprotons for days or more at a time by maintaining the trap at a temperature of 4 Kelvin. The storage density can theoretically be increased by forming electrically neutral anti-hydrogen atoms to address space charge and Brillouin trapping limits but this has not been demonstrated at a significant scale. Recent discussion has also centered on using photonic bandgap structures to store positrons by preventing excited positronium to decay to its ground state. It remains to be seen whether this can be scaled to store large quantities of antimatter.

The original Penn State antiproton trap, capable of transporting 10^{10} antiprotons (~10 femtograms), was 100 cm tall by 30 cm across and weighed 55 kg fully loaded [14]. The system mass to antiproton mass is therefore 10^9 kg/μg though it is unclear how, or even if, this can scale to the nanogram to microgram class storage levels needed for space applications. The particles would need

to be produced and then stored over a period of months to years without significant annihilation losses. The ability to transport antiprotons (in their traps) generated on the ground into orbit remains a serious obstacle even if ground based production can be scaled to much higher rates.

NATURAL ANTIMATTER PRODUCTION

High energy galactic cosmic rays (GCR) are pervasive through our galaxy and constantly bombard the upper atmosphere of Earth with energies up to 10^{20} eV per nucleon. The exact nature of the flux is uncertain, but the particles are believed to originate from events both in and out of our galaxy. [15] Moskalenko et al. [16] provides an overview of GCR propagation in the context of interstellar antiproton generation. The GCR flux can also interact with the Earth's atmosphere to locally produce antiparticles. [17] When a high energy proton strikes a particle in the interstellar medium or in a planet's atmosphere, its kinetic energy can be converted to matter when above the energy threshold,

$$E_{th} = m_P\left(2+\frac{4}{A}\right), \qquad \textit{Equation 1}$$

where m_p is the mass of a proton and A is the mass of the atmospheric or interstellar constituent struck by the incident particle. (Appendix A provides a derivation of this quantity.) A proton-proton reaction results in the two original protons plus a proton and antiproton generated through pair production such that

$$p + p \rightarrow p + p + p + \overline{p}. \qquad \textit{Equation 2}$$

Likewise, an equivalent process can generate a neutron/anti-neutron pair. The antineutron subsequently decays into an antiproton, positron, and neutrino with a half life of just over 10 minutes in the reference frame of the particle.

The ratio of protons to antiprotons is an important measurement in the search for dark matter as well as a number of other physical processes including bounding restrictions on the amount of antimatter which can exist in the universe. As a result, a significant number of experiments have been performed to measure the ratio between the natural proton background and the antiproton flux. Over a period of several decades measurements have been made in high altitude balloons, LEO satellites and spacecraft (including the space shuttle). Figure 10 and Figure 11 from Picozza et al.

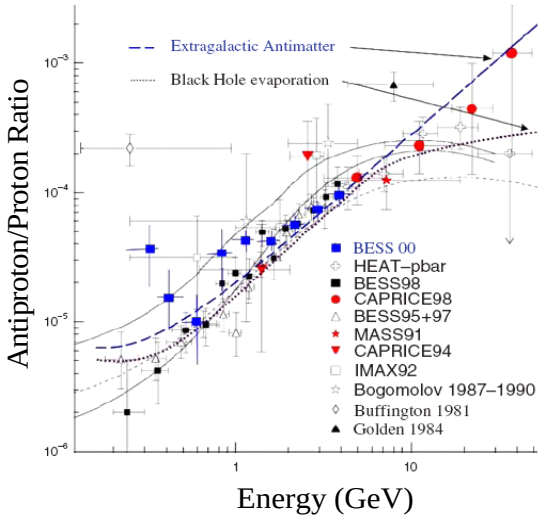

Figure 10 — Measured Proton/Antiproton Ratio. (Based on Picozza et al.)

[18] summarizes the resulting measurements obtained. The antiproton/proton ratio is approximately 10^{-4} when integrated over the total particle population though there is a strong dependence on the particle's energy. A dependence on solar cycle is also seen. [19] Positrons contribute to nearly 10% of the overall electron and positron flux.

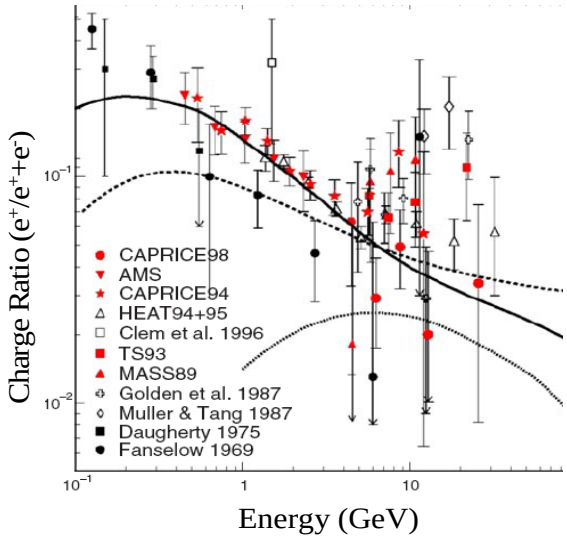

Figure 11 - Measured Positron Fraction. (Based on Picozza et al.)

MAGNETOSPHERIC TRAPPING

Charged particles moving in a magnetic field are influenced by the Lorentz force,

$$\mathbf{F} = q(\mathbf{v} \times \mathbf{B} + \mathbf{E}) \qquad \textit{Equation 3}$$

where q is the charge, $\boldsymbol{v}$ is the particle velocity, $\boldsymbol{B}$ is the magnetic field and $\boldsymbol{E}$ is the electric field. The path of antiprotons, positrons, and other charged particles will be heavily influenced by the magnetic field of a planet. As described by Walt [20], the magnetic field potential of the Earth is,

$$\psi = R_E \sum_{n=1}^{\infty} \left(\frac{R_E}{r} \right)^{n+1} \sum_{m=1}^{n} g_n^m \left(\cos m\phi + h_n^m \sin m\phi \right) P_n^m (\cos\theta), \qquad \textit{Equation 4}$$

where R_E is the radius of the Earth, r, θ, ϕ are the position variables of the point being considered, and the other terms are constants which represent empirically derived field parameters for the planet. The lowest order, and dominant term, of the Earth's magnetic field is a simple dipole.

When under the influence of the magnetic field, some fraction of internally generated particles is properly aligned to become trapped in the magnetic field of the Earth. This is identical to the normal trapping which occurs with protons, electrons and other nuclei to form the Van Allen radiation belts of the planet. The trapped particles follow a trajectory which spirals around magnetic field lines as shown in Figure 12.

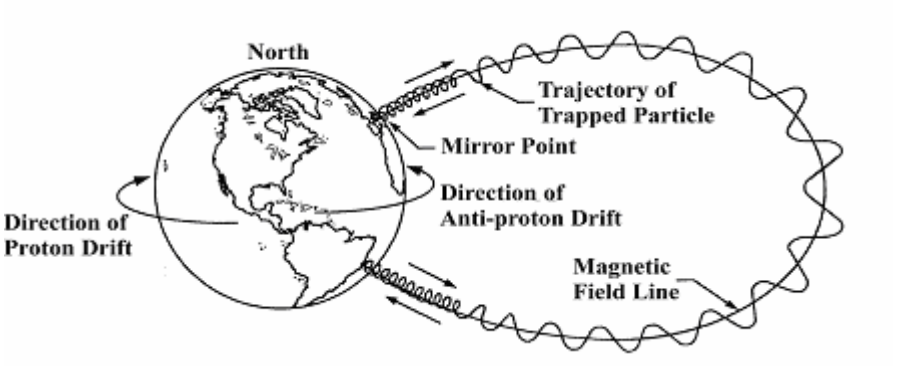

Figure 12 - Trapped charged particle motion in a magnetic field

The gyroradius, or the distance between the mean trajectory (guiding center) and the spiral radius is,

$$\rho = \frac{p_\perp}{Bq} = \frac{m_0 \gamma v_\perp}{Bq} \qquad \textit{Equation 5}$$

where $v_\perp$ is the particle's velocity perpendicular to the mean trajectory and γ is the relativistic correction factor for high energy particles. Particles of opposite charge will spiral in the reverse direction of each other.

The particles are trapped due to the influence of a mirroring force as the particle approaches the higher field strength near the poles. The mirror force,

$$F_z = -q v_\perp \frac{\rho}{2} \frac{\partial B_z}{dz} \qquad \textit{Equation 6}$$

is independent of the polarity of the particle's charge and forces the particle to bounce between mirror points in the Northern and Southern hemispheres. The pitch angle α,

$$\tan \alpha = \frac{v_\perp}{v_{||}} \qquad \textit{Equation 7}$$

is modified due to the mirror force as it approaches the mirror point near the poles. At a pitch angle of 90^0, the particle has been effectively repelled and bounces back to its mirror point in the opposite hemisphere. The approximate bounce period for Earth,

$$\tau_b = 0.117 \left(\frac{R_0}{R_E} \right) \frac{1}{\beta} \left[1 - 0.4635 \left(\sin \alpha_{eq} \right)^{3/4} \right] \text{sec} \qquad \textit{Equation 8}$$

is a function of the equatorial crossing distance R_o, and equatorial pitch angle α_{eq}, along with the velocity relative to light, β. The trapped particles are slowly transported through various diffusion processes (e.g. magnetic field fluctuations) [21] until a quasi-static balance between the source and loss functions is ultimately reached [22]. The radiation belt can be described as a six dimensional average phase space density (*f*) where the components represent the three position and three

momentum values for the trapped particle population. The time evolution of the generated radiation belts in phase space is described by diffusion coupled with appropriate source and loss terms such that,

$$\frac{\partial f}{\partial t} = \frac{\partial}{\partial L}\left[\frac{D_{LL}}{L^2}\frac{\partial f}{\partial L}\right] + Sources + Losses, \qquad \textit{Equation 9}$$

where L is the magnetic shell that the particle is traversing and D_{LL} is the diffusion constant which describes the radial diffusion of the particles due to the collective action of various natural mechanisms operating in the magnetosphere. These combined processes produce a quasi-static radiation belt of charged particles resident in the magnetic field lines of the planet. Barth et al. [23] and Hargreaves [24] describe the pertinent models for the environment surrounding the Earth. The empirically derived AP8 radiation belt model shown in Figure 13 gives the resulting fluxes expected for protons trapped in the Earth's radiation belts.

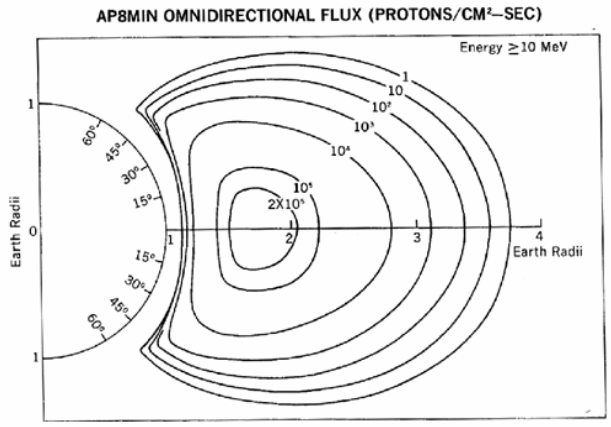

Figure 13 – Radiation belt proton fluxes (AP8).

Though traditionally the radiation belts are thought to be comprised mostly of high energy protons and electrons, antiparticles which are otherwise identical aside from their charge, can also be similarly trapped provided there is an appropriate internal source mechanism. The pair production mechanism described in equation (2) can act as such a source to populate the belt with antiprotons either directly or through antineutron decay. Given the fact that the AP8 radiation model predicts about 2.5 kg (E > 1 MeV) of protons and about 9 grams of electrons (E > 100 keV), it would appear that a large quantity of antiparticles are available for 'mining' assuming the ratio of antiparticles to particles is similar to the GCR flux impinging on the Earth. Discovering the fundamental truth of this statement is the primary motivation of this study.

CONCEPT VISION

A fundamental challenge still exists before trapped magnetospheric antiparticles can be utilized for space propulsion. Though the density is higher than background levels, the particles contained within the magnetic field are still extremely tenuous and must be concentrated in order to extract them efficiently. In 1960, Robert W. Bussard proposed using a magnetic scoop to collect proton fuel during an interstellar flight [25]. Calculations showed that a 10,000 km² intake area could provide 1g acceleration up to relativistic velocities. Subsequent papers by Fishback [26] and Martin [27] refined the performance based on improved assumptions and physical limitations. The fundamental problem limiting this technology is the inability to create a sustained fusion reaction using the interstellar flux without slowing the forward momentum of the vehicle.

Here we propose to use a Bussard type scoop placed in an equatorial orbit to concentrate the magnetospheric antimatter for collection. In fact, antimatter collection by interstellar scoops was recently proposed by Semay and Silvestre-Brac [28] to improve the performance of interstellar ram jets. The limitations of an interstellar jet are not relevant to planetary based antiparticle extraction since the purpose is not to accelerate the vehicle or to directly induce a fusion reaction.

A magnetic scoop placed along the equatorial plane in the inner belt with an apogee of about 3500 km and a perigee of approximately 1500 km, will encounter nearly the entire flux of the antiproton belt after repeated orbits. The vehicle motion of the interstellar ram jet is replaced by the relative motion of the particles bouncing between mirror points in both hemispheres. Thus, this configuration enables antiparticles to be extracted from the radiation belts for eventual practical use in spacecraft propulsion. Figure 14 shows a concept for a vehicle which provides such functionality.

Figure 14 – Artist's concept of proposed system implementation in orbit.

A large ring current flowing in a high temperature superconductor coil induces a large magnetic dipole moment. The resulting field, superimposed over existing natural fields, can influence the trajectory of charged particles in the spacecraft's vicinity. The particles will follow the field lines where they are concentrated as they approach the 'throat' of the collection system. The study of the efficiency of this process is the second major focus of this study. Interestingly, this same field can act as a mini-magnetosphere similar to the Earth's radiation belts. Degrading the energy of the particle and using electric and/or RF fields to transfer the particle to closed field lines while near the throat, introduces a mechanism where particles can be stably trapped and stored with relatively low loss rates.

Once trapped in the artificial magnetosphere surrounding the spacecraft, the antiprotons stored in the field can be directed to react with material near the throat to catalyze a nuclear reaction which subsequently produces ejecta which can be used to propel the vehicle with high efficiency. In this scenario, the magnetic field is also used to direct the trajectory of the ejecta debris and therefore acts as a magnetic nozzle. Finally, this same field acts as a radiation shield to protect equipment (and possibly astronauts) within the center region. Therefore the magnetic field acts as a multi-functional device. The functionality provided is:

- Antiparticle collection system
- Stable antiparticle fuel storage
- Nozzle and propulsion system
- Radiation shield

BACKGROUND SUMMARY

This program has the grand vision to provide the enabling technology for very high performance space propulsion. Here we outline the fundamental advantages and problems of antimatter propulsion and present a concept for a system which addresses these issues. The key points are:

- Antimatter has an energy density more than ten orders of magnitude higher than the best chemical propellants currently used in rocket systems.
    - Very small quantities (nanograms to micrograms) of antiprotons can be used to catalyze nuclear reactions and enable very aggressive interplanetary or pre-cursor interstellar exploration not possible with conventional systems.
    - Antimatter also offers revolutionary potential in a variety of other Earth based applications including sensing, medical treatment, and basic science research.
- The fundamental stumbling block preventing the realization of this potential is the extreme difficulty (and cost) associated with manufacturing and then storing the antiprotons for extended periods of time.
    - Particle accelerator production currently is limited to a few nanograms per year worldwide and is mostly dedicated to science research.
    - The cost of production is estimated to be upwards of $160 trillion per gram.
    - The current state of the art antiproton storage systems can only trap femtograms of antiprotons for days to weeks at a time. It is unclear if it is possible or how efficiently this could be scaled up to the levels needed for space propulsion. The specific mass of the current systems is more than a billion kilograms per microgram stored which implies limited feasibility for transporting the devices to orbit.
- In contrast, high energy cosmic rays which originate from outside our solar system constantly generate antiprotons when their kinetic energy is converted to mass during high energy collisions with other particles.
    - Interactions in the interstellar medium create a low flux source of antiprotons that continuously impinges on planetary magnetospheres.
    - The interaction of cosmic rays with the atmosphere of a planet, or other targets such as rings, can create natural supplies of antiprotons that become trapped in the radiation belts surrounding the planet.
- A large dipole magnetic field can be advantageously applied to collect the concentrated antiprotons from their natural environment offering the potential for a nearly limitless supply of antiprotons without the difficulties of Earth based production and storage.
    - A spacecraft surrounded by a ring of superconducting wire can be used to induce the required magnetic field for the scoop.
    - The mini-magnetosphere generated around the spacecraft can also be used to store the antiprotons for later use.
    - The magnetic field also offers an intrinsic shield against space radiation and can possibly be applied to assist in the propulsion system by directing the charged particle sources and thrust.

PRODUCTION MECHANISMS FOR THE EARTH'S PROTON BELT

A clear understanding of how the proton radiation belt is formed is helpful when studying the generation of its antimatter counterpart. There are two fundamentally different sources of protons which primarily populate the proton radiation belt. The first is Cosmic Ray Albedo Neutron Decay (CRAND) which is the primary source function for the high energy proton population. The second source is the diffusion of protons from an external source, namely the Sun. This external diffusion process primarily serves to populate the low energy portion of the belts, especially at higher L shells.

Ifedili [29] reviews the CRAND process. Figure 15 shows the fundamental nature of the CRAND process. The mechanism is driven by high energy cosmic rays that strike the upper atmosphere of the Earth which induce nuclear reactions in atmospheric nuclei. Many particles are generated some of which are free neutrons following trajectories which leave the atmosphere. The estimated flux of these 'albedo' neutrons are shown in Figure 16 based on a slab model simulation of nuclear transport within the Earth's atmosphere. The majority of the albedo neutrons are formed below 10 MeV due to the physics of the spallation process.

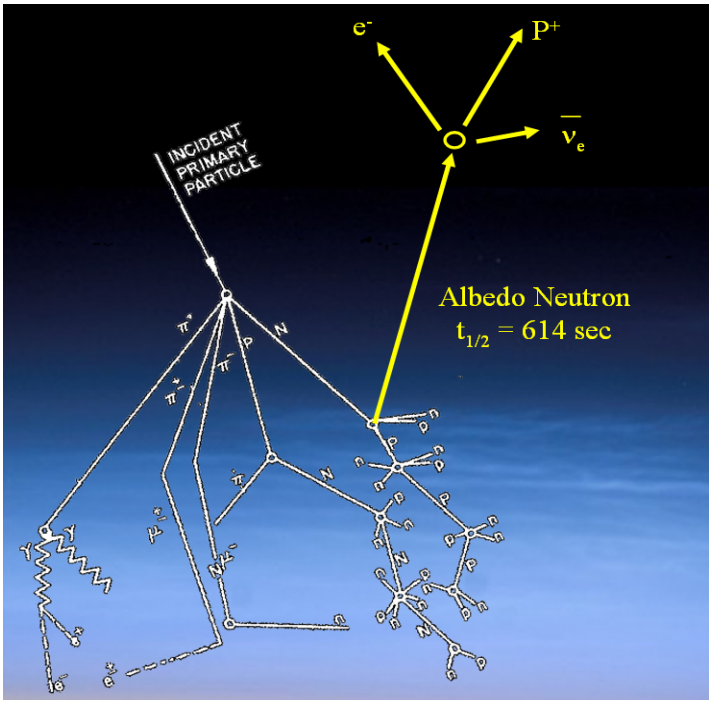

Figure 15 – Cosmic Ray Albedo Neutron Decay (CRAND)

Though neutrons are stable when bound in nuclei, they decay into an electron, proton, and anti-neutrino in their free state with a half life of just over 10 minutes. Though the majority of neutrons will be absorbed by the atmosphere or pass outside the influence of the Earth before decaying, a small fraction of the particles will decay while inside the magnetosphere. If the ejected proton is properly oriented with a velocity vector outside the loss cone for a particle at that energy and location, it will be stably trapped within the radiation belt. Neutrons which originate from the Sun can also decay in the magnetosphere, though this process (SPAND) is much less effective at populating the belts.

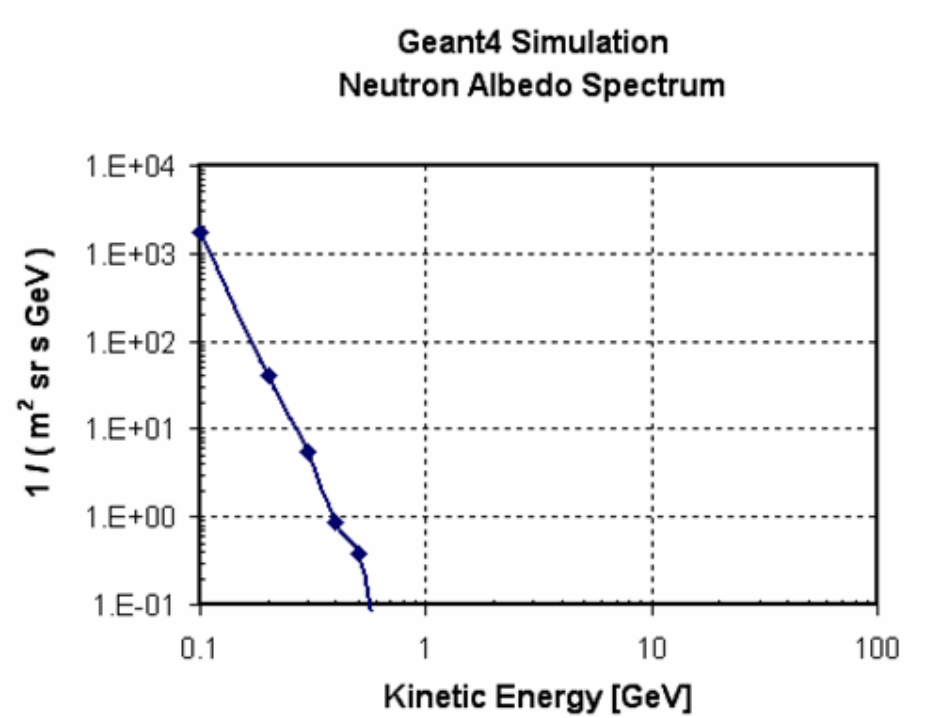

Figure 16 - Neutron Albedo Spectrum. (Earth)

Protons which originate outside of the magnetosphere can also make there way into the stable trapping regions of the radiation belts after interacting with the magnetic field of the planet. The field, which is itself fluctuating due to interactions with the solar wind, allows the protons to radially diffuse to low L shells. The contribution of this effect relative to the CRAND source is described by a semi-analytical model proposed by Jentsch [30]. Figure 17 shows the relative contribution of the different sources. The diffusive source is especially important at lower energies and higher L shells.

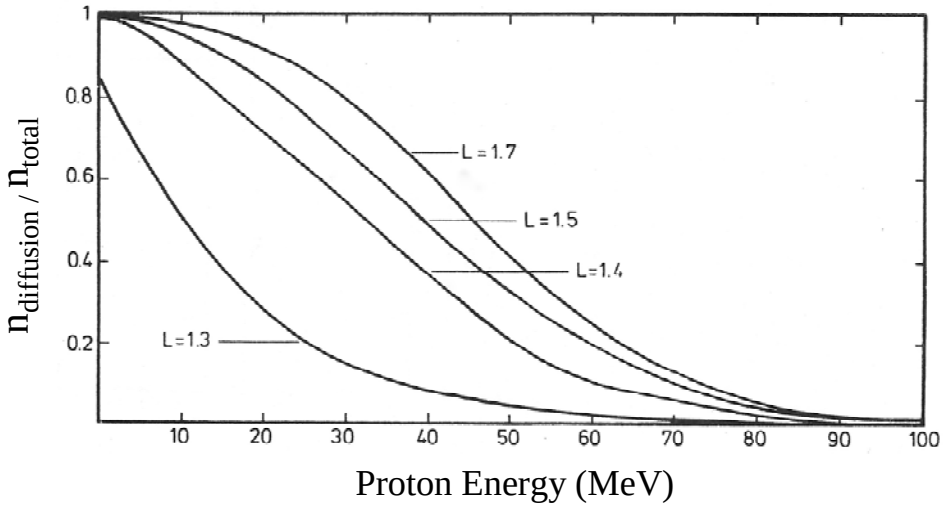

Figure 17 – Relative contribution of external and CRAND proton sources (Jentsch model).

PBAR AND NBAR SOURCE FUNCTIONS

We can now compare the source rate of antiparticles relative to their standard matter counterparts. The most energetic processes in the Sun are not sufficient for proton/antiproton or neutron/antineutron pairs to be created. Therefore, antiprotons will not be present in the solar wind which impinges on the Earth's magnetosphere, eliminating the external source as a possible way to populate the antiproton radiation belt. However, the galactic cosmic ray flux impinging on the atmosphere is energetic enough for pair production to occur. Geant4 is a toolkit for the simulation for the passage of particles through matter [31] which can be used to model these interactions. Figure 18 shows the estimated flux of antineutrons generated in the atmosphere of the Earth calculated by impinging the GCR proton spectrum on a Geant slab model of the atmosphere. The antineutrons will decay into a positron, antiproton, and neutrino with a half life of just over 10 minutes. The antineutrons which decay within the magnetosphere will act as a source function for the antiproton radiation belt.

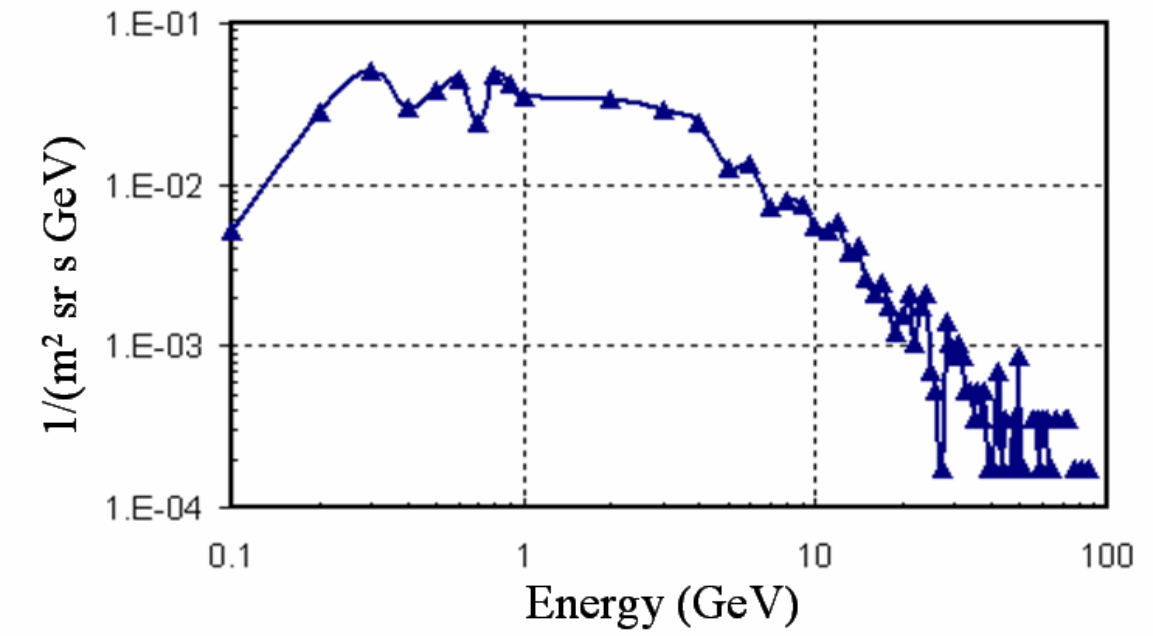

Figure 18 – Antineutron Atmospheric Production Spectrum.

The antineutron spectrum is substantial but unfortunately the particles are produced along a narrow corridor which approximates the original path of the impinging cosmic ray. Figure 19 shows the angular distribution relative to the generating particle as calculated by the software code Geant4. The majority of the antineutrons lie within a narrow 10 degree cone which means that most of the anti-neutrons will be at high energy on a downward trajectory away from the magnetosphere.

The antineutrons must go through a second scattering process with the atmosphere in order to reduce their energy and then traverse and decay within the magnetosphere. This secondary scattering process is far less efficient at generating albedo antineutrons relative to the spallation processes that is the source of the albedo neutrons. Pugacheva et al. [32], calculated the relative efficiency of albedo antineutron production at 1 part in about 10^9 at an energy of 100 MeV based on analytical relationships. Figure 20 shows preliminary calculations of the resulting albedo antineutron flux based on Geant4 simulations. Comparing the plot to Figure 16, we calculated the efficiency to be an energy dependent value which varies between ~1:10^5 and ~1:10^8 with an average generation efficiency of about 1:10^7 relative to the CRAND source.

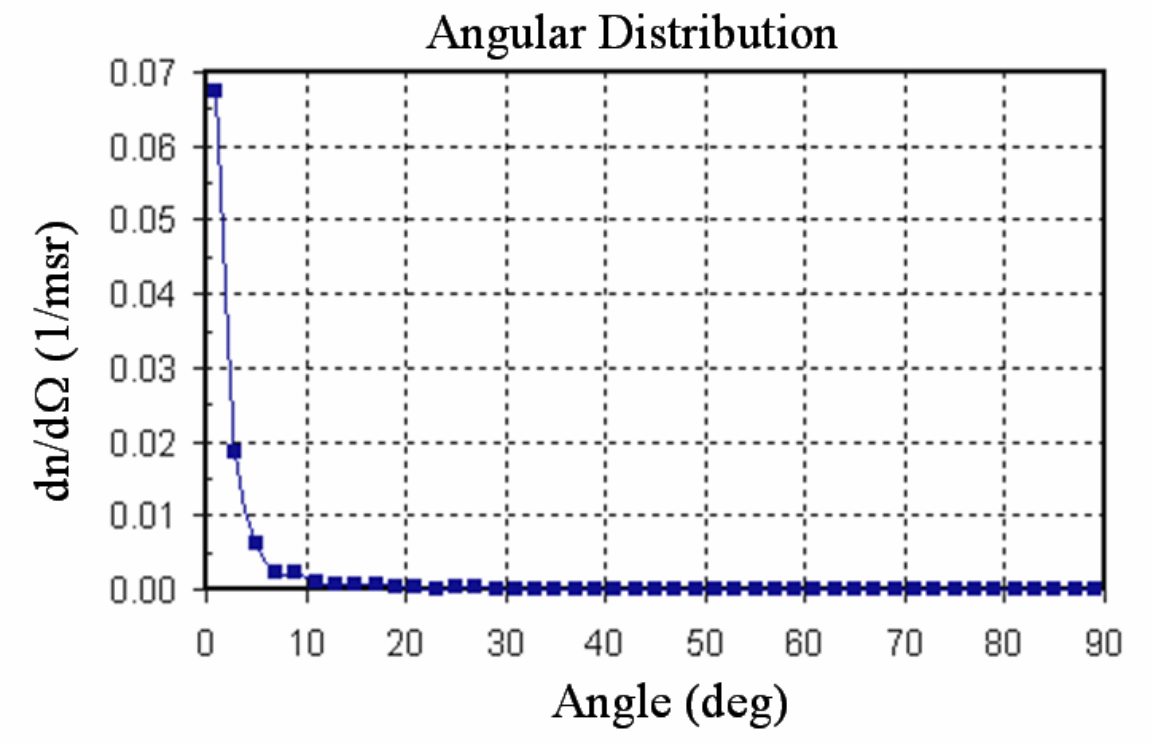

Figure 19 – Angular distribution of pair produced antineutrons.

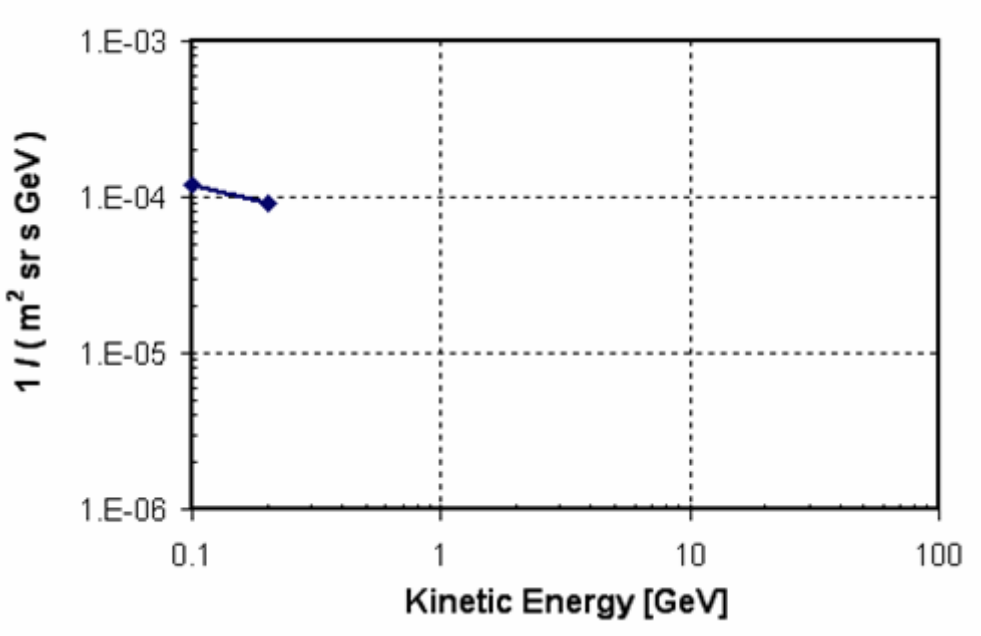

Figure 20 – Antineutron Albedo Spectrum.

Antiprotons can also be directly generated via pair production in the exosphere. This has been studied previously in several papers. [32, 33, 34, 35] Figure 21 shows the predicted production spectrum of antiprotons in the exosphere normalized to the density of the atmosphere based on Geant4 simulations. There is a careful balance here since production at lower altitudes results in much higher fluxes but also in much higher loss rates due to interactions with the upper atmosphere.

Unlike the antineutron decay process, antiprotons are trapped on the L shell where they are initially pair produced since their charge prevents them from freely traversing the magnetosphere to a higher L shell.

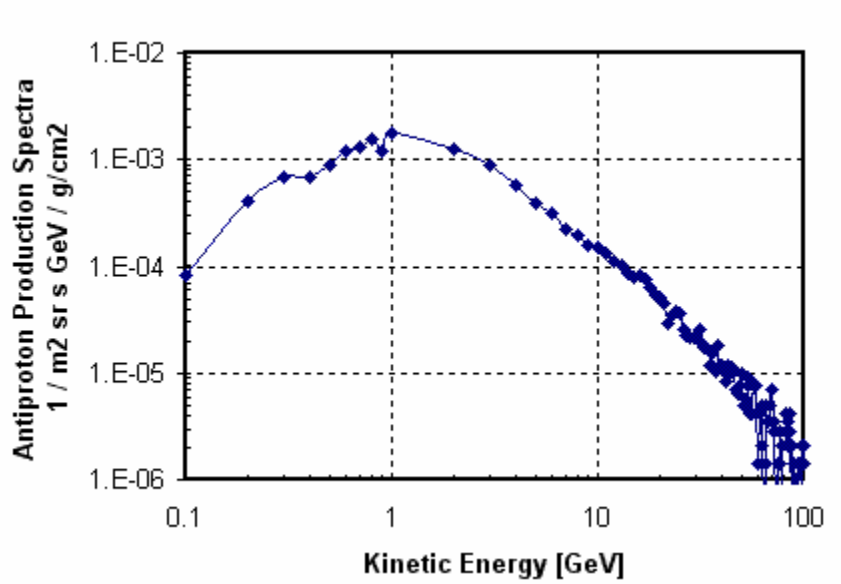

Figure 21 – Antiproton Production Spectrum in the Earth's Exosphere at L=1.2.

ANTIPROTON BELT FLUXES AND INTEGRATED MASS

The fluxes and integrated mass of antiprotons produced locally from these two sources and trapped within the magnetosphere can be estimated from the above data to determine its ultimate utility to spacecraft propulsion. Figure 22 shows the predicted fluxes from the CRANbarD source (antineutron decay). The curves were derived by starting with the AP8 radiation model to determine the total flux of protons and then using the Jentsch model (Figure 17) to subtract the protons that originated externally and diffused inward. The antiproton curve was then estimated by multiplying these fluxes by the ratio of albedo antineutrons to albedo neutrons. The plot shown conservatively assumes a constant ratio based on the estimates posed by Pugacheva et al. [32] Subsequent Geant4 simulations suggest this may be too conservative by several orders of magnitude. A more detailed analysis based on solving equation (9) should be completed to more accurately determine the true flux.

Figure 23 shows the estimated trapped antiproton fluxes from direct pair production in the exosphere. The values from an analysis by Spjeldvik et al. [35] show that the peak production location is at L=1.2. At lower altitudes, the generation of antiprotons increase but this is outweighed by their short lifetimes due to interactions with the upper atmosphere. At higher altitudes, the loss rates are substantially lower though there is insufficient material available to produce a substantial primary flux of antiprotons. The balance between these two effects produces the maximum flux at L=1.2 which then radially diffuses inwards and outwards due to fluctuations in the global magnetic field. It should be noted that the energy spectrum is shifted to considerably higher energies relative to the CRANbarD derived source. This likely will reduce the observed fluxes due to direct pair production of antiprotons since long term stability is limited for such high energy particles.

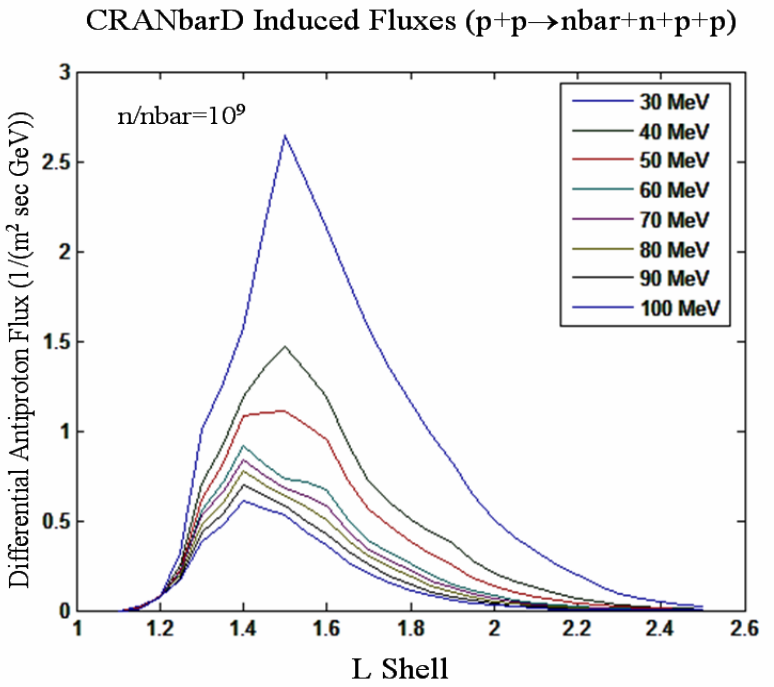

Figure 22 – Predicted antiproton fluxes originating from the CRANbarD source.

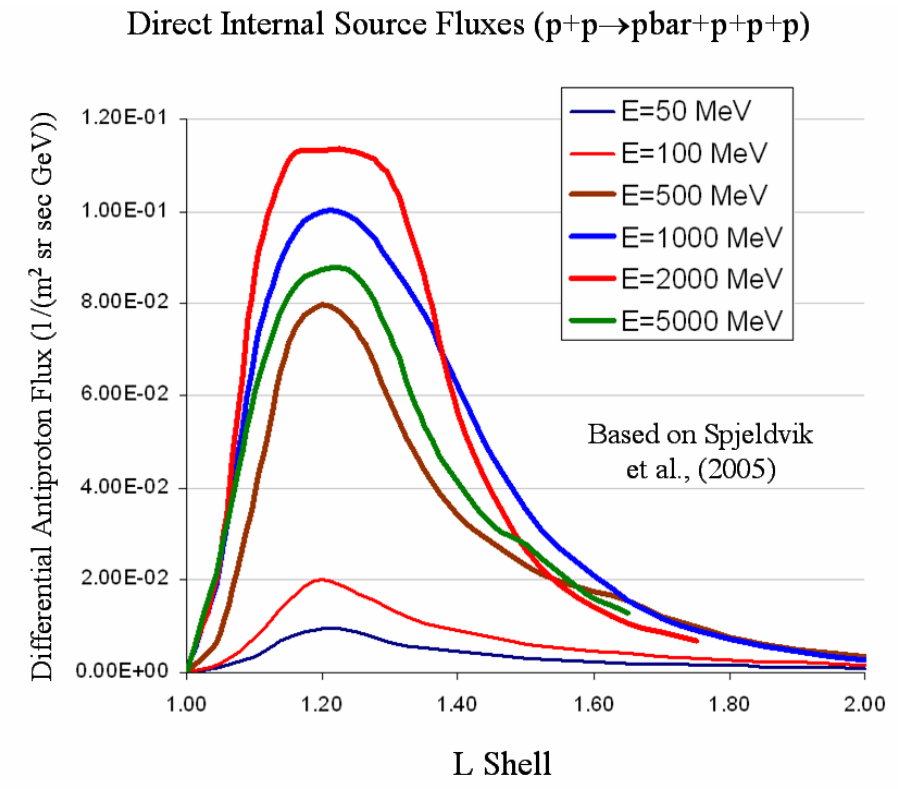

Figure 23 – Predicted antiproton fluxes from direct pair production.

By integrating through phase space, the total number of trapped antiprotons per L shell can be estimated. Figure 24 shows the total mass estimates following integration. The quasi steady state local supply of antiprotons from the direct pair production source is probably 0.1 nanograms or less with a peak about L=1.25. Instabilities in trapping may reduce this value further. In contrast, the antineutron decay source supply is conservatively estimated at 0.15 nanograms with a peak around L=1.9. Preliminary results from subsequent analyses have shown that this value may be up to two orders of magnitude higher which would imply a total supply of 15 nanograms or more trapped around the Earth.

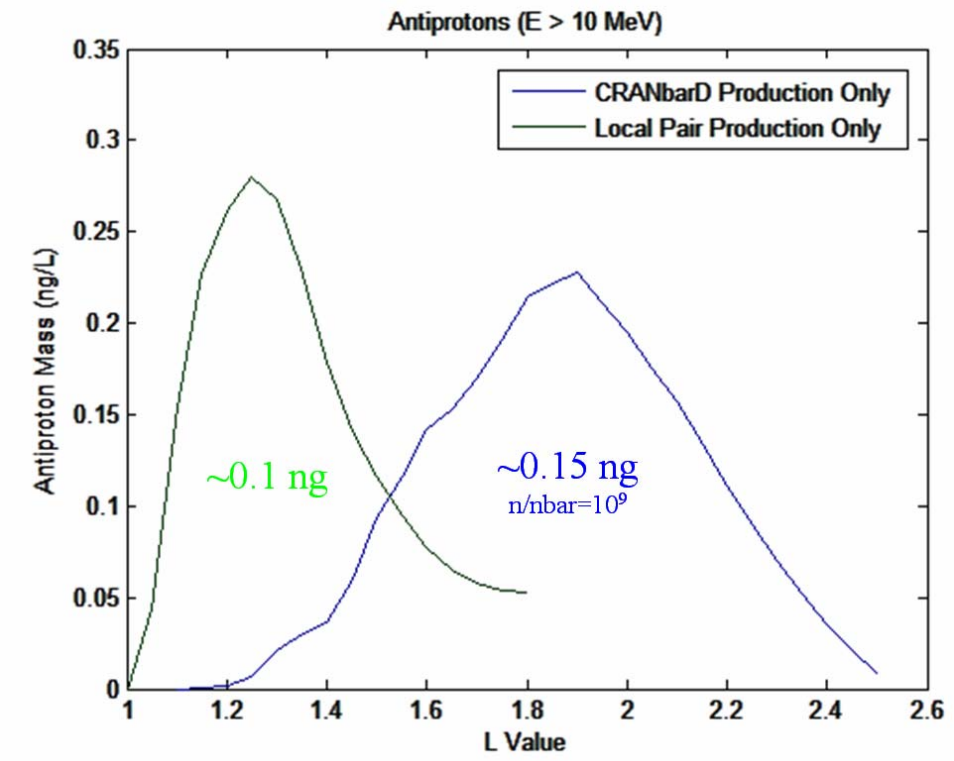

Figure 24 – Integrated mass estimates based on conservative antiproton fluxes estimates.

This predicted number of trapped antiprotons around the Earth is considerably lower than the initial estimates based on the GCR spectrum. The antineutron decay mechanism which primarily populates the belt is much less efficient than the standard CRAND source due to inefficiencies in the backscattering of antineutrons. Despite this, stable trapped antiparticle populations are predicted to exist in the magnetosphere of Earth (and other planets). A more detailed investigation will be needed to precisely determine the true fluxes and mass. For instance, the contribution of antineutrons produced at oblique angles to the atmosphere may substantially increase the overall flux since the antineutrons do not need to be fully backscattered to decay within the magnetosphere.

LOSS AND REPLENISHMENT RATES

Unfortunately the total mass of antiprotons predicted to be trapped around the Earth is relatively low. However, the question remains, how quickly is the supply replenished? Figure 25 shows the timescale of the relevant antiproton loss and transport processes operating in the magnetosphere. The two true loss mechanisms are from inelastic collisions with the atmosphere (annihilation) and instabilities at higher L shells (Appendix E). Coulomb losses are not true losses per se but instead degrade the energy of the trapped antiproton population. Radial diffusion is also not a true loss mechanism, but rather transports the particles to regions where annihilation or instability losses are

more likely to occur. Protons also experience losses due to charge exchange though this is not a relevant loss mechanism for antiprotons since there are no neutral anti-atoms in the atmosphere for the exchange to occur with.

The plot shows the annihilation loss timescale (time until 1/e of the flux is lost) as a function of the magnetic L shell (altitude) for particles with an equatorial pitch angle near 90 degrees. Particles with smaller pitch angles will be lost somewhat faster due to the higher loss rates when mirroring at lower altitudes. The particles are transported via radial diffusion in the magnetosphere. This is largely independent of particle energy, but is influenced by the severity of the ambient field fluctuations which is related to the level of solar activity. The timescale shown is the ensemble-average of the timescale for the particles to be transported a distance of $(\Delta L)^2$.

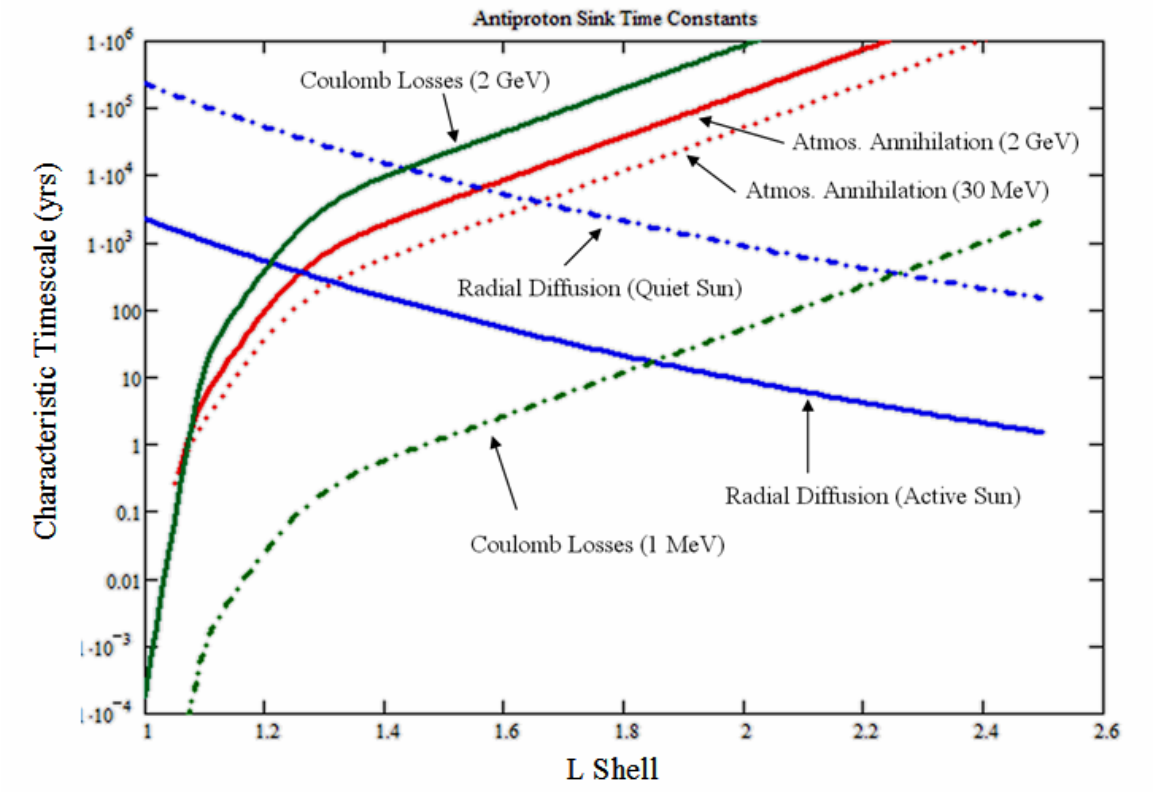

Figure 25 – Characteristic loss and transport timescale for antiprotons in the magnetosphere.

When combined with the Fokker-Planck equation, the overall replenishment rate is similar to that experienced by the proton belt where the timescale is measured to be on the order of a few years or less though the exact value is dependent upon the initial L shell where the antiproton is initially formed. However, this rate still yields an overall antiproton supply that is a few nanograms per year at best, and possibly less depending upon the exact fluxes generated via the various sources. Therefore, the Earth's natural antiproton supply does not appear to be as abundant as originally hoped. However, the levels predicted are still of significant practical interest and additional simulations may show that other sources, such as oblique angle atmospheric generation, may yield much larger total supplies than current estimates may imply.

SUMMARY OF IN SITU TRAPPING IN THE EARTH'S MAGNETOSPHERE

Analysis of the source and loss mechanisms for antiprotons in the Earth's magnetosphere yielded predictions for antiproton fluxes and replenishment rates. The following are the key points:

- Trapped antiprotons come from two primary sources which both originate from high energy galactic cosmic rays interacting with the upper atmosphere.
    - Pair produced anti-neutrons in the atmosphere are subsequently backscattered and decay into antiprotons while in the magnetosphere. (CRANbarD)
    - Antiprotons are directly generated via pair production in the exosphere with a peak at an altitude of about 1200 km (L=1.2).
- The total steady state trapped supply is estimated to be between 0.25 and 15 nanograms based on preliminary calculations.
    - The low end estimates for the total supply are not practical and the high end estimates are marginal for space propulsion applications.
    - This is much less than originally predicted due to the high energies and narrow angular distribution of the pair produced antineutrons.
    - Inefficiencies in the backscatter process reduce the magnitude of the albedo antineutron flux to be less efficient than the analogous neutron process by 1 part in 10^5 to 10^9.
    - The generation of antineutrons generated by cosmic rays striking the atmosphere at a narrow slant angle is not included in these estimates. Since these antineutrons do not need to be backscattered to enter the magnetosphere trapping region, this could represent a significant additional source of antiprotons.
    - We have conservatively assumed the 0.25 nanogram worst case prediction for all remaining calculations including extrapolations to the outer planets.
- The overall replenishment rate timescale is on the order of several years.

CHAPTER 4 – JOVIAN EXTRAPOLATIONS

The outer gaseous planets in our solar system are larger in size than the Earth and also have significantly stronger magnetic fields. Table 2 lists the selected parameters for the planets which have substantial magnetic fields. The Jovian planets have magnetic fields which are much stronger than those of the rocky planets. For instance, the dipole moment of Jupiter is nearly 20,000 times larger than Earth's. Measured radiation fluxes from robotic spacecraft significantly exceed those measured in the Earth's radiation belts. [36,37] Dessler [38] provides a detailed survey of the Jupiter environment and the models which describe it. One can therefore extrapolate and assume that these planets will also have much higher antiproton fluxes and total integrated mass. In this section, we will explore the relative differences between the production mechanisms which form the antiproton belts and develop scaling relationships to allow us to estimate the antiproton content of the Jovian planets.

Planet	Dipole Moment	Radius
Earth	7.9×10^{25} gauss cm^3	6378 km
Jupiter	1.5×10^{30} gauss cm^3	71492 km
Saturn	4.3×10^{28} gauss cm^3	60268 km
Uranus	3.8×10^{27} gauss cm^3	25559 km
Neptune	2×10^{27} gauss cm^3	24764 km

Table 2 – Radius and magnetic field parameters for selected planets.

The Jovian planets offer a significantly different environment for the production and loss of antiprotons relative to the region around Earth. Like Earth, antiprotons will be lost to the residual atmosphere, but the Jovian planets can also have moons, rings, gases, and dust within the trapping region which can absorb the antiproton flux. However, these same factors can sometimes improve the efficiency of the antiproton generation process. Together with the larger dipole moment and increased radius, there are numerous reasons why the source function from equation (9) will increase beyond the Earth's to yield a greater number of total antiprotons trapped in the planet's magnetosphere. Five such effects are outlined below. The first three sources (S1-S3) represent improvements in the CRANbarD process relative to Earth. The fourth source (S4) is unique to the Jovian planets which involves the generation of particles via interactions of the GCR with rings and other material near the planet. Finally the source S5 represents improvements in the direct pair production of antiprotons in the exosphere relative to Earth. Admittedly, the scaling is crude but it does provide insight into the most important mechanisms and natural antiproton sources in our solar system.

LOSS CONE REDUCTION (S1)

Stronger magnetic fields can increase the antineutron decay acceptance cone. Therefore, a larger percentage of the antineutrons that decay within the magnetosphere will be trapped. The improvement relative to the Earth can be given approximately as,

$$(S_{p1}/S_{earth}) \approx (\pi/2-\alpha_{pLC})/(\pi/2-\alpha_{earthLC}) \qquad \textit{Equation 10}$$

where α_{LC} is the loss cone angle for the planet (p) relative to Earth. This is likely to be a relatively minor effect.

TIME OF FLIGHT INCREASE (S2)

The magnetosphere of the Earth extends out to approximately 10 Earth radii. In comparison, a 10 MeV antineutron will travel greater than 4000 Earth radii over a time period equivalent to its half life. Therefore, only a very small fraction of the antineutrons will decay while within the trapping region of the planet. However, a greater percentage of the particles decay when path lengths (and flight times) are longer. Planets with larger magnetic fields (and thus trapping regions) will capture a larger fraction of the decay products.

The size of the trapping region can be estimated by comparing the particle gyro radius to the radius of curvature of the field lines. Increasing the radius of curvature for the same field strength enables trapping over wider regions. The magnetic field at a distance x from the planet is proportional to,

$$B \propto \frac{M}{x^3} \qquad \textit{Equation 11}$$

where M is dipole moment of the planet. The maximum distance for stable trapping at a given energy (Larmor limits) can be given as the point where the gyro radius is equal to no more than 10% the radius of curvature. (See Appendix E) The radius of curvature is approximately $x_{eq}/3$ so therefore,

$$\frac{x}{3} > 10\frac{p}{Bq} \rightarrow x^2 < \frac{Mq}{30p} \rightarrow x_{\max} \propto \sqrt{M} \qquad \textit{Equation 12}$$

Since the time of flight is related to the distance (d=vt), the maximum flight time in a planetary magnetosphere is proportional to the square root of the planet's magnetic dipole moment. Relating this to flight times in the Earth's magnetosphere gives,

$$\frac{flighttime_p}{flighttime_{Earth}} = \sqrt{\frac{M_p}{M_{Earth}}} \qquad \textit{Equation 13}$$

The number of neutrons that have decayed in the planet's rest frame after a time t is,

$$\frac{N_{decayed}}{N_0} = 1 - e^{-\lambda_{decay} t} \qquad \textit{Equation 14}$$

where λ_{decay} is the neutron's relativistic decay time constant ($\ln(2)/\tau_{1/2}$). When $t << \tau_{1/2}$ the number of particles that decay within a planet's magnetosphere relative to the number at Earth can be simplified to,

$$\frac{N_1}{N_2} \approx \frac{t_1}{t_2} \rightarrow \frac{S_{p2}}{S_{Earth}} \approx \sqrt{\frac{M_p}{M_{Earth}}} \qquad \textit{Equation 15}$$

.

Note that this expression is energy independent. Therefore, planets with stronger magnetic fields can trap a greater number of decay products from albedo antineutrons since the longer transit times enable a larger percentage of them to decay while within the trapping region. This becomes non-linear and breaks down as the flight time approaches the particle's relativistic half life, but offers a realistic scaling factor for the Jovian planets. This is a relatively major effect with the Jupiter source being two orders of magnitude more efficient relative to Earth.

INCREASE IN ANTINEUTRON ATMOSPHERIC PRODUCTION AREA (S3)

Antineutron pair production in the atmosphere increases with the available production area. Therefore, larger planets offer more atmospheric material (surface area) for the antineutron production to occur over. However, due to cutoff limitations, some portion of the source spectrum (GCR) may not strike the atmosphere, thus reducing the production rate. Appendix D shows the classic forbidden region due to rigidity cutoff limitations. This is primarily an issue near Jupiter where much of the production spectrum is cutoff below latitude of about 60 degrees. The overall effect scales approximately as,

$$S_{p3}/S_{earth} \approx (r_p^2/r_{earth}^2)(\lambda_{earthcut}/\lambda_{pcut}) \qquad \textit{Equation 16}$$

where r is the radius of the planet, and $\lambda_{\_cut}$ is the average cutoff latitude for the weighted production spectrum. This can be a relatively major effect, especially at Saturn where the surface area of the planet is almost two orders of magnitude larger than Earth.

ADDITIONAL ANTINEUTRON PRODUCTION TARGETS (S4)

The Jovian planets also have additional targets for pair production via interactions with the impinging GCR source. Examples of additional targets include rings, belts, moons, and gaseous concentrations. In particular the rings of Saturn and the Io gas torus surrounding Jupiter are enticing targets. There are no analogous generation sources around the Earth.

The production efficiency of antiprotons generated via antineutron decay is increased since the antineutrons produced in the belts (~Saturn) or dusty/gaseous regions (~Io Torus) do not need to be backscattered to decay within the belts. The Io torus and dust deposits are not thick enough (g/cm^2) to produce significant antineutron fluxes though the A and B rings of Saturn have nearly the ideal density (5-100 g/cm^2 [39]) for this process to occur.

Antineutrons produced in rings or other structures can directly exit the target and travel into the magnetosphere where the decay products can be trapped. This process is much more efficient than relying on the backscatter of antineutrons in the atmosphere. We can not ratio this effect to Earth since there is no analogous source, but it can be compared to the atmospheric production efficiency (S3). The efficiency improves by the relative path lengths for production (ρ_{atm}/ρ_{ring}), the approximate relative area (A_{ring}/A_p) over which pair production occurs, and the inverse of the antineutron backscatter ratio ($Q_{nbar}/Q_{nbaralb}$) which is calculated from monte carlo nuclear transport simulations (Geant4). The combined expression,

$$S_{p4}/S_{p3} \approx (Q_{nbar}/Q_{nbaralb})(A_{ring}/A_p)(\rho_{atm}/\rho_{ring}) \qquad \textit{Equation 17}$$

provides a very approximate estimate of the relative production efficiency for secondary antiproton generation via antineutron generation in the belts. This is a major effect for Saturn. Antiprotons will also be produced at approximately the same rate though they will be trapped on the same L shell as the production target (rings). Therefore, an antiproton will be quickly reabsorbed by the source that

initially generated it. The relative advantage of the production via antineutron decay is that the neutral antineutrons produced can travel away from the target before decaying.

INCREASE IN ANTIPROTON ATMOSPHERIC PRODUCTION AREA (S5)

The surface area of the outer planets will also help with the direct production of antiprotons which subsequently become trapped. Similar to the antineutron source (S3) this is restricted if the production surface is within the forbidden region for cosmic rays at that energy. Therefore, the generation of antiprotons at Jupiter will be reduced significantly due to rigidity cutoff limitations. Similar to S3, the overall effect scales approximately as,

$$S_{p5}/S_{earth} \approx (r_p^2/r_{earth}^2)(\lambda_{earthcut}/\lambda_{pcut}) \qquad \textit{Equation 18}$$

where the parameters are all equivalent to S3. The exception is S_{earth} which here represents the direct antiproton source at Earth instead of the CRANbarD source. In total, this can be a relatively major effect, especially at Saturn where the surface area of the planet is almost two orders of magnitude larger than Earth.

COMBINED SCALING EFFECTS

The effects of increasing the source function can be estimated by combining the above ratios. The following expression yields the estimated antiproton source relative to that of Earth,

$$S_p \approx (S_{p1}/S_{earth1})\,(S_{p2}/S_{earth2})\,(S_{p3}/S_{earth3})\,(S_{earth1\text{-}3}) + (S_{p4}/S_{earth1\text{-}3}) + (S_{p5}/S_{earth5}). \qquad \textit{Equation 19}$$

The value for $S_{earth1\text{-}3}$ represents the calculated CRANbarD source function while S_{earth5} represents the calculated source function for direct production of antiprotons in the exosphere. Table 3 shows the estimated values for each of the terms. The last column provides an estimate for the total mass of antiprotons trapped in the planet's magnetosphere. This does not include all relevant effects (loss and transport timescales, etc…) so it does not represent a truly complete (and accurate) estimate of the trapped mass. However, it does provide a rough guideline for the relative mass of antiprotons trapped in our Solar System.

	$S_{1\text{-}3}/S_{earth}$	S_1/S_{earth}	S_2/S_{earth}	S_3/S_{earth}	$S_4/S_{1\text{-}3}$	S_5/S_{earth}	Mass
	Nbar Related	*Loss Cone*	*Decay Time*	*Production Area*	*Rings (Nbar)*	*Direct Pbar*	*Trapped Pbar*
Earth	1	1	1	1	0	1	~0.25 ng
Jupiter	> 6 x 10^3	< 1.2	~ 140	~ 45	~ 0	~ 45	~1 μgm
Saturn	> 3 x 10^3	< 1.2	~ 25	~ 90	10^3 (?)	~ 90	~400 μgm
Uranus	> 110	< 1.2	~ 7	~ 15	~ 0	~ 15	~ 18 ng
Neptune	> 75	< 1.2	~ 5	~ 15	~ 0	~ 15	~ 13 ng

Table 3 – Coarse estimates for Jovian source scaling factors.

The limitation of this estimation technique is that is basely solely on extrapolations and coarse estimates for some of the variables. Though the values could easily be off by an order of magnitude or more, the results provide insight into interesting production phenomena within our solar system.

SUMMARY OF JOVIAN SCALING EFFECTS

Extrapolations of the Earth magnetosphere were made to estimate the trapped supply of antiprotons naturally surrounding the Jovian planets. Some of key findings are:

- The rings of Saturn are the largest source of locally generated antiprotons in the solar system. Nearly a half milligram of antiprotons are trapped based on coarse engineering extrapolations.
    - The fluxes are primarily formed by the decay of ring produced antineutrons in the magnetosphere. Antineutrons generated in the A&B rings do not have to be backscattered for trapping which drastically increases the production efficiency.
- Jupiter has a smaller trapped supply of antiprotons than originally anticipated due to the cutoff of the GCR production spectrum by its large magnetic field.
    - Approximately 1 μgm of antiprotons are spread throughout Jupiter's magnetosphere.
- Saturn and Jupiter both have relatively large supplies of antiprotons relative to that needed for selected propulsive concepts which utilize antiprotons to catalyze nuclear reactions. The disadvantage is that a spacecraft must first be sent there to collect the antiparticles.
    - Though Earth has a relatively small antiproton supply in terms of very high delta-v missions, the supply is likely large enough to enable a bootstrap mission where a spacecraft first stops in Earth orbit for a partial 'fuel up' and then travels to Saturn to extract most of the fuel for an interstellar precursor mission.
- The estimates are all based on extrapolations of conservative Earth supply estimates. A complete model of the Jovian radiation belts will be required to more accurately determine the true fluxes and integrated mass.

Positrons have also been suggested as a potential energy storage medium for space propulsion. However, the mass requirements are significantly larger since using them as a nuclear catalyst like antiprotons is not possible. Though their flux is far lower than protons, the galactic cosmic ray spectrum also includes electron and positron constituents. Measurements of the spectrum have also shown that for every 10 electrons there will be 1 positron incident on the atmosphere. Though the relative ratio of positrons to electrons is relatively high, the overall background mass flux is low. However, of more interest are several recent measurements of positrons produced by the Sun as well as trapped positrons measured in low Earth orbit.

LOCAL GENERATION

In 1998, the space shuttle flew the AMS-01 magnetic spectrometer as a precursor to the more permanent AMS-02 experiment which is due to be installed on the international space station. Interestingly, measurements of the positron and electron background showed that there were approximately four times as many positrons as electrons at an altitude of approximately 380 km. [40] A paper by Gusev et al. [41] explained this curious phenomenon as a result of the trapping of pion decay products as the lower portion of the proton radiation belts interacts with the upper atmosphere. This can be expected to yield a stably trapped positron population in low magnetic L shells. Though limited data and simulation results are available, applying this ratio to the AE8 model below L=1.2, implies that a total of 45 ng (E>1 MeV) to 11 μg (E>100 keV) of positrons are trapped in low Earth orbit. The replenishment rate would be high at these altitudes due to the relatively dense atmosphere below L = 1.2.

SOLAR POSITRONS

Recent measurements from RHESSI [42] have shown that positrons can be produced by the Sun under certain conditions. Though even the largest solar flares on the Sun are not energetic enough to produce antiprotons via pair production, the collision of plasma due to solar flares near the surface provides enough energy to produce positron/electron pairs. It was reported that the annihilation of nearly 1kg was observed after a large solar flare which was measured by observing the gamma rays produced during positron/electron annihilations near the Sun. However, it is unclear how many, if any of these positrons, are able to escape the production region without annihilating to travel outwards into the solar system. If we assume the 10% ratio from the GCR flux and apply it to the Earth's electron belt, a total trapped positron content of ~850 mg is predicted. This is probably overly optimistic since a significant outward flux seems unlikely given that one would expect this to be observable in the Earth's electron belt if a significant fraction made its way to Earth. None the less, this is an interesting phenomenon that may be of additional interest.

POSITRON SUMMARY

- Positrons generated as a result of the proton belt interacting with the upper atmosphere produce fluxes where the number of positrons exceeds the number of electrons.
- Solar positrons generated near the surface of the Sun have been experimentally observed. It is unclear how many if any of these make their way to Earth where they can be trapped in the magnetosphere.
- Significant fluxes of positrons may exist, though the exact magnitude is still uncertain. A quasi-static supply < 1 μgm is most likely.

The galactic cosmic ray (GCR) background includes a significant flux (Figure 26) of antiprotons generated by the interaction of particles in the interstellar medium. There is a distinctive peak around a particle energy of 2 GeV. Though still extremely tenuous by the standards of radiation belt fluxes, the antiproton content is significant over large scales. A question persists – how effectively can planetary magnetic fields help concentrate the GCR flux to assist extracting useful quantities of antiprotons from it?

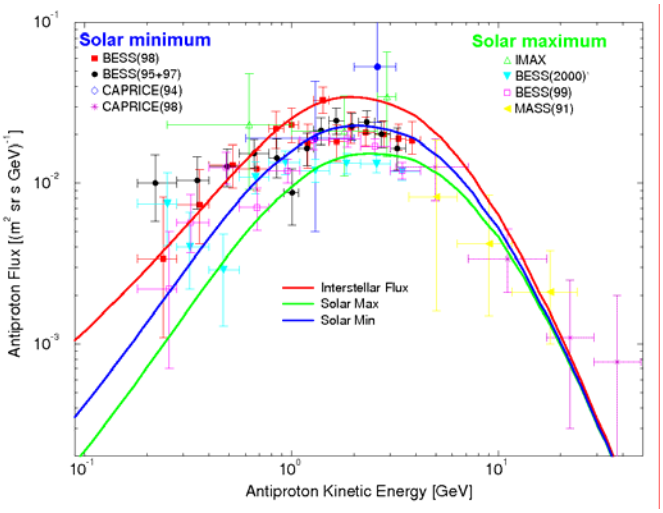

Figure 26 – Measured GCR antiproton flux with theory.

Table 4 shows the yearly impingement of antiprotons on the inner magnetospheres of the listed planets. Here we have defined the size of the magnetosphere to be a sphere with a radius equivalent to the approximate sunward side shock boundary where the magnetic pressure balances the solar wind pressure. [43] Within this volume around the Earth, a modest 4 grams of antiprotons (1 GeV < E < 10 GeV) pass through on a yearly basis. In comparison, the magnetosphere of Jupiter is the largest structure in our solar system and experiences an integrated flux of over 9 kg of antiprotons per year!

Planet	**Standoff Distance** ($2\rho v^2 = B^2/2\mu_0$)	**Antiproton Rate** (1 GeV < E < 10 GeV)	**Yearly Antiproton Impingement** (~inner magnetosphere)
Earth	11 R_{earth}	0.13 μg/sec	0.004 kg
Jupiter	45 $R_{jupiter}$	287 μg/sec	9.1 kg
Saturn	20 R_{saturn}	41 μg/sec	1.3 kg
Uranus	26 R_{uranus}	12 μg/sec	0.39 kg
Neptune	25 $R_{neptune}$	10 μg/sec	0.33 kg

Table 4 – GCR Antiproton Magnetosphere Impingement

A hint of possible concentration factors is given in the original work by Carl Störmer in the first half of the 20th century. [44] Störmer orbits were calculated by manually integrating the forces on a charged particle to determine its trajectory through a simple magnetic field. Störmer identified specific trajectories based on the particle rigidity (momentum relative to charge) and identified the limits of the forbidden regions through which particles of certain energy are not able to pass.

COMPUTATIONAL TECHNIQUE

We wish to study the motion of a charged particle, such as an antiproton, in the presence of magnetic and electric fields which make up the magnetosphere of a planet. The spatial domain has specified magnetic and electric fields which can vary as a function of both position and time. Ultimately, the path of the particle with a given charge (q) and mass (m_0) and an arbitrary set of initial spatial (x_o,y_o,z_o) and velocity conditions (u_o,v_o,w_o) needs to be determined. This simulation of these trajectories can be applied to a large scale Monte Carlo analysis to simulate the interaction of cosmic rays with the Earth's magnetic field.

The equations describing the physics of this motion can be represented with a system of six first order differential equations. The six derivatives of the particle's position,

$$\frac{d\vec{s}}{dt} = \vec{V}, \qquad \textit{Equation 20}$$

and relativistic momentum,

$$\frac{d\vec{p}}{dt} = q\left(\vec{V} \times \vec{B} + \vec{E}\right), \qquad \textit{Equation 21}$$

can be readily solved with a high order Runge-Kutta algorithm. A simulation environment to study the motion of the antiprotons was developed in matlab for this purpose. Though various solvers were evaluated, most simulations used an explicit Runge-Kutta 5th order formulation based on the Dorman-Prince pair [45] or a variable order Adams-Bashforth-Moulton PECE solver [46]. Both provide variable time step capabilities and error tolerance control (Appendix F). The initial models for the planet used a static dipole field model of the magnetosphere with no electric field present. Though the capability exists, higher order terms were not used in the model since the inner field of interest closely approximates an ideal dipole to the level of fidelity required. Figure 27 shows an example trajectory from a single particle simulation.

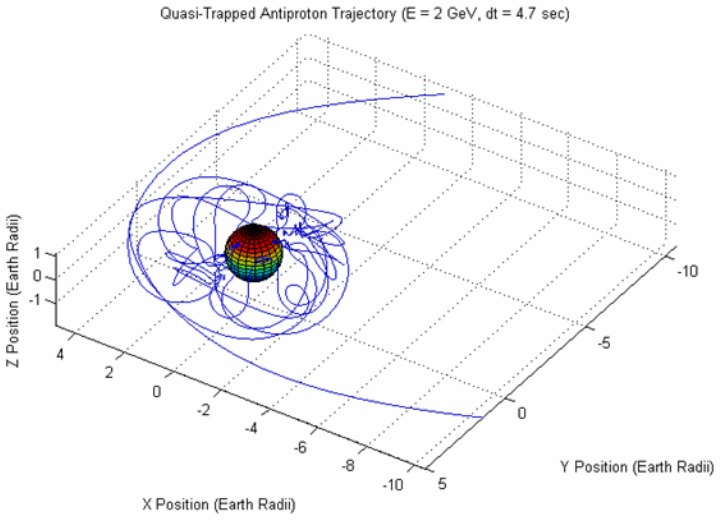

Figure 27 – Example GCR antiproton trajectory around Earth.

Monte Carlo runs for random trajectories (10^5-10^6 total particles) could be easily run over the course of several hours or an evening on a 2.0 GHz multi-CPU desktop machine. The starting conditions consisted of uniformly distributed points on a sphere [47] for position with randomly oriented inward facing vectors for the initial starting velocity. The particles were traced until they struck the atmosphere of the planet ($r=R_{earth}$) or they left the simulation environment ($r > 11\ R_{earth}$ for Earth).

EARTH FLUX

Figure 28 shows the results of simulations based on the Earth's magnetosphere interacting with the GCR antiproton flux for particles with an energy of 2 GeV. The plot of the left shows the locations where particles passed through a plane aligned with the magnetic pole of the planet. The Störmer forbidden region (rigidity cutoff) for particles at this energy can clearly be seen in the graph. The plot on the right shows the predicted fluxes of GCR antiprotons. An increase due to the funneling of charged particles along field lines was observed near the poles. This mechanism provides a flux increase of approximately a half order of magnitude relative to the background GCR flux at 1AU.

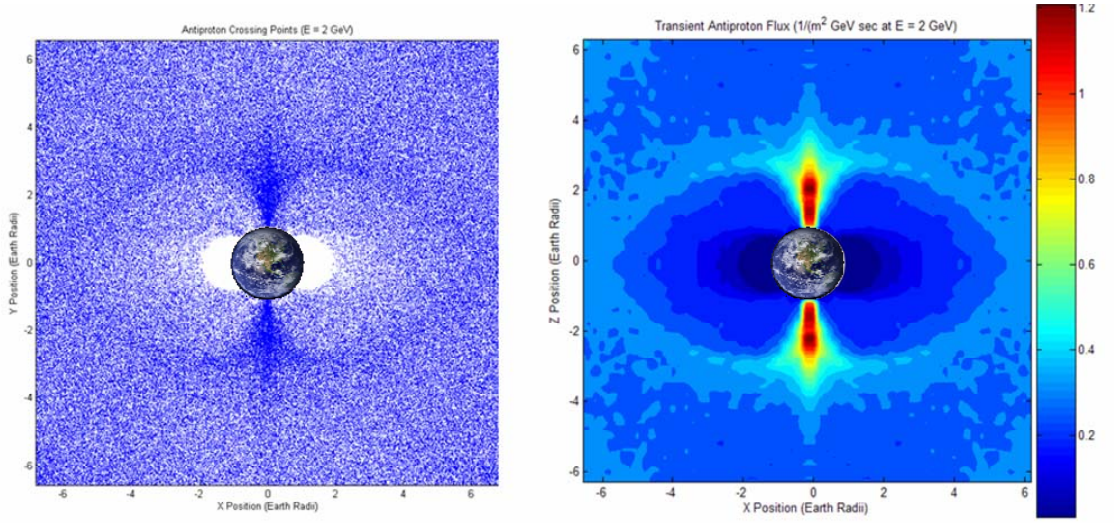

Figure 28 – Predicted antiproton flux in the vicinity of the Earth. (E=2 GeV)

Figure 29 shows the flux for several different particle energies. The magnitude of the flux has been normalized to the background value for that energy level. The peak concentration is approximately a half order of magnitude greater than the background flux and independent of the incident particle energy. However, the spatial extent over which this concentration occurs is dependent upon the particle's rigidity with the high concentration extending over a smaller region for higher energy particles.

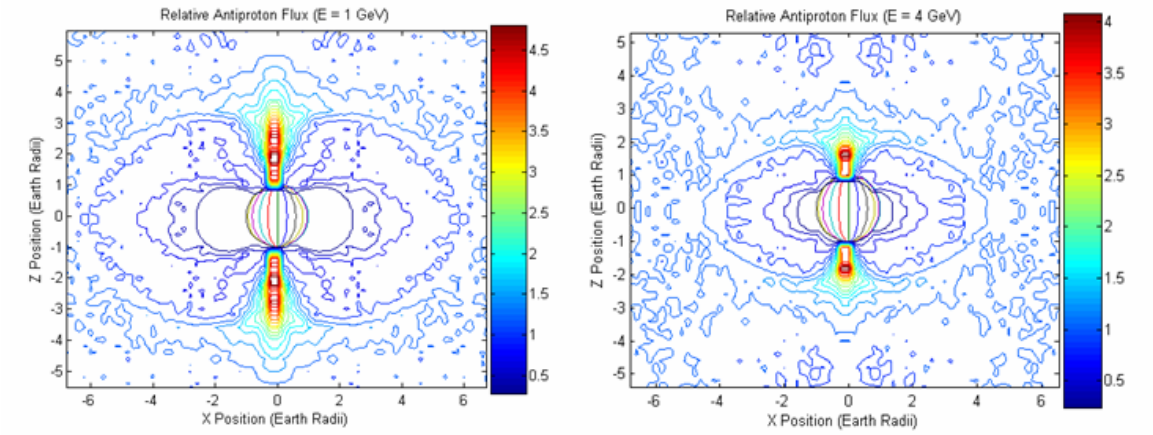

Figure 29 – GCR flux relative to background at 1 GeV and 4 GeV around Earth.

JUPITER FLUX

Figure 30 shows the equivalent flux for the Jupiter system. One should note the spatial scale relative to the Earth simulation since it is normalized by the radius of the planet. The domain shown is therefore about 75 times larger in each direction relative to the Earth plots. The influence of Jupiter's tremendous magnetic field is clearly evident. The Störmer forbidden region extends out to over 20 $R_{jupiter}$ for the 2 GeV particles shown in the plot. The magnetic funnel effect near the magnetic poles is also seen with the maximum flux about one and one half orders of magnitude higher than the background GCR flux.

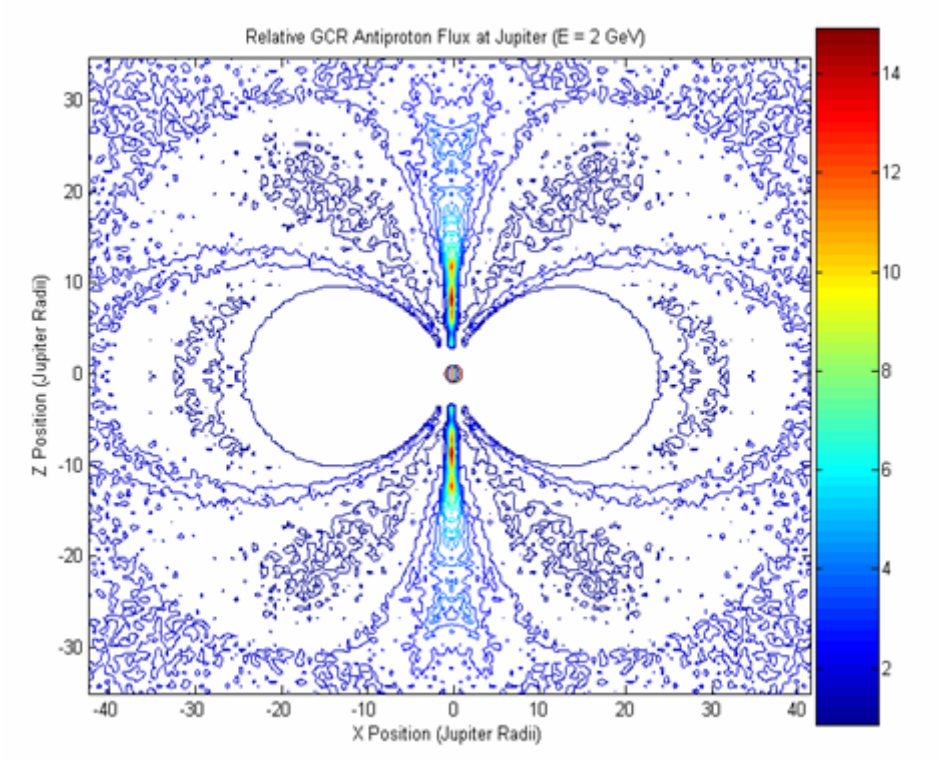

Figure 30 – GCR antiproton flux in the vicinity of Jupiter relative to background (E=2 GeV)

OPTIMAL ORBITS TO MAXIMIZE INTEGRATED FLUX

Utilizing the higher fluxes of antiprotons near the poles to increase the collection rate can be a challenge due to the required orbital dynamics of spacecraft capable of flying through these regions. Orbits that pass through the high flux zones are restricted to high inclination polar orbits. Unfortunately, a large portion of the orbital period will be spent in the near equatorial regions within the forbidden regions where the background flux is low (Figure 31). If significant trapped radiation belts are present in the forbidden regions this scenario may become more advantageous. The electrodynamics of a magnetic scoop operating in such a field would also be an issue since torque would be applied on a spacecraft in a polar orbit.

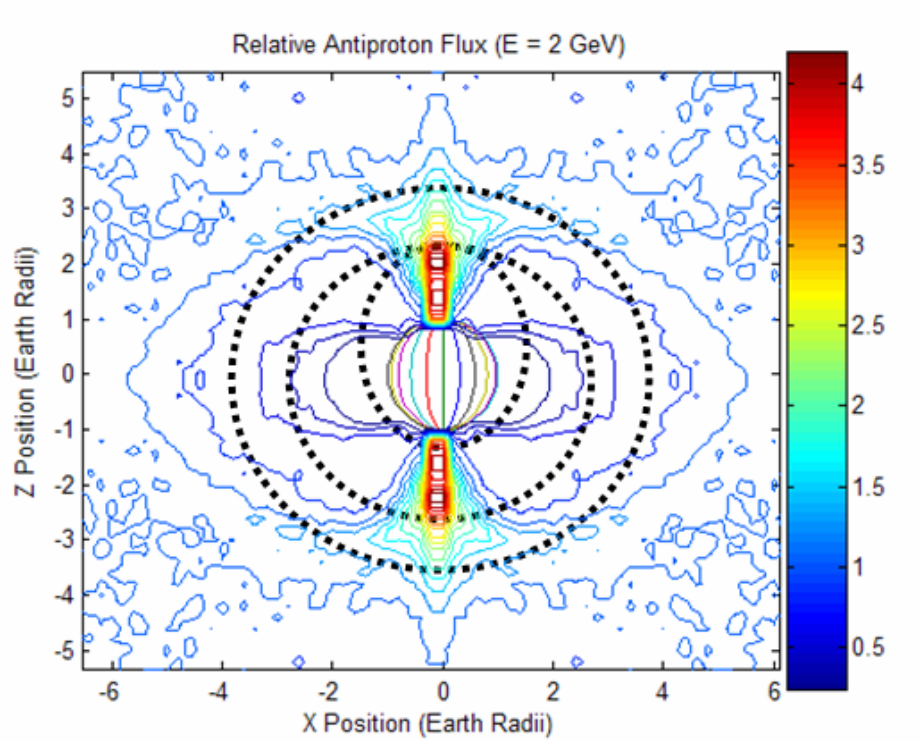

Figure 31 – Example polar orbits overlaid on the 2 GeV antiproton flux map.

Ideally the collection spacecraft should be placed in a near equatorial orbit for optimal stability and maximum integrated flux intensity. This allows the spacecraft to pass through the radiation belts or to extract portions of the GCR spectrum when orbiting beyond the forbidden regions. The magnetic field of the planet can help in the collection process by biasing the pitch angle of the incident particles. Figure 32 shows the pitch angle of GCR 2 GeV antiprotons passing through the equatorial plane. The particles have a tendency to follow field lines as they are deflected by the planet's magnetic field. Therefore the antiprotons are coming from a restricted portion of the sky which can greatly assist when collecting the particles via a magnetic scoop. (Chapter 8)

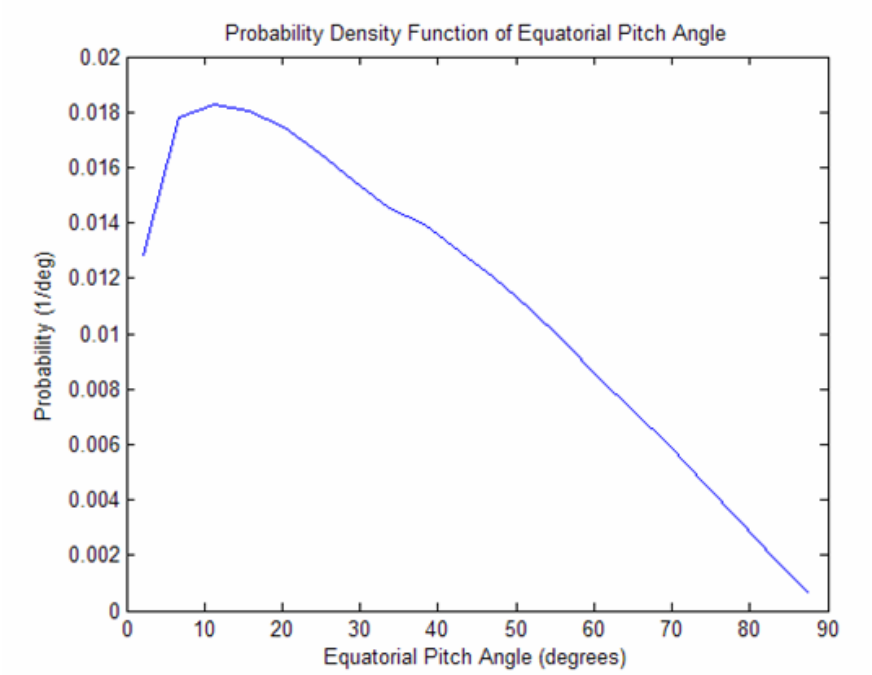

Figure 32 – Equatorial pitch angle of GCR particles near Earth. (E = 2GeV)

SUMMARY OF TRANSIENT GCR FLUX RESULTS

- Simulations of the motion of charged GCR particles traversing a planetary magnetic field were completed to determine the relative level of flux concentration provided by the global field.

- Above the poles of the Earth, the flux was concentrated by approximately a half order of magnitude relative to the GCR background flux.

    - A spacecraft placed in an orbit to take advantage of this would also pass through the forbidden regions during its equatorial pass. This would reduce the total integrated flux unless antiprotons trapped in the radiation belts were present in the equatorial areas.

- Jupiter provides a similar type of flux enhancement with the local flux over the poles approximately one and one half orders of magnitude higher than the background level.

- Transient GCR antiprotons passing the equatorial region are preferentially biased to a relatively narrow and small pitch angle. This could improve collection performance significantly.

Though the original program plan called for focusing exclusively on natural phenomena in planetary magnetic fields, the scope was expanded to survey other potential renewable, high flux sources of antiprotons accessible to spacecraft in our solar system. Several ideas which include extensions of natural phenomena as well as purely artificial means are explored in this section.

INDUCED QUASI-STABLE TRAPPING OF GCR FLUX

Imprecise tolerance control during early transient GCR flux simulations showed an anomalous radiation belt being generated around L=3 as shown in Figure 33. Investigation revealed that numerical errors allowed the energy of particles to vary by as much as 0.01% in as the GCR particle approached the Earth. A small subset of the incoming particles became quasi-trapped for short periods of time. Though the average resident time in the Earth's magnetosphere was only about 0.25 seconds for 2 GeV particles, the quasi-trapped particles became trapped for multiple seconds or even many minutes. The result of this extended time in the Earth's vicinity was the generation of a quasi-stable antiproton population near the rigidity cutoff point. The maximum observed flux was 25 times the background GCR flux for 2 GeV antiprotons at L=2.75. A spacecraft in an equatorial orbit at this altitude would experience a large antiproton flux which would be continuously replenished. It is unknown if degrading the energy further will expand this effect. However, one may surmise that a larger subset of the incident trajectories would be trapped to produce a larger flux magnification.

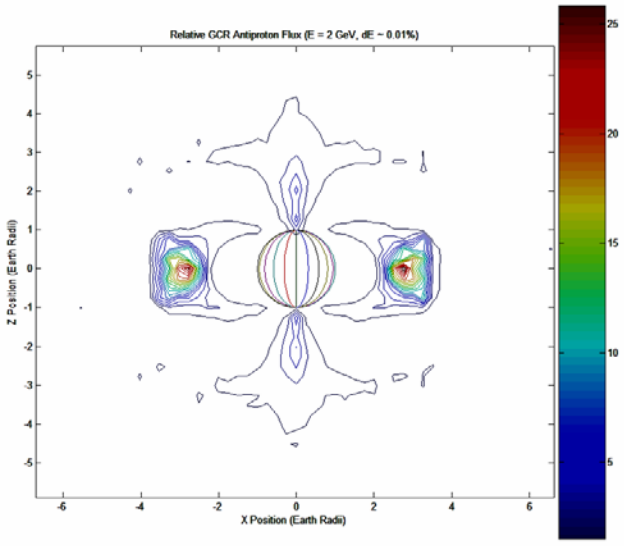

Figure 33 – Relative flux of the quasi-stable GCR radiation belt (E = 2 GeV).

The energy degradation could potentially occur during major fluctuations in the magnetic field. The fluctuations will induce an electric field by the relation in Maxwell's equation,

$$\nabla \times E = -\frac{\partial B}{\partial t}. \qquad \textit{Equation 22}$$

Unfortunately the magnetic fluctuations are unlikely to be strong enough to consistently degrade the antiproton energy sufficiently for noteworthy fluxes to develop. One intriguing possibility is that the

energy be degraded artificially by human intervention to induce this effect and artificially generate the quasi-stable antiproton belt. RF fields generated on the ground and/or electric fields in orbit could potentially induce this effect. However, this is likely to be a very power intensive process and it may not prove worthwhile based on economic viability.

PAIR PRODUCTION DUE TO GCR INTRACTIONS WITH COMET TAILS

Another intriguing possibility for high antiproton generation is from the tail of comets. As a comet approaches the Sun, solar heating causes luminous tails stretching for millions of kilometers to form. The solar heating and radiation pressure cause surface volatiles to evaporate and form several distinct tails based on the size and mass of the released particles. (Figure 34) An ion trail flows directly away from the Sun while the hydrogen envelope forms another tail slightly offset. Of particular interest is a slightly curved dust tail which slightly lags the motion of the comet.

Figure 34 – Comet Hale-Bopp showing separated tails.

The dust tail offers a substantial distributed mass of material with which GCR protons can interact to form proton/antiproton pairs. A portion of pair produced antineutrons may also decay which offers a secondary source of antiprotons. A spacecraft flying near the comet could intercept the antiprotons though it is unclear if there is sufficient density to generate significant fluxes. However, this is an interesting possibility that should be explored in more detail.

AUGMENTED ANTIPROTON GENERATION

So far we have relied exclusively on natural processes based on the flux of high energy galactic cosmic rays to produce antiproton/proton and antineutron/neutron pairs. In comparison, Earth based generation currently relies entirely on the collision of high energy proton or ion beams with a target in a particle accelerator. This process is relatively inefficient though numerous suggestions have been put forth to improve the energy efficiency of the generation process. [48,49,50] The concept of moving the generation process to Earth orbit has also been previously suggested. [51] Space based production has the intrinsic advantage that the generated antiparticles do not have to be transported to orbit from the ground.

What is perhaps even more exciting and appealing is the potential to place the generator within the magnetic confinement region. All previous concepts have assumed that the antiprotons would first be generated, then cooled and finally transferred to a storage trap. This cooling and transfer process leads to inherent losses which reduce the total collection efficiency. However, in the case of a planetary magnetosphere or a mini-magnetosphere generated by the magnetic field of a spacecraft, the generator can be placed within the trap. This becomes feasible due to the high vacuum environment in space along with the large volume external trapping provided by the dipole field. Placing the generator in this way enables a significant improvement in the capture efficiency and

overall energy efficiency of the process. Table 5 shows estimates for this in situ generation process based on the scaling of Forward's numbers relative to antiproton generation at CERN and Fermilab.

	CERN	**Fermilab**	**In Situ**
Incident Proton Energy (GeV)	26	120	200
Generation Efficiency (pbar/p)	0.4%	4.7 %	8.5%
Angular Capture Efficiency	20%	30%	100%
Momentum Capture Efficiency	1%	1.2%	85%
Handling Efficiency	5%	18%	80%
Total Efficiency (pbar/p)	4×10^{-7}	3×10^{-5}	0.058
Overall Energy Efficiency	1.4×10^{-9}	2.5×10^{-8}	2.7×10^{-4}
Rate at 100 kWe (Prometheus)			9.5 μg/yr
Rate at 1 GWe			95 mg/yr

Table 5 – Antiproton generation efficiency. (Based on Forward, 1985)

If we take the power available in orbit to be the projected electrical power generated by a Project Prometheus source or a large solar power array, nearly 10 micrograms of antiprotons could be generated and stored per year. This represents a significant quantity of antimatter which could be used for very aggressive space propulsion and exploration. The concept is also quite appealing since additional antiprotons could be generated over the course of the trip during transit to further propel to vehicle. A much larger power source (GWe) could conceivably enable milligram class quantities of antiprotons to be generated. This level of antiproton generation is sufficient to propel small interstellar probes to a significant fraction of c.

SUMMARY OF OTHER ANTIPROTON SOURCES

- Transient antiprotons in the GCR background which are slightly degraded in energy could possibly form a quasi-stable radiation belt near the Earth which would be replenished very quickly (minutes). Though this is unlikely to occur consistently due to natural phenomena, it could possibly be induced artificially.

- Antiprotons generated by the interaction of galactic cosmic rays with the tail of a comet could produce transient fluxes larger than the GCR background. The generated antiprotons could then be efficiently captured for subsequent use. This should be studied in more detail to determine feasibility.

- Artificially generating antiprotons in magnetospheres (natural or otherwise) would be very valuable and efficient. By effectively locating the particle accelerator within the magnetic 'bubble', the system can produce and trap antiparticles with high efficiency which can then be used for propulsion. Leveraging the development of a space qualified nuclear reactor (Project Prometheus) or 100 kWe solar arrays would enable ~10+ μgm to be collected in orbit per year.

The processes discussed in the previous sections naturally produce fluxes of antiparticles that can be used for space propulsion among other things. However, the fluxes are still relatively tenuous when compared to the storage density desired for operational applications. A method that allows the flux to be concentrated, collected, and then stored must be devised before we can take advantage of the natural supply of antiparticles. We have proposed the use of a magnetic scoop to concentrate the antiparticles from the space environment. The concentrated flux can then be transferred to the mini-magnetosphere that forms around the scoop to store the antiparticles for long periods of time. A magnetic scoop placed in a low inclination orbit can be designed to intercept nearly the entire antiproton supply trapped in a planet's radiation belt. The scoop can also be optimized to operate in deep space where it can trap portions of the background flux.

COLLECTION PHYSICS AND EFFICIENCY

The physics governing the operation of the antiparticle scoop are similar to the Bussard scoop proposed for interstellar propulsion. However, a few key distinctions should be made between the two. The major challenges associated with the Bussard scoop are not relevant since the collector does not need to accelerate the vehicle or directly induce fusion reactions. Instead, the vehicle motion of the ram jet is replaced by the relative motion of the particles bouncing between mirror points in both hemispheres. There is no need to induce nuclear reactions directly in the inlet stream since there is no desire to accelerate the vehicle during the collection process. The two concepts also differ in the factors that influence the collection efficiency. Depending upon the relative forward momentum and magnetic field strength, an incident particle has some probability of being mirrored out of the magnetic scoop. In addition, very high energy particles will have gyro radii which may exceed the dimensions of the collector which will also reduce the efficiency of the collection process. Interstellar protons are expected to be only thermally agitated relative to the vehicle motion while radiation belt antiparticles will be spiraling along field lines with some pitch angle dependence. The ratio of particles within the acceptance cone based on these factors differs between the two scenarios.

Figure 35 shows our hypothetical magnetic scoop. A dipole moment is formed as high current passes through a wire loop. This is described in any introductory text on electromagnetism. [52] Incident antiprotons will be guided by the field lines similar to their motion in the Earth's magnetic field. The far field magnetic intensity at a distance s from the center is,

$$B = \frac{\mu_0 \cdot N \cdot I \cdot r^2}{4s^3}\sqrt{1+3\sin^2(\lambda)} \qquad \textit{Equation 23}$$

where μ_0 is the permeability of free space, N is the number of loops in the coil, I is the current in each loop, r is the radius of the loop, and λ is the angle relative to the normal. Therefore, the region of influence where the magnetic field exceeds the ambient field (B_0) extends out to a maximum distance of,

$$s_{\max} = \sqrt[3]{\frac{\mu_0 \cdot N \cdot I \cdot r^2}{2B_0}} \; . \qquad \textit{Equation 24}$$

The pitch angle of the incident particle will increase as it approaches the throat where the magnetic field intensity is greatest. The mirror point where the particle is repelled and returns along its original trajectory occurs when the pitch angle reaches 90 degrees. For any arbitrary magnetic field configuration, the relationship between the pitch angle (α)„ particle momentum (p), and magnetic field strength (B) is given as,

$$\frac{p_1^2 \sin^2(\alpha_1)}{B_1} = \frac{p_2^2 \sin^2(\alpha_2)}{B_2} \qquad \textit{Equation 25}$$

for any two points in along the particle's trajectory. [20] This expression remains valid even if an electric potential parallel to the field lines changes the particle's momentum.

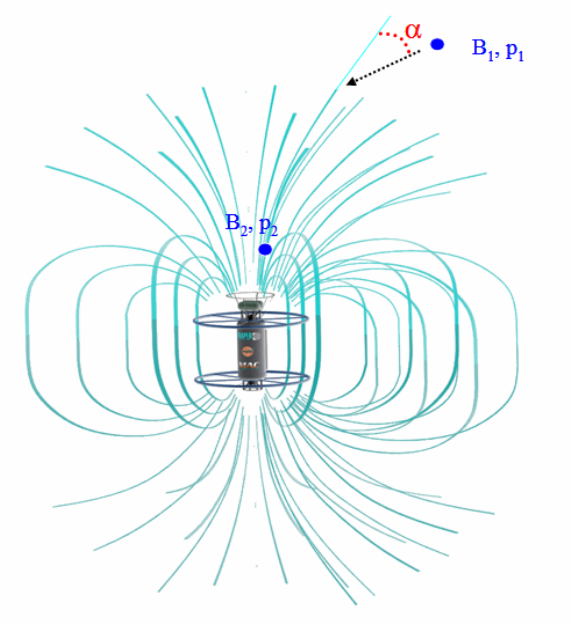

Figure 35 – Magnetic scoop with field lines.

From Equation 25 one can calculate the maximum pitch angle for acceptance based on the ambient field strength and the magnetic field at the throat. Solving for the maximum pitch angle due to magnetic reflection gives,

$$\alpha \max_{\text{Re flection}} = \frac{p_m}{p_0}\sqrt{\frac{B_0}{B_m}}. \qquad \textit{Equation 26}$$

The gyro radius (Larmor radius) represents a separate limitation on the ability to collect particles with the magnetic field. Equation (5) gives the gyro radius of the particle in the ambient field as it approaches the collection device. If the gyro radius exceeds the radius of influence for the collector, the particle will not be trapped. The Larmor limit is given as,

$$\alpha \max_{Larmor} = \sin^{-1}\left(\left(\frac{B_0 q}{2p_0}\right)\sqrt[3]{\frac{\mu_0 \cdot N \cdot I \cdot r^2}{2B_0}}\right) \qquad \textit{Equation 27}$$

The maximum pitch angle accepted into the collector is the minimum value of the reflection and Larmor limited cases. Figure 36 plots the maximum radius of influence and acceptance angle for a magnetic scoop operating in the interplanetary magnetic field (IMF) at 1AU and in low Earth orbit at an altitude of 6400 km. The data is plotted as a function of coil radius.

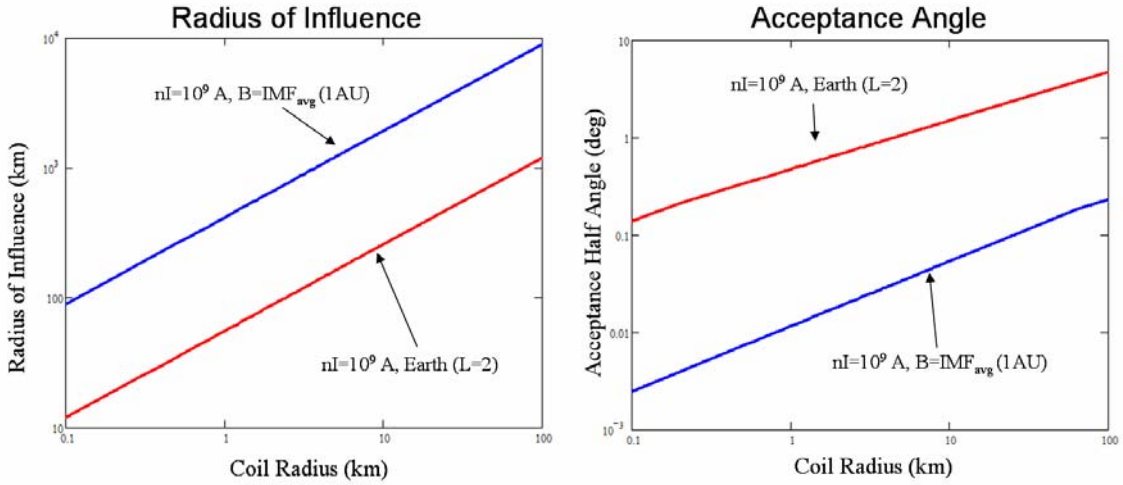

Figure 36 – Radius of influence and maximum acceptable angle to magnetic scoop.

The plots show that very large loops with tremendous electrical current running through them (or many loops with lower current) have the ability to influence particle trajectories within a radius extending out thousands of kilometers. Even with only the lowest GCR background flux, milligrams or more of antiprotons will still pass within this sphere of influence for such systems each year. Systems with more modest parameters are still capable of influencing particles in a sphere measuring tens to hundreds of kilometers per side and yearly fluxes in the microgram range based on the limited GCR background flux.

The limitation of the collection is of course the maximum acceptance angle. If we require that the antiprotons approach the coils to within one diameter (z_m=2r), where the energy can be degraded and the particle's trajectory transferred to a closed field line for trapping, the maximum acceptance angle will be a few degrees and often much less. This is a fundamental issue that limits the collection efficiency of the scoop. The maximum acceptance angle can be increased by applying electric or RF fields to pull the particle in. The increase in acceptance angle scales linearly with the change in the particle's momentum from its initial value on approach to that near its mirror point. This technique may be effective for improving the collection efficiency of low energy particles but would likely be difficult to implement in a practical manner for high energy particles due to their very high initial kinetic energy.

ESTIMATED ANTIPROTON COLLECTION RATE

We can calculate the overall collection rate based on some ambient antiproton flux. Figure 37 shows the estimated collection rate assuming the worst case flux of the omni-directional GCR antiproton background. The specific mass of the system improves as the coil radius increases. With a 50 km diameter coil, the coil mass is estimated to be less than 1 metric ton per microgram collected per year. Operating the device in higher flux regions will improve the performance significantly. The engineering current density used in the mass estimates is a value proposed by Zubrin [53] as potentially feasible in the 10-20 year time frame. This assumes significant improvements (by about two orders of magnitude) in superconductor technology relative to the current state of the art. Relying on currently available commercial technology would be prohibitive from a mass perspective for all but the smallest systems.

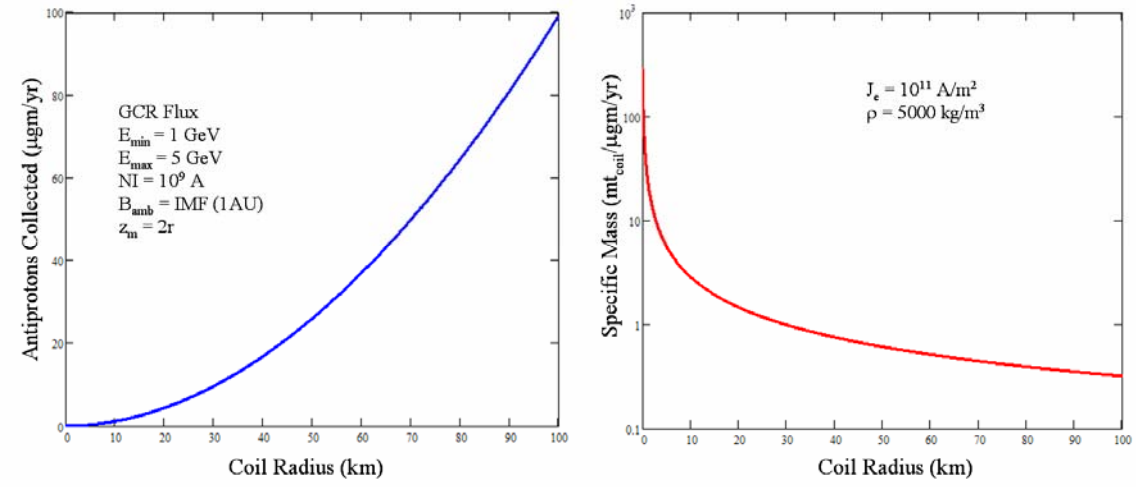

Figure 37 – *Antiproton collection rate and mass efficiency for the GCR background flux.*

The total rate of collection with a very large 100 km coil system could be as high as 100 micrograms per year for the worst case flux. Smaller systems of a more practical size would still be able to collect a few micrograms per year at these flux levels. This is three orders of magnitude faster than the current capabilities of Earth based accelerator production. In addition, collection rates would improve substantially if operating within planetary radiation belts or near other antiproton production targets. Extracting the lower energy radiation belt particles (MeV instead of GeV) improves performance in a number of ways - the fluxes are higher, the lower energy regime reduces the gyro radius collection limit, and the particles are easier to trap in the external dipole field. However, the limitation of radiation belt extraction is the total supply limit compared to the infinite supply offered by the GCR background. This is especially true for Earth. One potential solution would be to use a bootstrap design where a small portion of the Earth antiproton population would be extracted to propel the vehicle to Saturn where much more could be collected to propel the vehicle on its true mission. The vehicle could also collect from the GCR background during the transit periods.

COLLECTOR TRADEOFFS

The values shown in the above plots are for a subset of the potential design and operational parameter space. There are a number of interesting tradeoffs that should be considered. The first is the best location in terms of the ambient magnetic field intensity. For a given antiproton flux, does performance improve when operating in a high ambient magnetic field (deep within a planetary magnetosphere) or does the collection rate increase when the system is operated in the lowest ambient field possible?

Low Earth orbit may seem optimal for collection since the relative change in the field between the collector throat and the ambient field is reduced. The acceptance cone would therefore increase due to the smaller relative change. However, the region where the coil field dominates over the ambient is reduced, thus minimizing the incident flux due to the smaller sphere of influence. These effects are combined in Figure 38 for several high current cases. The collection rate and mass efficiency improves as the ambient field is reduced. Therefore, operating the greatest distance possible from a planet is optimal. Of course, there is an additional dimension to this tradeoff since the largest fluxes are likely to occur within a planetary magnetosphere. However, comets are an enticing option since they potentially offer high fluxes with low ambient fields – the best of both worlds.

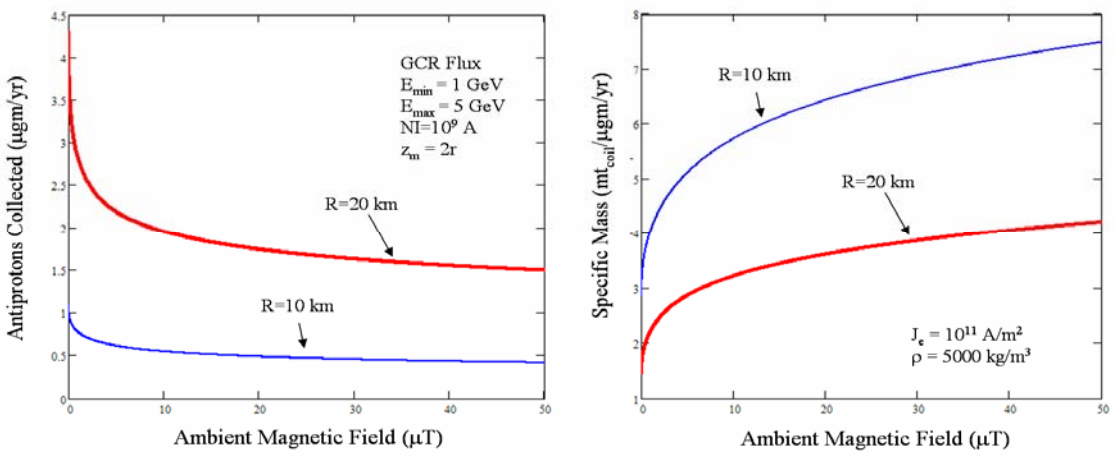

Figure 38 – Optimal ambient field magnitude for collection.

There is also a tradeoff for the optimal ring current as shown in Figure 39. Here we define the total ring current to be the product of the number of coils and the current in each. Several interesting effects are observed. The first is that operating in different ambient magnetic fields does not play a large role in efficiency when the ring current is lower than about 10^8 amp-turns. The mass efficiency is also flat below this current level. The effects seen in Figure 38 only become apparent at higher currents. The change in behavior represents a change in the limiting factor for collection. At the lower current limits, it is in the Larmor radius limited region while it is reflection limited at the higher values. The exact shift point depends upon the energy of the incident particle – the 10^8 Amp-turns value represents the critical point for particles in the 1-5 GeV range. The shift would occur at lower currents for trapped antiprotons in the MeV range.

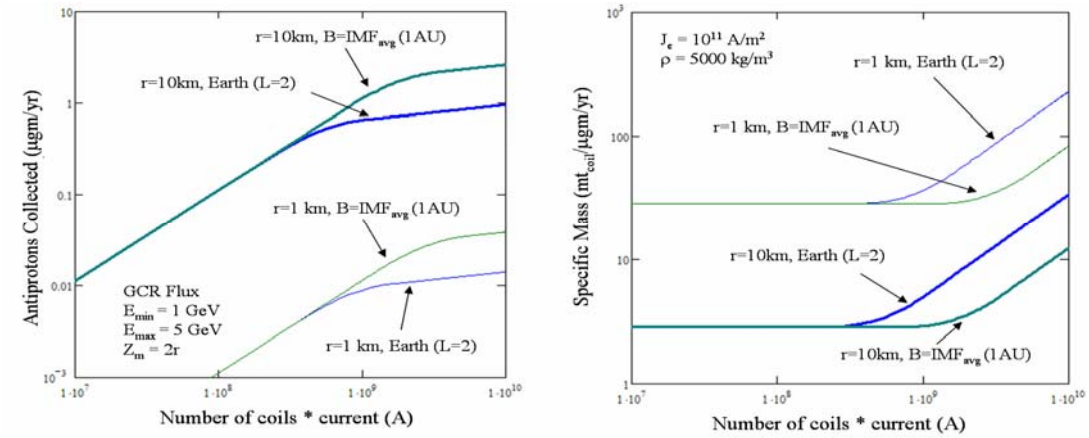

Figure 39 – Optimal ring current for collection.

Figure 40 shows the estimated mass of the high current system (NI=10^9 amp-turns) based on commercially available superconductor technology and projected superconductor performance in the time frame of this program. Very large coils become prohibitive from a mass perspective, even with substantial improvements in superconductor performance. The cost of ground launch will likely limit the maximum ring size to be much less than 10 km in radius for the high current case. This probably represents a practical (economic) limit for system performance though the exact point is dependent upon many additional variables including political support.

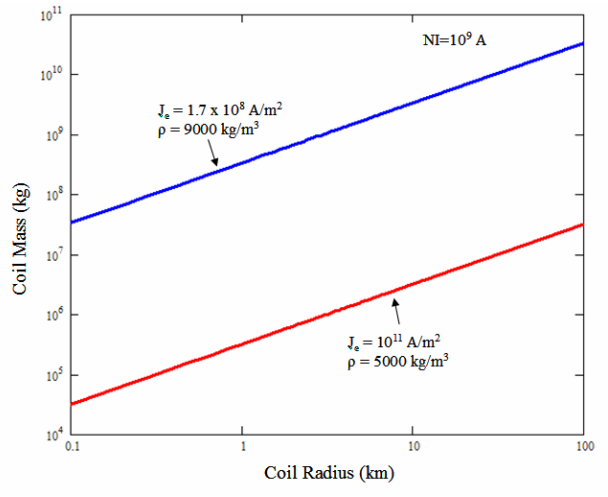

Figure 40 – Coil mass based on current and projected superconductor technology. (NI=10^9 A)

POWER REQUIREMENTS

Though the current loops will be made of a superconductor to support the large required currents, there will still be some occasional losses which need to be compensated for. Of more importance to the maximum power required for the system is the need to initially charge the coils within a limited period of time. The magnetic field generated by the current loops stores a tremendous amount of energy. From an initial starting state with no current, a power system should be able to charge the system to its operational state within days or weeks. This is a relatively minor issue for small loops, but becomes a major concern for very large systems where 10^{14} Joules or more may be stored in the magnetic field. Figure 41 shows the power required to charge various loop sizes to different final current states. The values can be quite large and perhaps prohibitive on the very high end.

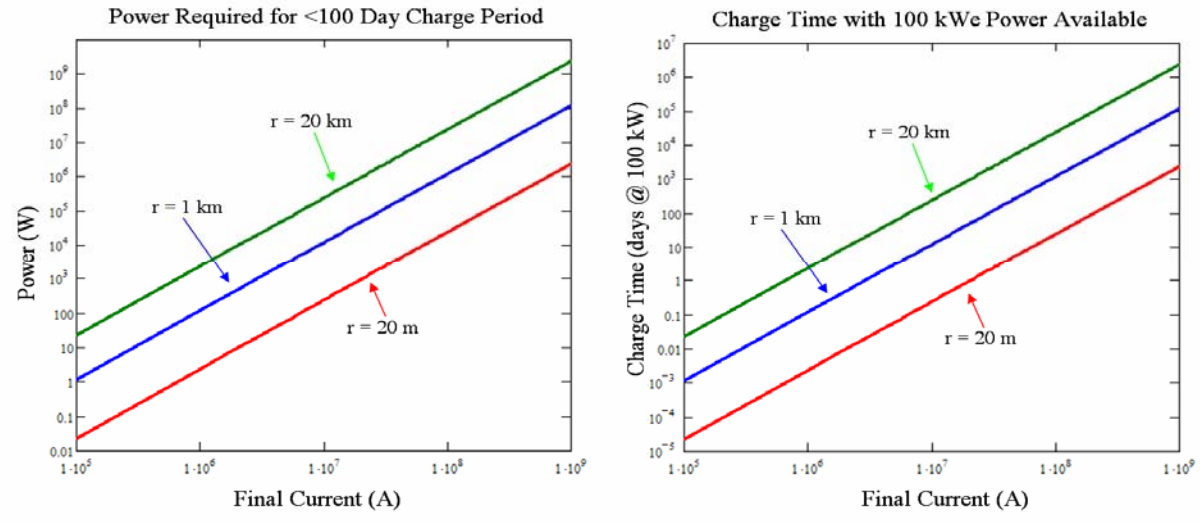

Figure 41 – Power requirements for the collection system.

THERMAL CONTROL

The superconducting loops required for use in the loop operate at cryogenic temperatures. Even the latest high temperature superconductors will need innovative cooling systems to achieve high current densities and maximize performance. Active cooling and/or bringing consumable cryogenic liquids to cool the coils will not be feasible for very large systems. Instead we must rely on passive cooling systems which are well established in the space industry – though perhaps not at this scale. Passive cooling works by using selective coatings to reduce the absorbtivity (α) in the optical spectrum where most of the Solar energy is concentrated, while maximizing the emissivity (ε) in the infrared region of the spectrum so heat can be dissipated to the cool 3K deep space background. This is especially challenging when operating near planets since there will be a large view factor to the relatively warm planet.

Ideally, a single film with a low absorbtivity/emissitivy ratio could be used for cooling, though directionally oriented multi-layer insulation (MLI) may be required to cool the coils when operating near Earth. Figure 42 shows the calculated temperature based on the effective solar absorptivity/emissivity ratio. To keep the coil temperature below 100K (and preferably much lower) MLI insulation would be required when operating near Earth. Zubrin [53] covers this in detail and therefore will not be duplicated here. Operating the device at Jupiter or beyond is likely to be feasible with second surface film coatings only since Sheldahl currently offers a product with the desired solar absorptance to emittance ratio. Details of the thermal control system will need to be investigated in more detail as part of future research activities.

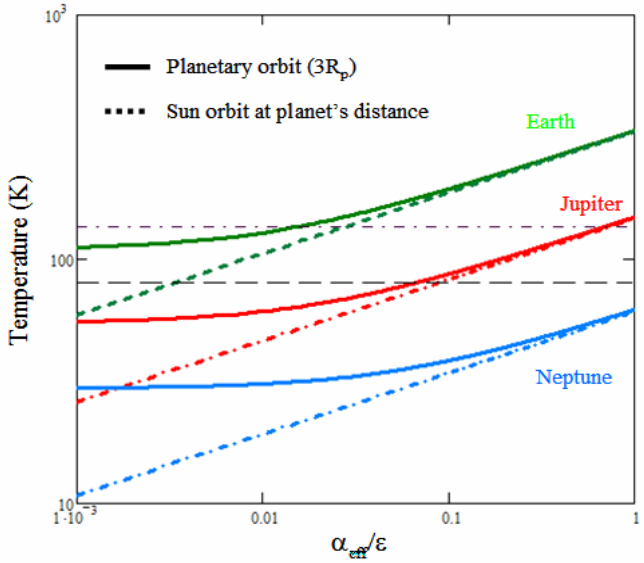

Figure 42 – Average coil temperature for various operating scenarios.

TORQUE AND EXTERNAL FORCES

Operating a spacecraft with a large intrinsic dipole field may introduce large torques or external forces based on its interaction with the external environment. A current loop experiences a torque when exposed to an ambient magnetic field that forces the dipole to align with the local field lines. If no damping is present, the loop will precess around the field lines due to any initial misalignment. There will be no net external force induced when the coils are located within a constant field though translation can occur due to field gradients.

Ideally, the collector should be aligned with the local field lines to maximize the collection efficiency since incident particles will be spiraling along the local field lines as they approach the collector's sphere of influence. The natural tendency of the system will cause it to become aligned with the ambient field as desired. The exception to this would be a spacecraft in a polar orbit. This type of orbit would force the system to rotate as the local field lines rotate relative to the spacecraft as the spacecraft's latitude changed. AC currents can eliminate the torque (and translations) if operation in this mode is desired. However, this will make trapping difficult and is unlikely to be practical for large systems.

SUMMARY OF COLLECTION SYSTEM

- A magnetic scoop can be used to concentrate charged particles for eventual extraction.
    - Loops of high temperature superconducting wire produce the desired magnetic dipole.
    - Particles spiral along the magnetic field lines towards the throat of the collector.
    - As the particles approach the throat, electric fields, RF fields, and/or an energy degrader (mass) can be used to trap the incident particles on closed field lines where they can be stored for future use.
- Performance efficiency is fundamentally limited by two effects with the actual collection rate equal to the worst case of the two.
    - Magnetic reflection causes particles to be mirrored out of the device before being captured near the throat. It is functionally dependent upon the initial angle of incidence of the particle and the magnitude of the magnetic field at the throat relative to ambient.
    - Particles in the ambient magnetic field that have a gyro radius larger than the collector dimensions will not be captured. This effect is functionally dependent upon the angle of incidence, particle energy, ambient magnetic field, and the spatial extent of the collector.
- Kilometer scale loops with very high effective currents are capable of influencing particle trajectories over a radius of hundreds to thousands of kilometers. The acceptance angle is relatively narrow, often much less than one degree.
- Despite the low relative efficiency, such systems are still capable of collecting hundreds of micrograms of antiprotons per year in the worst case GCR background flux.
    - Collecting particles with much lower energies and higher fluxes (radiation belts) will improve collection efficiency and rates substantially.
    - Radiation belt extraction is limited by the total available supply and replenishment rate.
- A high power source is required to initially generate the large currents in the loop over a reasonable period of time.
- Passive thermal cooling should be used to keep the coils at super-conducting temperatures.
    - MLI insulation will be required for spacecraft operating within Jupiter's orbit.
- The current loop will naturally want to self-align with the ambient magnetic field which is the desired configuration for collection.

TECHNOLOGY DEVELOPMENT REQUIREMENTS

The proposed collection system does not require the development of any fundamentally new technology to make it work. However, significant improvements in several key areas are essential to ensure the system is both economically and technically feasible. Of particular importance is technology development in the area of high temperature, low specific mass superconductors. Relying on state of the art superconductors that are available commercially now will yield systems that are not competitive from a mass perspective.

The following list summarizes the technology gaps and their relative development priorities. Most of the technologies are also relevant to other NASA programs (e.g. Project Prometheus) with related development likely to progress independent of this program.

Technology Gap: Low mass, high strength, long strand, ultra-high current loops

- Requirement: High temperature superconductors with $J_e > \sim 10^{10}$ A/m^2 at 90K and L>100m.
- Priority: Essential for collecting from natural low flux antiproton background, highly desirable for systems with artificial augmentation.

- Technology Gap : In-orbit power
  - Requirement : Space qualified nuclear reactor with P >= 100 kWe
  - Priority: Highly valuable though solar power is potentially another option.
- Technology Gap : High efficiency, orbital antiproton generator
  - Requirement: Orbital particle accelerator with beam power = 200 GeV.
  - Priority: Essential for artificial augmentation, not needed if natural antiproton sources are used.
- Technology Gap : Passive cooling systems
  - Requirement: Reduced mass multi-layer thermal blankets for passive temperature control of large structures with $T_{max} < 90$K at 1 AU.
  - Priority: Improvements in reducing mass or operating temperature valuable; reduces requirements on HTS.
- Technology Gap : Affordable Lift
  - Requirement: Reduced cost to orbit. ($/kg)
  - Priority: Not required, but helpful.

NEXT STEPS

This phase I program investigated the basic feasibility of extracting antiparticles from the natural environment for use in space propulsion. Most of the fundamental issues have been investigated to first order which has given us a feel for the major effects and potential of the technology. However due to the limited time and resources available in a phase I study, many of the estimates were based on ad hoc extrapolations. A great deal of additional analysis, experiments, and testing will be required to precisely quantify the potential of the technology. The following are some of the key items that need to be explored in more detail during the proposed phase II program and beyond.

- Improve fidelity of the antiproton source and flux level estimates
    - Estimates of the antineutron derived antiproton fluxes are entirely based on coarse extrapolations of the AP8 radiation belt model. There are numerous uncertainties introduced during the application of this method. A complete radiation belt model, based on solving the full transport equations described in Appendix C, should be completed during phase II. This will require more detailed modeling of the source and loss mechanisms (below).
    - The current antiproton source models are highly dependent on the albedo antineutron backscatter spectrum. The Geant results used for the calculations in phase I were based on coarse simulations of a simple slab model of the atmosphere. The slab model does not account for forward scattering at grazing angles in the atmosphere. The higher flux introduced by GCR focusing over the poles is also not included. A simulation that includes a full field model with all of these effects needs to be completed.
    - A far more detailed model with better energy dependent statistics needs to be completed during phase II. The phase I results had limited resolution due to the limited statistics provided by the initial simulations.
    - Radiation belt models of Saturn and other planets should be completed rather than extrapolating from Earth based measurements.
        - This will require detailed modeling of the source and loss mechanisms specific to the Jovian planets. In particular, modeling the induced fluxes and absorption from Saturn's rings is of great interest.
    - Models of the source fluxes from various other natural phenomena should be completed to quantity the actual fluxes produced by comets, etc…
- Increase the magnetic scoop model fidelity and supplement with experimental data.
    - The current efficiency estimates are all based on analytical equations which describe the simplified motion of charged particles in a magneto-static field. The true behavior of the plasma is more complex and needs to be explored in greater detail. To start, detailed transport modeling needs to be completed based on a full 3D time dependent field model of the scoop. The specifics of the transfer to the closed field lines needs to be designed and verified with more detailed modeling and experiments (below).

- Experimental verification of the plasma trapping design can be completed by trapping electrons in a scale model placed in a plasma test chamber.

- Detailed models of the loss rates and other phenomena should be completed with Geant and other modeling tools.

- Design specifics should be worked out in more detail; this includes thermal and power subsystem design.

- The economic and technical feasibility of the system should be further explored.

  - The relative technical risk and economics should be compared to other (Earth based) production and storage technologies.

  - The viability of artificially augmenting antiproton supplies with an in-orbit generator should be investigated in more detail.

- The system design should be refined.

  - The integrated propulsion system needs to be flushed out to determine if transferring the particles to another vehicle for use is required.

  - The relative value of intrinsic radiation shielding should be quantified.

- Precursor and flight system concepts should be explored in more detail

  - The development program will progress through the following sequence

    - Analytical modeling

    - Detailed modeling

    - Experimental ground based verification

    - Science verification by piggybacking on other missions

    - Proof of concept LEO flights

    - Flight system development

  - Probable flight opportunities should be investigated.

- A more detailed look at the technology development requirements should be completed.

  - This, along with risk estimates should be used to refine the feasibility estimates.

  - Identifying key development elements that are common to other exploration or science missions is essential to maximize the probability of success. In particular, identifying other high value science objectives (e.g. the search for dark matter) that share similar science goals should be emphasized to maximize the return on investment for potential experiments and flight opportunities.

CHAPTER 10 – INTEGRATED SUMMARY AND CONCLUSIONS

The following section combines the summary points from each chapter and lists the major conclusions derived from the phase I work.

BACKGROUND

- Antimatter has an energy density more than ten orders of magnitude higher than the best chemical propellants currently used in rocket systems.
    - Very small quantities (nanograms to micrograms) of antiprotons can be used to catalyze nuclear reactions and enable very aggressive interplanetary or pre-cursor interstellar exploration not possible with conventional systems.
    - Antimatter also offers revolutionary potential in a variety of other Earth based applications including sensing, medical treatment, and basic science research.
- The fundamental stumbling block preventing the realization of this potential is the extreme difficulty (and cost) associated with manufacturing and then storing the antiprotons for extended periods of time.
    - Particle accelerator production currently is limited to a few nanograms per year worldwide and is mostly dedicated to science research.
    - The cost of production is estimated to be upwards of $160 trillion per gram.
    - The current state of the art antiproton storage systems can only trap femtograms of antiprotons for days to weeks at a time. It is unclear if it is possible or how efficiently this could be scaled up to the levels needed for space propulsion. The specific mass of the current systems is more than a billion kilograms per microgram stored which implies limited feasibility for transporting the devices to orbit.
- In contrast, high energy cosmic rays which originate from outside our solar system constantly generate antiprotons when their kinetic energy is converted to mass during high energy collisions with other particles.
    - Interactions in the interstellar medium create a low flux source of antiprotons that continuously impinges on planetary magnetospheres.
    - The interaction of cosmic rays with the atmosphere of a planet, or other targets such as rings, can create natural supplies of antiprotons that become trapped in the radiation belts surrounding the planet.
- A large dipole magnetic field can be advantageously applied to collect the concentrated antiprotons from their natural environment offering the potential for a nearly limitless supply of antiprotons without the difficulties of Earth based production and storage.
    - A spacecraft surrounded by a ring of superconducting wire can be used to induce the required magnetic field for the scoop.
    - The mini-magnetosphere generated around the spacecraft can also be used to store the antiprotons for later use.
    - The magnetic field also offers an intrinsic shield against space radiation and can possibly be applied to assist in the propulsion system by directing the charged particle sources and thrust.

LOCAL EARTH PRODUCTION AND TRAPPING

- Trapped antiprotons come from two primary sources which both originate from high energy galactic cosmic rays interacting with the upper atmosphere.
    - Pair produced anti-neutrons in the atmosphere are subsequently backscattered and decay into antiprotons while in the magnetosphere. (CRANbarD)
    - Antiprotons are directly generated via pair production in the exosphere with a peak at an altitude of about 1200 km (L=1.2).
- The total steady state trapped supply is estimated to be between 0.25 and 15 nanograms based on preliminary calculations.
    - The low end estimates for the total supply are not practical and the high end estimates are marginal for space propulsion applications.
    - This is much less than originally predicted due to the high energies and narrow angular distribution of the pair produced antineutrons.
    - Inefficiencies in the backscatter process reduce the magnitude of the albedo antineutron flux to be less efficient than the analogous neutron process by 1 part in 10^5 to 10^9.
    - The generation of antineutrons generated by cosmic rays striking the atmosphere at a narrow slant angle is not included in these estimates. Since these antineutrons do not need to be backscattered to enter the magnetosphere trapping region, this could represent a significant additional source of antiprotons.
    - We have conservatively assumed the 0.25 nanogram worst case prediction for all remaining calculations including extrapolations to the outer planets.
- The overall replenishment rate timescale is on the order of several years.

JOVIAN EXTRAPOLATIONS

- The rings of Saturn are the largest source of locally generated antiprotons in the solar system. Nearly a half milligram of antiprotons are trapped based on the coarse engineering extrapolations.
    - The fluxes are primarily formed by the decay of ring produced antineutrons in the magnetosphere. Antineutrons generated in the A&B rings do not have to be backscattered for trapping which drastically increases the production efficiency.
- Jupiter has a smaller trapped supply of antiprotons than originally anticipated due to the cutoff of the GCR production spectrum by its large magnetic field.
    - Approximately 1 μgm of antiprotons are spread throughout Jupiter's magnetosphere.

- Saturn and Jupiter both have relatively large supplies of antiprotons relative to that needed for selected propulsive concepts which utilize antiprotons to catalyze nuclear reactions. The disadvantage is that a spacecraft must first be sent there to collect the antiparticles.
    - Though Earth has a relatively small antiproton supply in terms of very high delta-v missions, the supply is likely large enough to enable a bootstrap mission where a spacecraft first stops in Earth orbit for a partial 'fuel up' and then travels to Saturn to extract most of the fuel for an interstellar precursor mission.
- The estimates are all based on extrapolations of conservative Earth supply estimates. A complete model of the Jovian radiation belts will be required to more accurately determine the true fluxes and integrated mass.

POSITRONS

- Positrons generated as a result of the proton belt interacting with the upper atmosphere produce fluxes where the number of positrons exceeds the number of electrons.
- Solar positrons generated near the surface of the Sun have been experimentally observed. It is unclear how many if any of these make their way to Earth where they can be trapped in the magnetosphere.
- Significant fluxes of positrons may exist, though the exact magnitude is still uncertain. A quasi-static supply < 1 μgm is most likely.

GCR FOCUSING

- Simulations of the motion of charged GCR particles traversing a planetary magnetic field were completed to determine the relative level of flux concentration provided by the global field.
- Above the poles of the Earth, the flux was concentrated by approximately a half order of magnitude relative to the GCR background flux.
    - A spacecraft placed in an orbit to take advantage of this would also pass through the forbidden regions during its equatorial pass. This would reduce the total integrated flux unless antiprotons trapped in the radiation belts were present in the equatorial areas.
- Jupiter provides a similar type of flux enhancement with the local flux over the poles approximately one and one half orders of magnitude higher than the background level.
- Transient GCR antiprotons passing the equatorial region are preferentially biased to a relatively narrow and small pitch angle. This could improve collection performance significantly.

OTHER NATURAL ANTIPROTON SOURCES

- Transient antiprotons in the GCR background which are slightly degraded in energy could possibly form a quasi-stable radiation belt near the Earth which would be

replenished very quickly (minutes). Though this is unlikely to occur consistently due to natural phenomena, it could possibly be induced artificially.

- Antiprotons generated by the interaction of galactic cosmic rays with the tail of a comet could produce transient fluxes larger than the GCR background. The generated antiprotons could then be efficiently captured for subsequent use. This should be studied in more detail to determine feasibility.

- Artificially generating antiprotons in magnetospheres (natural or otherwise) would be very valuable and efficient. By effectively locating the particle accelerator within the magnetic 'bubble', the system can produce and trap antiparticles with high efficiency which can then be used for propulsion. Leveraging the development of a space qualified nuclear reactor (Project Prometheus) or 100 kWe solar arrays would enable ~10+ μgm to be collected in orbit per year.

COLLECTION SYSTEM

- A magnetic scoop can be used to concentrate charged particles for eventual extraction.
    - Loops of high temperature superconducting wire produce the desired magnetic dipole.
    - Particles spiral along the magnetic field lines towards the throat of the collector.
    - As the particles approach the throat, electric fields, RF fields, and/or an energy degrader (mass) can be used to trap the incident particles on closed field lines where they can be stored for future use.
- Performance efficiency is fundamentally limited by two effects with the actual collection rate equal to the worst case of the two.
    - Magnetic reflection causes particles to be mirrored out of the device before being captured near the throat. It is functionally dependent upon the initial angle of incidence of the particle and the magnitude of the magnetic field at the throat relative to ambient.
    - Particles in the ambient magnetic field that have a gyro radius larger than the collector dimensions will not be captured. This effect is functionally dependent upon the angle of incidence, particle energy, ambient magnetic field, and the spatial extent of the collector.
- Kilometer scale loops with very high effective currents are capable of influencing particle trajectories over a radius of hundreds to thousands of kilometers. The acceptance angle is relatively narrow, often much less than one degree.
- Despite the low relative efficiency, such systems are still capable of collecting hundreds of micrograms of antiprotons per year in the worst case GCR background flux.
    - Collecting particles with much lower energies and higher fluxes (radiation belts) will improve collection efficiency and rates substantially.
    - Radiation belt extraction is limited by the total available supply and replenishment rate.
- A high power source is required to initially generate the large currents in the loop over a reasonable period of time.

- Passive thermal cooling should be used to keep the coils at super-conducting temperatures.
    - MLI insulation will be required for spacecraft operating within Jupiter's orbit.
- The current loop will naturally want to self-align with the ambient magnetic field which is the desired configuration for collection.

CONCLUSIONS AND RECOMMENDATIONS

- Earth has a minimal (0.25 - 15 ng) trapped supply of antiprotons. This is replenished over a period of several years. The low level is due to inefficiencies in backscattering albedo antineutrons from the atmosphere. Significant fluxes of positrons may exist, though a quasi-static supply < 1 μg is most likely.

- Saturn has the largest trapped antiproton supply in the Solar System (estimated at ~400 μg) due to high antineutron production from GCR interactions with its ring system. The flux of transient antiprotons produced in the ring system is also predicted to be significant.

- The antiparticle estimates are based on approximate extrapolations. Full radiation belt models should be completed for the Earth and Jovian planets. This will include detailed radiation transport analyses to precisely quantify the source and loss terms.

- High energy (GeV) antiprotons in the natural Galactic Cosmic Ray (GCR) background are very tenuous but are partially concentrated by planetary magnetic fields. Though not as desirable as collecting them from stable radiation belt supplies (MeV), extraction from the GCR background is also feasible.

- Local transient antiproton fluxes from planetary rings (Saturn), comet tails, and other phenomena may significantly exceed background GCR fluxes.

- Though Earth has a relatively small antiproton supply in terms of very high delta-v missions, the total content is enough to enable a bootstrap mission where a spacecraft first stops in Earth orbit for a partial 'fuel up' and then travels to Saturn to extract most of the fuel for the full mission. Antiprotons from the GCR background can be collected during transit.

- A magnetic funnel formed from passively cooled high temperature superconducting loops can be used to collect significant quantities of antiprotons from low GCR background levels or in regions of high intensity local production (Saturn). However, significant improvements in superconductor performance will be required before this is practical at a large scale.

- A magnetic bottle formed from the same superconducting loops can be used to safely store antiprotons for long periods of time. Particles and antiparticles at various energies can coexist in the same device since the large trapped volume (km^3 or more) and natural vacuum afforded by the space environment minimizes losses.

- Artificially generating antiprotons in magnetospheres (natural or otherwise) would be very valuable and efficient. By effectively locating the particle accelerator within the magnetic 'bubble', the system can produce and trap antiparticles within high efficiency which can then be used for propulsion. Leveraging the development of a space qualified nuclear reactor (Project Prometheus) or 100 kWe solar array would enable ~10+ μgm to be collected in orbit per year.

APPENDIX A – LAB FRAME THRESHOLD ANTIPROTON PRODUCTION KINEMATICS

The following appendix derives the formula for the kinetic energy required in the lab frame for antiproton production just at threshold. The collision is assumed to be a high-energy proton striking an atomic nucleus. The reaction can be symbolized as follows:

$$p + A \rightarrow p + A + p + \bar{p} \qquad \textit{Equation 28}$$

with

p = proton,

A = atomic nucleus, and

$\bar{p}$ = antiproton.

Note that we have an extra proton on the right hand side since we need to conserve baryon number.

There are two useful frames for describing this reaction. One of them is the lab frame (target at rest) and the other is the center of mass frame where the total momentum is identically zero. Just at threshold the production of antiprotons can be easily illustrated in both frames with the use of the following scattering diagrams shown in Figure 43 below.

Scattering Diagram for Antiproton Creation Just at Threshold:

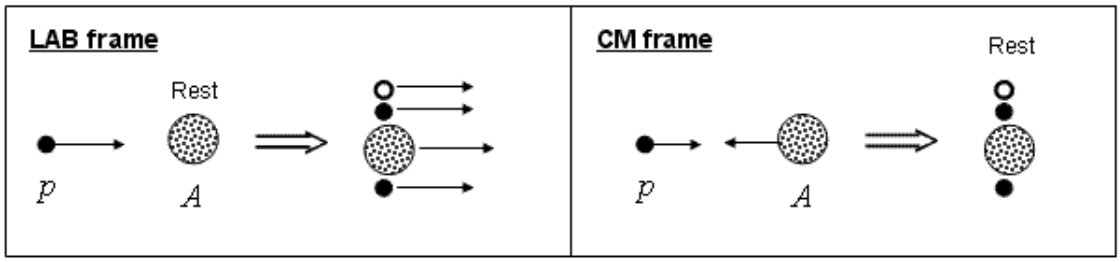

Figure 43 - Scattering diagrams for antiproton creation just at threshold. The left panel illustrates the reaction in the laboratory frame (target at rest) and the right panel illustrates the reaction in the center of mass frame from where at threshold the final particles are at rest.

We seek to derive a formula for the threshold kinetic energy in the lab frame for antiproton production. Clearly in the center-of-mass frame the threshold kinetic energy is simply $2m$ where m is the mass of a proton. However, in the lab frame more energy is needed since the final particles emerge with finite momentum. To derive the general formula it is convenient to express momentum and energy conservation using the 4-momentum notation of Einstein. Conservation of 4-momentum then gives the following expression in the lab and center-of-mass frames.

$$P_p^{lab} + P_A^{lab} = P_{p'}^{lab} + P_{A'}^{lab} + P_{p''}^{lab} + P_{\bar{p}}^{lab} \qquad \textit{Lab–Frame} \qquad \textit{Equation 29}$$

$$P_p^{cm} + P_A^{cm} = P_{p'}^{cm} + P_{A'}^{cm} + P_{p''}^{cm} + P_{\bar{p}}^{cm} \qquad \textit{CM–Frame} \qquad \textit{Equation 30}$$

Now here's a trick. The lab frame and CM frame are related by a Lorentz transformation Λ. This transformation is used this to connect the lab and CM frame and is expressed as follows:

$$P_p^{lab} + P_A^{lab} = \Lambda(P_p^{cm} + P_A^{cm}) \qquad \textit{Equation 31}$$

The trick occurs when taking the square of both sides since the Lorentz factor become unity, and therefore we don't actually need to know what it is, and leads to the equality:

$$(P_p^{lab} + P_A^{lab})^2 = (P_p^{cm} + P_A^{cm})^2 \ . \qquad \textit{Equation 32}$$

Using equation 30 we can then rewrite equation 32 as follows:

$$(P_p^{lab} + P_A^{lab})^2 = (P_{p'}^{cm} + P_{A'}^{cm} + P_{p''}^{cm} + P_{\bar{p}}^{cm})^2 \ . \qquad \textit{Equation 33}$$

We are almost there... Using equation 33 we can easily evaluate the Lorentz invariant length for the right hand side of the equation since by definition just at threshold in the CM frame the final particles are all at rest. Therefore in the center of mass frame, just at the antiproton production threshold, the final state particle 4-momenta are:

$$P_{p'}^{cm} = (m,\vec{0})$$
$$P_{A'}^{cm} = (Am,\vec{0})$$
$$P_{p''}^{cm} = (m,\vec{0})$$
$$P_{\bar{p}}^{cm} = (m,\vec{0})$$

The resultant 4-momentum vector for the right hand side then becomes

$$P_{p'}^{cm} + P_{A'}^{cm} + P_{p''}^{cm} + P_{\bar{p}}^{cm} = (Am + 3m,\vec{0})$$

whose square is simply $(Am+3m)^2$. Plugging this back into Equation 6 and factoring out the m^2 term we then obtain:

$$(P_p^{lab} + P_A^{lab})^2 = m^2(A+3)^2 \ . \qquad \textit{Equation 34}$$

Completing the square of the left hand side of Equation 34 we then obtain the relation:

$$(P_p^{lab})^2 + 2P_p^{lab}P_A^{lab} + (P_A^{lab})^2 = m^2(A+3)^2 \ . \qquad \textit{Equation 35}$$

We can now further reduce the left hand side of the equation using the following expressions for the 4-momentum vectors in the lab frame

$$P_p^{lab} = (m + K_{thr}^{lab}, \vec{p}_p^{lab})$$
$$P_A^{lab} = (Am, \vec{0}) \qquad \text{(target at rest)}$$

and the fact that

$$(P_p^{lab})^2 = m^2 .$$

Substituting these 4-momenta into equation 8 yields the following:

$$m^2 + 2Am(m + K_{thr}^{lab}) + (Am)^2 = m^2(A+3)^2 . \qquad \textit{Equation 36}$$

Equation 36 can then be solved for the threshold kinetic energy to yield the formula for the lab-frame proton threshold kinetic energy required for antiproton production from a target of atomic weight A:

$$K_{thr}^{lab} = m\left(2 + \frac{4}{A}\right). \qquad \textit{Equation 37}$$

The following atmospheric models and annihilation cross sections were used to calculate loss rates in the radiation belts. The number density for constituents of the Earth's atmosphere as a function of altitude and other parameters are given by the Mass-Spectrometer-Incoherent-Scatter (MSIS) model [55]. Figure 45 shows values for typical atmospheric conditions.

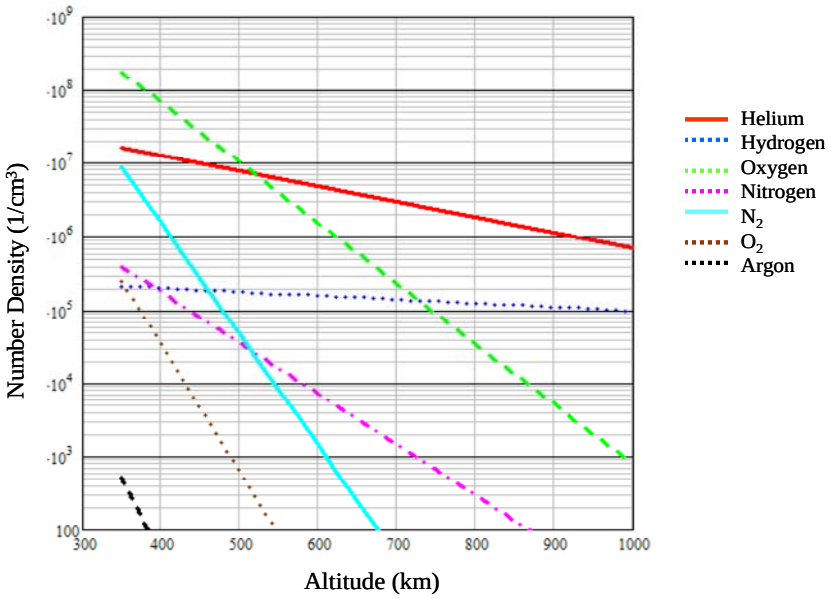

Figure 45 – Atmospheric number density.

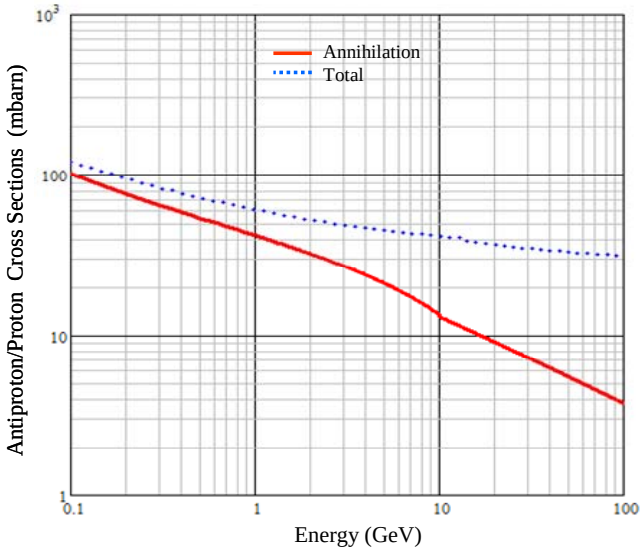

Figure 44 – Proton/antiproton interaction cross section.

The cross sections for antiprotons interacting with protons are given by Tan et al. [56] and are shown in Figure 44. Interactions with the atmospheric constituents are quantified with the cross sections given by Letaw et al. [57] and are shown in Figure 46.

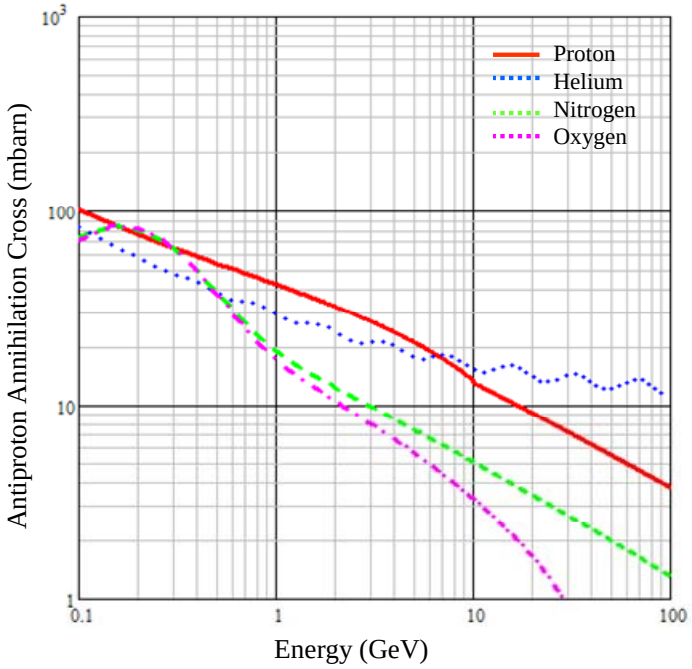

Figure 46 – Cross section for antiproton annihilation with the atmosphere.

Introduction:

With application to an ensemble of energetic charged particles in mind, we choose to define time scales that are appropriate to the statistical behavior of the particles. Thus we begin with the description of the distribution function **f**. In principle this distribution function can be written in terms of the six free variables: spatial coordinates (e.g., Cartesian) and velocity component expressed in those coordinates, forming a six-dimensional parameter space (**x, y, z; v_x, v_y, v_z).** It is customary to perform a Jacobian transformation to a suitable parameter space where the particle dynamics is advantageously described: the so-called adiabatic-invariant space.

Thus one expresses the distribution function in terms of the three adiabatic invariants, μ, **J** and Φ as traditionally defined (e. g., Schulz and Lanzerotti, 1974; Spjeldvik and Rothwell, 1986), μ being the gyration invariant (related to the particle magnetic moment), **J** the bounce invariant (related to the particle energy along the **B**-field), and Φ the azimuthal drift-invariant (related to the geomagnetic **L**-shell parameter). Let us denote the charged particle's local pitch angle (the angle between the instantaneous velocity vector and the local magnetic field vector) as α.

Useful Coordinates:

By the mirror equation (e.g., Roederer, 1970):

$$\sin \alpha / B = \sin \alpha_0 / B_0 = 1 / B_m \qquad \textit{Equation 38}$$

the local pitch angle, α, is related to its value, α_0, when the particle crosses (or is located on) the magnetic equatorial plane. The value of the local pitch angle $\alpha = \pi/2$ (so that $\sin \alpha = 1$) occurs at the mirror-points (where $B = B_m$). Except near the dayside magnetopause region (typically around **L**=10) where the geomagnetic field is very compressed, all energetic charged particles cross the magnetic equator during bounce-motion every half-bounce time, τ_b.

In the dipolar magnetic field approximation to the real geomagnetic field (approximately valid, as an idealization, in the **L**=1.1-6.6 region), one can express the geomagnetic field induction magnitude as:

$$B = (B_E/L^3)\,(4 - 3\cos^2\lambda) / \cos^6\lambda \qquad \textit{Equation 39}$$

where $B_E \sim 0.312$ gauss is the Earth's magnetic induction value at the longitudinally averaged magnetic equator on the surface of the Earth, and λ is geomagnetic dipole-latitude. In this notation, subscript-0 on the various quantities denote those quantities' values at $\lambda = 0$ degrees (i. e., on the magnetic equator).

For a given equatorial pitch angle, α_0, the corresponding mirror-latitude, $\lambda=\lambda_m$ (in the dipole approximation) is given by:

$$\sin \alpha_0 / B_0 = 1 / B_m = (L^3/B_E) \cos^6 \lambda_m / (4 - 3 \cos^2 \lambda_m) \qquad \textit{Equation 40}$$

and thus λ_m is a function of both α_0 and **L**. This equation is transcendental, but a numerical relationship is readily obtained.

Proton transport equation:

Radiation belt theory leads to a formulation of an equation for the transport (by diffusion) of the energetic protons based on stochastic fluctuations of the geomagnetic and geoelectric fields. Empirically the geoelectric field variability is important for thermal and suprathermal plasma, and for energetic particles up to so-called "ring-current" energies (i.e., below several tens of keV per particle), while the geomagnetic field variability appear to control the diffusive transport of the more energetic particles (above a few keV). Thus there is an overlapping energy range where both types of fluctuating fields co-influence particle transport.

For equatorially mirroring protons ($\lambda = \lambda_m = 0$; $\alpha = \alpha_0 = \pi/2$) one can write the energetic proton diffusive transport equation in the form:

$$(\partial f/\partial t) = S + L^2 (\partial/\partial L) [L^{-2} D_{LL} (\partial f/\partial L)] + (\partial f/\partial \mu) (\partial \mu/\partial t) - \Diamond f \qquad \textit{Equation 41}$$

where $S = S(L,E,\alpha_0=\pi/2)$ denotes the strength of an internal proton source (such as the CRAND process), $D_{LL} = D_{LL}(L,E,\alpha_0=\pi/2)$ denotes the radial diffusion coefficient (which depends on the combined B- and E-field fluctuations statistics), and $\Diamond = \Diamond(L,E,\alpha_0=\pi/2)$ is the charge exchange loss frequency per unit distribution function.

Here, the factor $(\partial \mu/\partial t)$ is akin to energy degradation, as described by Rossi and Olbert (1970) (on pp. 219-222): $(\partial \mu/\partial t) = (\partial \mu/\partial E) (\partial E/\partial t)$ where $\mu = E\sin^2\alpha_0/B$ so that $(\partial \mu/\partial E) = E\sin^2\alpha_0/B$ and for equatorially mirroring particles: $(\partial \mu/\partial E) = 1/B_0$

Characteristic Time Scales:

One can define characteristic time scale based on each of the physical processes that control the distribution function, **f**:

1. Overall evolution time scale for the distribution of energetic protons as a whole:

$$\tau_{OVERALL} = f / (\partial f/\partial t) \qquad \textit{Equation 42}$$

2. Source time scale for any effective internal source (such as CRAND):

$$\tau_{SOURCE} = f / S(L,E,\alpha_0=\pi/2) \qquad \textit{Equation 43}$$

3. Without a priori knowledge of the distribution functions themselves, radial diffusive transport time scale for radial distribution spread can be statistically defined from the form of the diffusion coefficient:

$$\mathbf{D_{LL} = (1/2) <(\Delta L)^2> / (\tau_{DIFFUSE})} \qquad \textit{Equation 44}$$

where $\mathbf{<(\Delta L)^2>}$ denotes the ensemble-average of the shifts in L-shell location, $\mathbf{\Delta L}$, that arise from the influence of the fluctuating geoelectric and geomagnetic fields. From this we a-priori to any **f**-determination extract an approximate value of the diffusion time scale by considering the time it takes for the mean-square spreading to equal one unit L-shell:

$$\tau_{DIFFUSE} = 1 / [2\, D_{LL}(L,E,\alpha_0=\pi/2)] \qquad \textit{Equation 45}$$

Of course, a more accurate time scale determination must also take into account the energetic proton distribution, **f**, itself also:

$$\mathbf{\tau_{DIFFUSE} = f / \left\{ L^2 \; \partial/\partial L \left[L^{-2} D_{LL}(L,E,\alpha_0=\pi/2) \; (\partial f/\partial L) \right] \right\}} \qquad \textit{Equation 46}$$

4. Proton losses by charge exchange that neutralizes the energetic particle (or in principle any other instantly acting loss mechanism) can be expressed by the probability that such a process takes place, as quantified by the interaction cross section: τ_{LOSS}, the speed of the energetic proton with respect to the (near stationary) neutral atom of the exosphere:

$$\mathbf{\Diamond \sim 1/ \tau_{LOSS}} \qquad \textit{Equation 47}$$

so that

$$\mathbf{\tau_{LOSS} = [1 / (\sigma_{LOSS}\, v)] / <DENS>} \qquad \textit{Equation 48}$$

where <DENS> is the energetic proton trajectory-averaged number density of the exospheric neutral atoms under consideration (i.e., atomic hydrogen, helium, atomic oxygen, molecular oxygen, etc).

5. Proton losses by (distant) Coulomb collisions is described by:

$$\mathbf{\tau_{COUL} = f / [(\partial f/\partial \mu)\, (\partial \mu/\partial t)].} \qquad \textit{Equation 49}$$

This, however, is only the time scale for energy degradation by a factor of e=2.71…, and so not the e-folding loss time for actual particle loss (i.e., it only describes phase space transfer towards lower energies, or lower magnetic moments). Eventually, by being reduced in energy by this "friction", the protons (or any other particles species subject to these distant electric force encounters) will be lost by other mechanisms (such as charge exchange, etc…).

APPENDIX D – STÖRMER'S FORBIDDEN REGIONS

The motion of a charged particle traversing a magnetic field is governed by the Lorentz force which is given in Equation 3. This must be solved numerically to estimate the trajectory of a particle in the magnetic field of a planet since there is no closed form solution which describes this motion. However, in the first half of the last century, Carl Störmer managed to define an inner region in which cosmic rays are not able to penetrate due to the shielding properties of the planet's magnetic field. The boundary of this forbidden region is described by,

$$r_{forbidden} = \sqrt{\frac{M_p q}{m_0 \gamma v}} \frac{\cos^2 \lambda}{1+\sqrt{1+\cos^3 \lambda}} \qquad \textit{Equation 50}$$

where M_p is the dipole moment of the planet, q is the particle charge, m_0 is the rest mass, γ is the correction factor for relativistic particles, v is the particle's velocity, and λ is the geomagnetic latitude. Recent work by Kress et al [58] has shown interesting time variations in the cutoff as the result of dynamic conditions in the magnetosphere as it responds to solar wind fluctuations.

Figure 47 shows the calculated cutoff locations as a function of latitude and planet radii for idealized static magnetic fields around Earth, Jupiter, and Saturn. The cutoff for a 6 GeV proton approaching the Earth is at approximately a 30 degree latitude. However, 20 GeV protons have full access to the atmosphere at any latitude. In comparison, a 20 GeV proton approaching Jupiter is cutoff below a latitude of 60 degrees and can only approach to about L=9.

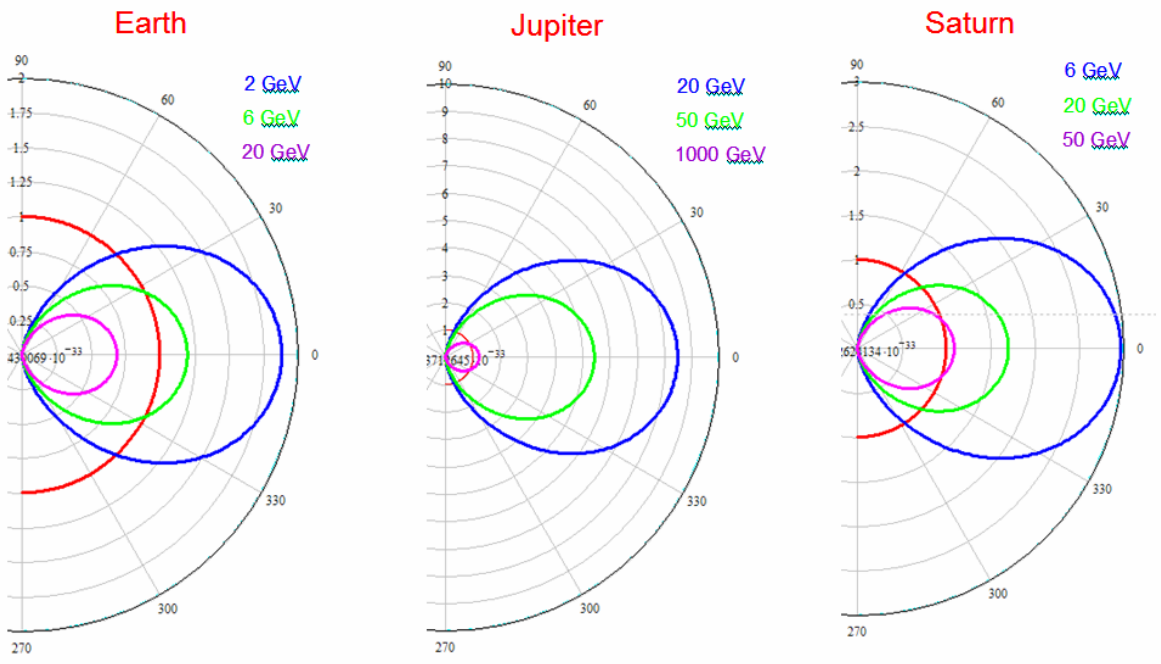

Figure 47 – Störmer forbidden regions for Earth, Jupiter, and Saturn at various energies.

APPENDIX E – TRAP STABILITY

The challenges associated with plasma confinement are well studied due to its applicability to fusion power. Rayleigh-Taylor, current driven, and drift instabilities contribute to losses though various trap geometries and approaches have been proposed to minimize these effects. [59] Single component antiparticle plasmas have traditionally been stored with Penning-Malmberg traps to prevent annihilations with surrounding matter. [60] An axial magnetic field is used to confine the particles radially while high potential electrodes contain axial motion. The positron storage density is generally limited by space charge effects which are caused by Debye shielding of the confinement potential. A 1000 V potential enables the storage of approximately 10^{10} positrons. In comparison, the bound on antiproton confinement is generally associated with the Brillouin limit which describes the maximum achievable density for which the Lorentz force provided by the magnetic field can balance the repulsive and centrifugal forces generated by the rotating plasma. In a 1T magnetic field the plasma density is limited to 10^9 $1/cm^3$. The traditional Brillouin limit to trapping is not a major factor in radiation belt plasmas due to the very large spatial extent of the dipole field trapping region. Distributing one milligram of antiprotons through a cubic kilometer yields a number density of 10^5 $1/cm^3$. Therefore, storage in dipole fields surrounding a space vehicle should not be limited by the traditional factors that are a concern for Earth based traps.

The near dipole magnetic field of the Earth is very effective at trapping high energy charged particles for extended periods of time. The transport and loss mechanisms detailed in Appendix C can be solved to calculate the residence time which can be measured in years. However, in the absence of magnetic fluctuations which induce radial diffusion across L shells and losses from interactions with the atmosphere at lower altitudes, the particle lifetime could effectively be considered infinite for very low density plasmas with minimal pitch angle scattering (long interaction lengths).

This stable trapping scenario can be closely approximated by an artificial magnetosphere surrounding a spacecraft. Much like the terrestrial radiation belts, the particles are trapped on closed field lines within the forbidden region (Appendix D) of the dipole. However, long term stable trapping relies on consistently conserving the adiabatic invariants. For instance, radial diffusion is the result of solar induced dynamic effects in the magnetosphere which can cause the invariants to be violated. The alfvén criterion describes the limit of stable trapping based on the conservation of the first adiabatic invariant. [61] Hudson et al. [62] describes particle stability limits in the Earth's magnetosphere as it reacts to dynamic changes introduced by magnetic storms based on related adiabatic parameters.

Violating one of the adiabatic invariants leads to instabilities and chaotic motion. In particular, if the radius of gyration is very large relative to the scale of the field, the magnetic field seen by the particle is not constant through its periodic gyration motion and the first invariant is violated. This eventually allows the particle to escape and effectively limits what could be considered stably trapped. The trapped particles can be considered to be trapped forever until the gyration radius begins to approach the radius of curvature for the field line about which it is gyrating. [32] Equation 5 defines the radius of gyration which is shown in Figure 48 as a function of the ambient field strength for several proton and electron energies.

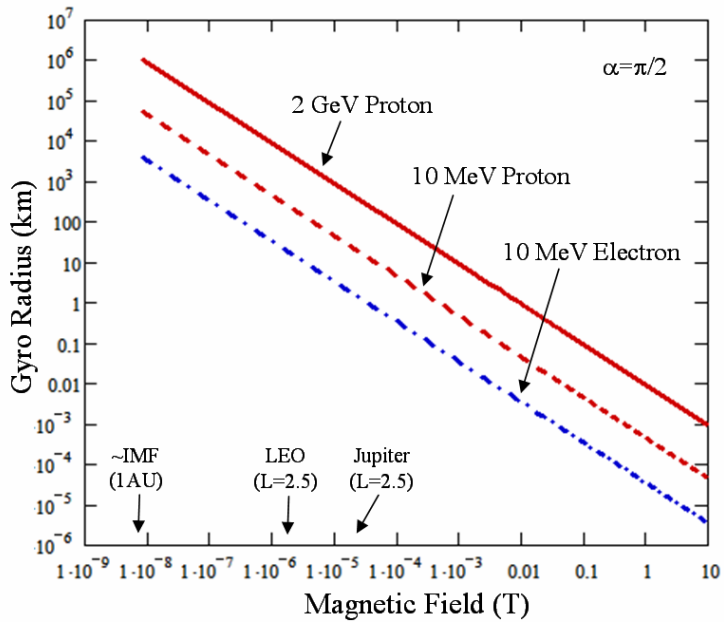

Figure 48 – Radius of gyration as a function of magnetic field strength for several cases.

For a simple dipole, the radial location of a given field line with r = R_0 near the equator is,

$$r = R_0 \sin^2(\theta) \qquad \textit{Equation 51}$$

In polar coordinates, the radius of curvature is given by,

$$RC = \frac{\left(r^2 + r_\theta^2\right)^{3/2}}{\left|r^2 + 2r_\theta^2 - rr_{\theta\theta}\right|} \qquad \textit{Equation 52}$$

where $r_\theta = dr/d\theta$. [63] Differentiating Equation 51 and applying it to Equation 52 yields an expression for the radius of curvature which is functionally dependent upon the latitude but remains constant when normalized by L shell. In the trapping region the minimum radius of curvature occurs at the equator with a value equal to $R_0/3$ or L/3 in a dipole field.

Pugacheva's criteria [32] for long term stability assumes that the gyration radius must be less than 10% of the radius of curvature for the field line on which it resides. Based on this, stable trapping occurs when,

$$\frac{L}{3} > 10\frac{p}{Bq} \qquad \textit{Equation 53}$$

The maximum extent of the stable trapping region can be solved for the Earth or artificially generated dipole using the above relation. Figure 49 shows the estimated values for the Earth, Jupiter, and several dipole field strengths. Strictly speaking, the radius of curvature calculations is for the far field. Therefore as the radius begins to approach the coil radius, the solution needs to be modified to account for near field modifications to the field geometry. A more formal treatment of the trap stability limits due to the adiabatic stability criterion is presented by Northrop [64], Schulz [65], and Chirikov [66].

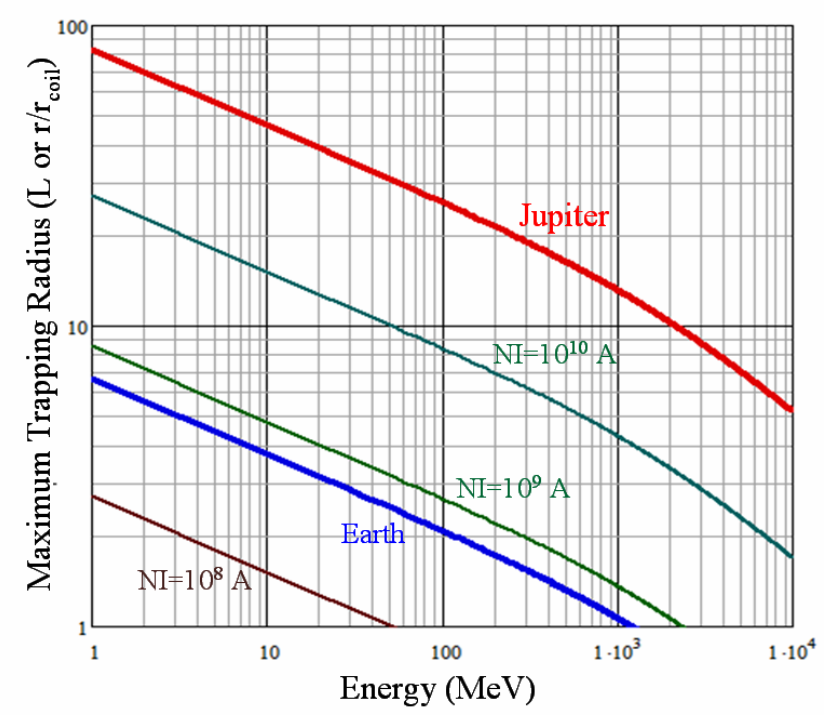

Figure 49 – Maximum trapping region for antiprotons.

APPENDIX F – PARTICLE ADVANCEMENT AND ERROR CONTROL

The motion of a charged particle, such as an antiproton, in the presence of magnetic and electric fields which make up the magnetosphere of a planet is governed by forces described the Lorentz equation. The geomagnetic field through which it is transported can vary as a function of both position and time. Ultimately, the path of the particle with a given charge (q) and mass (m_0) based on a arbitrary set of initial spatial (x_o,y_o,z_o) and velocity conditions (u_o,v_o,w_o) needs to be determined. This simulation of these trajectories can eventually be applied to a large scale Monte Carlo analysis to simulate the interaction of cosmic rays with the Earth's magnetic field.

The equations describing the physics of this motion can be represented with a system of six first order differential equations. The six derivatives of the particle's position,

$$\frac{d\vec{s}}{dt} = \vec{V}, \qquad \textit{Equation 54}$$

and relativistic momentum,

$$\frac{d\vec{p}}{dt} = q\left(\vec{V} \times \vec{B} + \vec{E}\right). \qquad \textit{Equation 55}$$

can be represented as,

$$\frac{dx}{dt} = u, \qquad \textit{Equation 56}$$

$$\frac{dy}{dt} = v, \qquad \textit{Equation 57}$$

$$\frac{dz}{dt} = w, \qquad \textit{Equation 58}$$

$$\frac{du}{dt} = \frac{q\sqrt{1-\left(\frac{\sqrt{u^2+v^2+w^2}}{c}\right)^2}}{m_0}\left(v \cdot B_z - w \cdot B_y\right), \qquad \textit{Equation 59}$$

$$\frac{dv}{dt} = \frac{q\sqrt{1-\left(\frac{\sqrt{u^2+v^2+w^2}}{c}\right)^2}}{m_0}\left(w\cdot B_x - u\cdot B_z\right), \qquad \textit{Equation 60}$$

$$\frac{dw}{dt} = \frac{q\sqrt{1-\left(\frac{\sqrt{u^2+v^2+w^2}}{c}\right)^2}}{m_0}\left(u\cdot B_y - v\cdot B_x\right), \qquad \textit{Equation 61}$$

in scalar representation since,

$$\vec{p} = m_0\gamma\vec{V}, \qquad \textit{Equation 62}$$

where the relativistic correction factor,

$$\gamma = \frac{1}{\sqrt{\left(1-\beta^2\right)}} = \frac{1}{\sqrt{\left(1-\left(V/c\right)^2\right)}}. \qquad \textit{Equation 63}$$

As a first pass, the Earth's magnetosphere can be represented as a static magnetic dipole with no electric field. A simple dipole model of the Earth in spherical coordinates is,

$$B_r = -2B_0\left(\frac{R_{earth}}{r}\right)^3\cos(\theta) \qquad \textit{Equation 64}$$

$$B_\theta = -B_0\left(\frac{R_{earth}}{r}\right)^3\sin(\theta) \qquad \textit{Equation 65}$$

or

$$B_x = \frac{3\cdot x\cdot z\cdot M}{\left(\sqrt{x^2+y^2+z^2}\right)^5} \qquad \textit{Equation 66}$$

$$B_y = \frac{3 \cdot y \cdot z \cdot M}{\left(\sqrt{x^2 + y^2 + z^2}\right)^5} \qquad \textit{Equation 67}$$

$$B_z = \left(\frac{3 \cdot z^2}{\left(\sqrt{x^2 + y^2 + z^2}\right)^2} - 1 \right) \frac{M}{\left(\sqrt{x^2 + y^2 + z^2}\right)^3} . \qquad \textit{Equation 68}$$

in Cartesian coordinates where M is the magnetic moment of the Earth (-7.84×10^{15} Tm^3). These equations can be readily solved with a high order Runge-Kutta algorithm. A simulation environment to study the motion of the antiprotons was developed in matlab for this purpose. Though various solvers were evaluated, most simulations used an explicit Runge-Kutta 5th order formulation based on the Dorman-Prince pair [45] or a variable order Adams-Bashforth-Moulton solver [46]. The initial models for the planet used a static dipole field model of the magnetosphere with no electric field present though a more detailed magnetosphere model could be included if so desired. However, a simple dipole field can quite accurately represent the inner field region of a magnetosphere with minimal computational overhead.

The particle advancement algorithms provide variable time step capabilities and error tolerance control. These are very important features to minimize the computational requirements which allow us to maximize the number of trajectories studied in the Monte Carlo analysis. Utilizing variable time steps during the solution allows the algorithm to quickly process portions of the trajectory where there is little change in the vector momentum. Automatic error control enables the time step to be chosen to minimize the computational burden for a desired level of accuracy. Care must be taken however, since minor errors can quickly propagate as demonstrated in Figure 50.

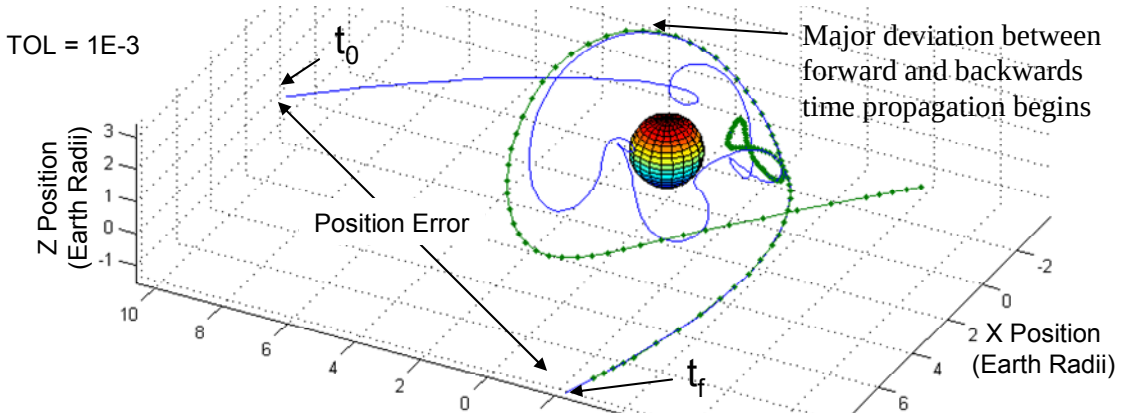

Figure 50 – Particle trajectory error due to low tolerances and error propagation.

The accuracy of the transport code was first validated semi-quantitatively against rigidity cutoff limits. A study was subsequently initiated to determine the required level of computational accuracy to maximize the number of trajectories calculated per unit time while preventing major errors such as the one shown in the previous figure. The two charts in Figure 51 show the distribution of position errors at two error tolerance levels. The errors are quantified by first calculating the forward trajectory and then recalculating the trajectory of a particle with a negative charge propagating from the final position with reversed momentum values of the final point on the initial trajectory. After the equivalent time span, the final position of the second trajectory is compared to the initial position of the first trajectory. The difference is the error shown.

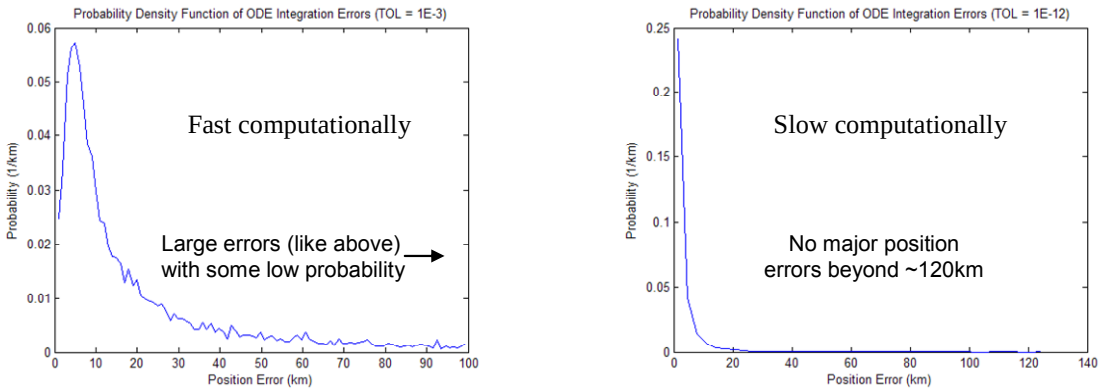

Figure 51 – Probability density function for ODE integration errors.

When many random trajectories are compared, the majority of the errors are 20 km or less, which is extremely small given the overall scale of the magnetosphere under consideration. However, a small subset of the long lived trajectories can experience large deviations like the one shown in Figure 50. However, this can be avoided by using a tighter error tolerance. Though this is computationally slower by a significant factor, it avoids the erroneous results such as the one shown. Despite the slowdown from the tighter error control, a moderately powerful desktop computer from today can calculate, in a very short period of time, what would have taken Carl Störmer's graduate students decades by hand in the first half of the last century.

REFERENCES

1. Sanger, E., "The Theory of Photon Rockets," *Ing. Arch.*, Vol 21, 1953.
2. Schmidt, G.R., H.P. Gerrish, J.J. Martin, G.A. Smith, and K.J. Meyer, "Antimatter Requirements and Energy Costs for Near-Term Propulsion Applications", *Journal of Propulsion and Power*, Vol. 16, No. 5, September-October 2000.
3. Schmidt, G.R., H.P. Gerrish, J.J. Martin, G.A. Smith, and K.J. Meyer, "Antimatter Production for Near-term Propulsion Applications", *Joint Propulsion Conference and Exhibit*, Los Angles, CA, 1999, AIAA-99-2691.
4. Howe, S.D., and G. P. Jackson, "Antimatter Driven Sail for Deep Space Exploration", NIAC 2004 Fellows Meeting Presentation, October 2004.
5. Gaidos, G., et al, "Antiproton- Catalyzed Microfission/Fusion Propulsion Systems for Exploration of the Outer Solar System and Beyond," AIAA 98-3589, July 1998.
6. Forward, R. L, and J. Davis, "Mirror Matter: Pioneering Antimatter Physics", *Wiley Science Additions,* 1988.
7. Gray, L., and T. E. Kalogeropoulos, "Possible Bio-Medical Application of Antiprotons", *IEEE Transactions in Nuclear Science*, Vol. NS-29, No. 2, April 1982.
8. Augenstein, B.W., "RAND Workshop on Antiproton Science and Technology, October 6-9,1987: Annotated Executive Summary," *RAND Note N-2763-AF*, October 1988.
9. LaPointe, M. R., "Antimatter Production at a Potential Boundary," *Joint Propulsion Conference and Exhibit,* July 2001, AIAA-2001-3361.
10. Hora, H., "Estimates of the Efficient Production of Antihydrogen by Lasers of Very High Intensities," *OptoElectronics*, Vol 5, 1973, pp. 491–501.
11. Crowe, E.G., "Laser Induced Pair Production as a Matter-Antimatter Source," *Journal of the British Interplanetary Society*, Vol. 36, 1983, pp. 507–508.
12. Chapline, G. "Antimatter Breeders," *Journal of the British Interplanetary Society*, Vol 35, pp. 423–424, 1982.
13. Cassenti, B.N., "Concepts for the Efficient Production and Storage of Antimatter," *AIAA–93–2031*, presented at the 29th Joint Propulsion Conference, Monterey, CA, Jun 28–30, 1993.
14. Holzscheiter, M.H., R. A. Lewis, E. Mitchell, J. Rochet, and G. A. Smith, "Production and Trapping of Antimatter for Space Propulsion Applications", *AIP Conference. Proceedings*. 387, 1493 (1997)
15. Biermann, P.L. and G. Sigl, "Introduction to Cosmic Rays", arXiv:astro-ph/0202425 v1 22 Feb 2002
16. Moskalenko, I.V., A. W. Strong, J. F. Ormes, and M.S. Potgieter, "Secondary Antiprotons and Propagation of Cosmic Rays in the Galaxy and Heliosphere", *The Astrophysical Journal*, 564, January 10, 2002.
17. Huang, C.Y., L. Derome, and M. Buenerd, "Secondary Antiproton Flux Induced by Cosmic Ray Interactions with the Atmosphere", *Physical Review D.*, Vol 68, pgs 053008, 2003.
18. Picozza, P., and A. Morselli, "Antimatter research in space", *Journal of Physics G: Nuclear and Particle Physics*, 29 (2003), 903-911.
19. Labrador, A. W., and R.A. Mewaldt, "Effects of Solar Modulation on the Low-Energy Cosmic-Ray Antiproton/Proton Ratio", *The Astrophysical Journal*, 480:371-376, 1997 May 1.
20. Walt, M., "Introduction to Geomagnetically Trapped Radiation", Cambridge University Press, 1994.
21. Schulz, M. and L.J. Lanzerotti, "Particle Diffusion in the Radiation Belts", *Springer-Verlag*, 1974.
22. Spjeldvik, W. N., "Equilibrium Structure of Equatorially Mirroring Radiation Belt Protons", *Journal of Geophysical Research*, Vol. 82, No. 19, July 1, 1977.
23. Barth, J.L., C.S. Dyer, and E.G. Stassinopoulos, "Space, Atmospheric, and Terrestrial Radiation Environments", *IEEE Transactions on Nuclear Science*, Vol. 50, No. 3, June 2003.
24. Hargreaves, J.K., "The Solar-Terrestrial Environment", *Cambridge Atmospheric and Space Science Series*, 1992.
25. Bussard, R.W., "Galactic matter and interstellar flight", *Astronautica. Acta.* Vol 6, pp 179-94, 1960.
26. Fishback, J. F., "Relativistic Interstellar Spaceflight", *Astronautica Acta*, Vol 15, pp 25-35, 1968
27. Martin, A.,R., "Magnetic Intake Limitations on Interstellar Ramjets", *Astronautica Acta*, Vol. 18, pp 1-10, 1973.
28. Semay, C., and B. Silvestre-Brac, "The equation of motion of an interstellar Bussard ramjet", *European Journal of Physics*, Vol 26, pp 75-83, 2005.
29. Ifedili, S.O., "Atmospheric Neutrons and Their Contributions to the Earth's Radiation Belts", *Journal of Geomagnetic and Geoelectric*, **43**, 255-266, 1991.

30. Jentsch, V., "On the Role of External and Internal Source In Generating Energy and Pitch Angle Distributions of Inner-zone Protons", *Journal of Geophysical Research*, Vol. 86, p.701-710, Feb 1981.
31. Agostinelli et al., "Geant4: A Simulation Toolkit", Nuclear *Instruments and Methods*. A506:250-303, 2003.
32. Pugacheva, G., A.A. Gusev, U.B. Jayanthi, N.J. Schuch, W.N. Spjeldvik, and C. H. Choque, "Antiprotons confined in the Earth's inner magnetosphere", *Astroparticle Physics* 20, pgs 257-265, 2003.
33. Gusev, A.A., U.B. Jayanthi, K.T. Choque, G. I. Pugacheva, N. Schuch and W.N. Spjeldvik, "Antiproton radiation belt produced by cosmic rays in the Earth's magnetosphere.", *Geophysical Research Letters*, Vol.30, No. 4, 1161, 2003.
34. Derome, L, "Atmospheric Protons and Antiprotons from sea level to satellite altitudes", *28th International Cosmic Ray Conference*, pgs. 2069-2071, 2003.
35. Spjeldvik, W.N., A.A. Gusev, I.M. Martin, G.I. Pugacheva, S. Bourdarie, and N.J. Schuch, "Theory for Antiproton Content of Planetary Magnetospheres", *IAGA-Scientific Symposia*, Toulouse, France; July 18-29, 2005.
36. Divine, N., and H. B. Garrett, "Charged Particle Distributions in Jupiter's Magnetosphere", *Journal of Geophysical Research*, Vol. 88, No. A9, pgs. 6889-6903, September 1, 1983.
37. Garret, H.B. et al., "A Revised Model of Jupiter's Inner Electron Belts: Updating the Divine Radiation Model", *Geophysical Research Letters*, Vol. 32, L04104, doi:10.1029/2004GL021986, 2005.
38. Dessler, A. J. (editor), "Physics of the Jovian Magnetosphere", Cambridge University Press, 1983.
39. Nicholson, P. D., and L. Dones, "Planetary Rings", *Reviews of Geophysics*, Supplement, pgs 313-327, April 1991.
40. Aguilar, M., et al., "The Alpha Magnetic Spectrometer (AMS) on the International Space Station: Part I – results from the test flight on the space shuttle", *Physics Reports* 366, pg 331-405, 2002.
41. Gusev, A.A., U.B. Jayanthi, I.M. Martin, G. I. Pugacheva, and W.N. Spjeldvik, "On Positron Radiation Belt in the Earth's Magnetosphere.", *Brazilian Journal of Physics*, Vol. 30, No. 3, Sept. 2003.
42. Share, G. H. et al, "High-Resolution Observation of the Solar Positron-Electron Annihilation Line", *The Astrophysical Journal*, 595:L85-L88, 2003 October 1.
43. Kallenrode, M., "Space Physics: An Introduction to Plasmas and Particles in the Heliosphere and Magnetospheres", *Springer Books*, pg 367, 2004.
44. Störmer, C., "The Polar Aurora", *Oxford University Press*, 1950.
45. Dormand, J. R. and P. J. Prince, "A Family of Embedded Runge-Kutta Formulae," *Journal of Computational and Applied Math*, Vol. 6, pp 19-26, 1980.
46. Shampine, L. F. and M. K. Gordon, "Computer Solution of Ordinary Differential Equations: the Initial Value Problem", *W. H. Freeman*, 1975.
47. Weisstein, E.W., "Sphere Point Picking", From *MathWorld* - A Wolfram Web Resource. http://mathworld.wolfram.com/SpherePointPicking.html
48. Forward, R. L., "Antiproton Annihilation Propulsion", *AFRPL TR-85-034*, September 1985.
49. Cassenti, B., "Mass Production of Antimatter for High-Energy Propulsion", *Journal of Propulsion and Power*, Vol. 16, No. 1, January-February 2000.
50. Jackson, G., "Commercial Production and Use of Antiprotons", *Proceedings of EPAC 2002*, Paris, France, 2002.
51. Haloulakos, V., and A. Ayotte,, "The Prospects For Space-Based Antimatter Production", *AIAA-91-1987*, Joint Propulsion Conference, Sacramento, CA, June 24-26, 1991.
52. Grant, I.S., and W.R. Phillips, "Electro-magnetism, 2nd Edition", Chapter 4, *Wiley*, 1990.
53. Zubrin, R., "The Magnetic Sail", *Phase I NIAC Final Report*, January 7, 2000.
54. Ohanian, H. C., "Classical Electrodynamics", Chapter 11, *Simon and Schuster*, 1988.
55. Hedin, A. E., "MSIS-86 Thermospheric Model", *Journal of Geophysical Research*, 92, 4649, 1987. Available online at: http://modelweb.gsfc.nasa.gov/atmos/msis.html
56. Tan, L.C., and L.K. Ng, "Calculation of the Equilibrium Antiproton Spectrum", *Journal of Physics G: Nuclear Physics*, 9, pgs. 227-242, 1983.
57. Letaw, J.R., R. Silverberg, C.H. Tsao, "Proton-nucleus total inelastic cross sections – an empirical formula for E greater than 10 MeV", *Astrophysical Journal Supplement Series*, Vol. 51, pgs. 271-275, March 1983.
58. Kress, B.T., M.K. Hudson, K.L. Perry, and P.L. Slocum, "Dynamic Modeling of Geomagnetic Cutoff for the 23-24 November 2001 Solar Energetic Particle Event", *Geophysical Research Letters*, Vol. 31, L04808, doi:10.1029/2003GL018599, 2004.
59. Chen, F.F., "Introduction to Plasma Physics", *Plenum Press*, 1974.

60. Greaves, R.G., and C.M. Surko, "Antimatter Plasmas and Antihydrogen", *Physics of Plasmas*, 4(5), May 1997.
61. Hovestadt, et al., "Evidence for Solar Wind Origin of Energetic Heavy Ions in the Earth's Radiation Belt", *Geophysical Research Letters*, Vol. 5, No. 12, December 1978.
62. Hudson, M.K., et al., "Radiation Belt Formation during Storm Sudden Commencements and Loss During Main Phase", *Advances in Space Research*, 21(4), pgs 597-607, February 1998.
63. Gray, A., "Modern Differential Geometry of Curves and Surfaces with Mathematica, 2nd edition" *CRC Press*, 1997.
64. Northrop, T.G., "The Adiabatic Motion of Charged Particles", *Interscience Publishers*, 1963.
65. Schulz, M., "The Magnetosphere" in "Geomagnetism" edited by J.A. Jacobs, Vol 4. pp 202, *Academic Press*, 1991.
66. Chirikov, B.V., "Particle Dynamics in Magnetic Traps", *Reviews of Plasma Physics*, Vol. 13, 1987.